DEPARTMENT OF MEDICAL BIOCHEMISTRY AND BIOPHYSICS
Division of Molecular Structural Biology
Karolinska Institutet, Stockholm, Sweden

CELL WALL REMODELING PROTEINS IN *MYCOBACTERIUM TUBERCULOSIS*: STRUCTURE, FUNCTION AND INHIBITION

Eva Maria Rebrova (Steiner)

Eva Maria Rebrova,
was born 1984 in Austria (Kirchdorf/Krems), grew up in a tiny mountain village and eventually studied after graduating from IT-Commercial Academy. She received her Master of Science (MSc) in Molecular Biology at the University of Vienna and joined the PhD grogram at Karolinska Institutet in 2012 in the protein crystallography group of Prof. Gunter Schneider and Dr. Robert Schnell.

Karolinska Institutet

Stockholm 2017

Cover art produced by ShapeSciFx (http://shapescifx.com) based on an original idea by Eva Maria Rebrova

All previously published papers were reproduced with permission from the publisher.

Published by Karolinska Institutet.
Printed by E-Print AB 2017

ISBN 978-91-7676-848-8

CELL WALL REMODELING PROTEINS IN *MYCOBACTERIUM TUBERCULOSIS*: STRUCTURE, FUNCTION AND INHIBITION

THESIS FOR DOCTORAL DEGREE (Ph.D.)

Friday, 17th November 2017, 10:00 a.m.

Samuelssonsalen, Scheelelaboratoriet, Tomtebodavägen 6
Karolinska Institutet, Solna

By

Eva Maria Rebrova (Steiner)

Principal Supervisor:
Dr. Robert Schnell
Karolinska Institutet
Department of Medical Biochemistry and Biophysics
Division of Molecular Structural Biology
Stockholm, Sweden

Co-supervisor:
Prof. Gunter Schneider
Karolinska Institutet
Department of Medical Biochemistry and Biophysics
Division of Molecular Structural Biology
Stockholm, Sweden

Opponent:
Prof. Juan A. Hermoso
Instituto Quimica-Fisica "Rocasolano", CSIC
Department of Crystallography and Structural Biology
Madrid, Spain

Examination Board:
Prof. Sherry L. Mowbray
Uppsala Universitet
Department of Cell and Molecular Biology, Structural and Molecular Biology
Uppsala, Sweden

Dr. Pål Stenmark
Stockholm Universitet
Department of Biochemistry and Biophysics
Stockholm, Sweden

Prof. Martin Rottenberg
Karolinska Institutet
Department of Microbiology, Tumor and Cell Biology
Stockholm, Sweden

Dedicated to my beloved family!

‘I think, at a child's birth, if a mother could ask a fairy godmother to endow it with the most useful gift, that gift would be curiosity.’

— Eleanor Roosevelt

ABSTRACT

The complex and peculiar cell wall architecture is vital for the survival of *M. tuberculosis* in the host and therefore an established target for several currently used drugs. Understanding of the cell wall maintenance and the underlying biochemical mechanisms in this pathogen is expected to aid the development and evaluation of novel anti-TB therapies. Within the scope of this thesis peptidoglycan remodeling enzymes including the essential transpeptidase Ldt_{Mt2}, an NlpC/P60 hydrolase, RipA and a non-catalytic NlpC/P60 variant, RipD were investigated.

Ldt_{Mt2}, essential in *M. tuberculosis* for intra-host survival, forms the prevalent 3-3 cross-links within the cell wall peptidoglycan. The structure of Ldt_{Mt2} was solved, a model of the three-domain protein located in the periplasm was proposed and the covalent adduct formation with β-lactam antibiotics was observed. The systematic analysis of several β-lactams identified faropenem displaying the fastest binding kinetics and resulting in the formation of a stable adduct. These results and the high-resolution structure of Ldt_{Mt2} with this adduct representing the inactivated state describes the detailed action of faropenem, which is the most efficient β-lactam in killing *M. tuberculosis in vitro* and inside macrophages.

During mycobacterial cell division, daughter cell separation requires endopeptidases from the NlpC/P60 protein family. RipD the first non-catalytic member from this family that retains PG binding activity and carries a long penta-peptide repeat sequence in C-terminal position was characterized. RipA comprises a well-characterized C-terminal endopeptidase domain of the NlpC/P60-type and an N-terminal domain of unknown function. The N-terminal domain was previously implicated in inhibition of the catalytic activity by blocking the C-terminal domain. Here we show that it is not the N-terminal domain but the lid-module of the inter-domain linker that limits the active site access. The structure of the N-terminal domain was solved by X-ray crystallography revealing an elongated domain built by two long α-helices. Small angle X-ray scattering in combination with the X-ray structures of the two individual domains was used to model the periplasmic RipA protein suggesting a rigid, hairpin-like N-module connected to the catalytic domain by a flexible linker. This domain organization allows for a defined range of movement of the catalytic domain implicated the spatially controlled cell wall degradation.

LIST OF SCIENTIFIC PAPERS

I. Böth Dominic, **Steiner Eva Maria**, Stadler Daniela, Lindqvist Ylva, Schnell Robert & Schneider Gunter (2013) Structure of Ldt_{Mt2}, an L,D-transpeptidase from *Mycobacterium tuberculosis*. *Acta Crystallogr D* **69**(3), 432–41.

II. **Steiner Eva Maria**, Schneider Gunter & Schnell Robert (2017) Binding and processing of β-lactam antibiotics by the transpeptidase Ldt_{Mt2} from *Mycobacterium tuberculosis*. *FEBS J* **284**(5), 725–741.

III. Böth Dominic, **Steiner Eva Maria**, Izumi Atsushi, Schneider Gunter & Schnell Robert (2014) RipD (Rv1566c) from *Mycobacterium tuberculosis*: adaptation of an NlpC/P60 domain to a non-catalytic peptidoglycan-binding function. *Biochem J* **457**(1), 33–41.

IV. **Steiner Eva Maria**, Lyngsø Jeppe, Guy Jodie, Bourenkov Gleb, Lindqvist Ylva, Schneider Thomas R., Pedersen Jan Skov, Schneider Gunter and Schnell Robert. The Structure of the N-terminal Module of the Cell Wall Hydrolase RipA and its Role in Regulating Catalytic Activity. *Manuscript in preparation.*

PUBLICATIONS NOT INCLUDED IN THE THESIS

Eva Maria Steiner, Dominic Böth, Philip Lössl, Francisco Vilaplana, Robert Schnell & Gunter Schneider (2014) CysK2 from *Mycobacterium tuberculosis* is an O-Phospho-l-Serine-Dependent S-Sulfocysteine Synthase. *J Bacteriol.* **196**(19), 3410–3420.

Katharina Brunner, **Eva Maria Steiner**, Rudraraju Srilakshmi Reshma, Dharmarajan Sriram, Robert Schnell & Gunter Schneider (2017) Profiling of *in vitro* activities of urea-based inhibitors against cysteine synthases from *Mycobacterium tuberculosis*. *Bioorg & Med Chem Letters* **27**, 4582–4587.

CONTENTS

LIST OF ABBREVIATIONS

AEC	airway epithelial cell
AFB	acid-fast-bacilli
AG	arabinogalactan
AM	alveolar macrophage
APA	6-aminopenicillanic acid
Ara*f*	arabinofuranose
ART	antiretroviral therapy
ASL	airway surface liquid
ATP	adenosine triphopshate
BCG	bacille Calmette-Guérin
BIA	biapenem
CAMP	cationic antimicrobial peptide
CD	circular dichroism
CD4/8+	cluster of differentiation 4/8 plus cells
CLR	C-type lectin receptor
CP	carboxypeptidation
CR	complement receptor
CWCx	cell wall extract
DAG	diacylglycerol
DC	dendritic cell
DNA	deoxyribonucleic acid
DORI	doripenem
DPG	diphosphatidylglycerol
DTNB	dithio-nitrobenzoate
EP	endopeptidase
ERTA	ertapenem
FARO	faropenem
FAROdal	faropenem daloxate
FDC	fixed-dose combination
Gal*f*	galactofuranose
GlcN	glucosamine
GlcNAc	*N*-acetylglucosamine
GPL	glycopeptidolipid
GT	glycosyltransferase
HIV	human immunodeficiency virus
HMW	high-molecular-weight
IFN-γ	interferon gamma
IFT	indirect Fourier transformation
Ig	immunoglobulin
IGRA	interferon-gamma release assay
IM	inner membrane
ITC	isothermal titration calorimetry
LAM	lipoarabinomannan
LM	lipomannan
LTBI	latent tuberculosis infection
MA	mycolic acid
mAGP	mycolyl-arabinogalactan-peptidoglycan
m-DAP	*meso*-diaminopimelic acid

MERO	meropenem
MDR	multi-drug resistant
MHC	major histocompatibility complex
MOA	mechanism of action
MOP	multidrug/oligosaccharidyl-lipid/polysaccharide
Mtb	*Mycobacterium tuberculosis*
MTBC	*Mycobacterium tuberculosis* complex
MurNAc	*N*-acteylmuramic acid
NK	natural killer cell
NlpC/P60	new lipoprotein C and a 60 kDa protein
NOD	nucleotide-binding oligomerization domain
OM	outer membrane
PAMP	pathogen-associated molecular pattern
PBP	penicillin-binding-protein
PDB	protein database
PE	phosphatidylethanolamine
PEN	penicillin-G
PIM	phosphatidylinositol mannoside
PIP	piperacillin
PG	peptidoglycan
PRR	pattern recognition receptor
RIF	rifampicin
RMS	reverse micellar solution
RNA	ribonucleic acid
RNS	reactive nitrogen species
ROS	reactive oxygen species
Rpf	resuscitating-promoting factor
RR	rifampicin-resistant
R&D	research and development
SAXS	small-angle X-ray scattering
SEC	size exclusion chromatography
TB	tuberculosis
TEBI	tebipenem
TLR	toll-like receptor
TNF-α	tumour necrosis factor alpha
TP	transpeptidase
TST	tuberculin skin test
UT/DP	uridine tri/diphosphate
WHO	World Health Organization
XDR	extensively-drug resistant

INTRODUCTION

1. TUBERCULOSIS – A GLOBAL CHALLENGE

Mycobacterium tuberculosis (*Mtb*) the causative agent of the chronic infectious disease tuberculosis (TB) is a highly efficient pathogen. In 2015 about 10 million new TB cases were estimated world wide and 60% of the new cases account for six countries: India, Indonesia, China, Nigeria, Pakistan and South Africa. The number of multi-drug resistant TB (MDR-TB) represents about 3.3% of the new cases (Figure 1). In 2015 about 580,000 people were newly eligible for MDR-TB treatment but only 20% were enrolled. The crisis of MDR-TB detection and treatment is particularly problematic in the five countries that accounted for more than 60% of the resulting gap: India, China, the Russian Federation, Indonesia and Nigeria. A bit more than half of notified TB patients had a documented human immunodeficiency virus (HIV) test result. 78% of patients diagnosed with the 'HIV-TB syndemic' are enrolled to antiretroviral therapy (ART), which is significantly higher compared to MDR-TB patients (WHO report 2016).

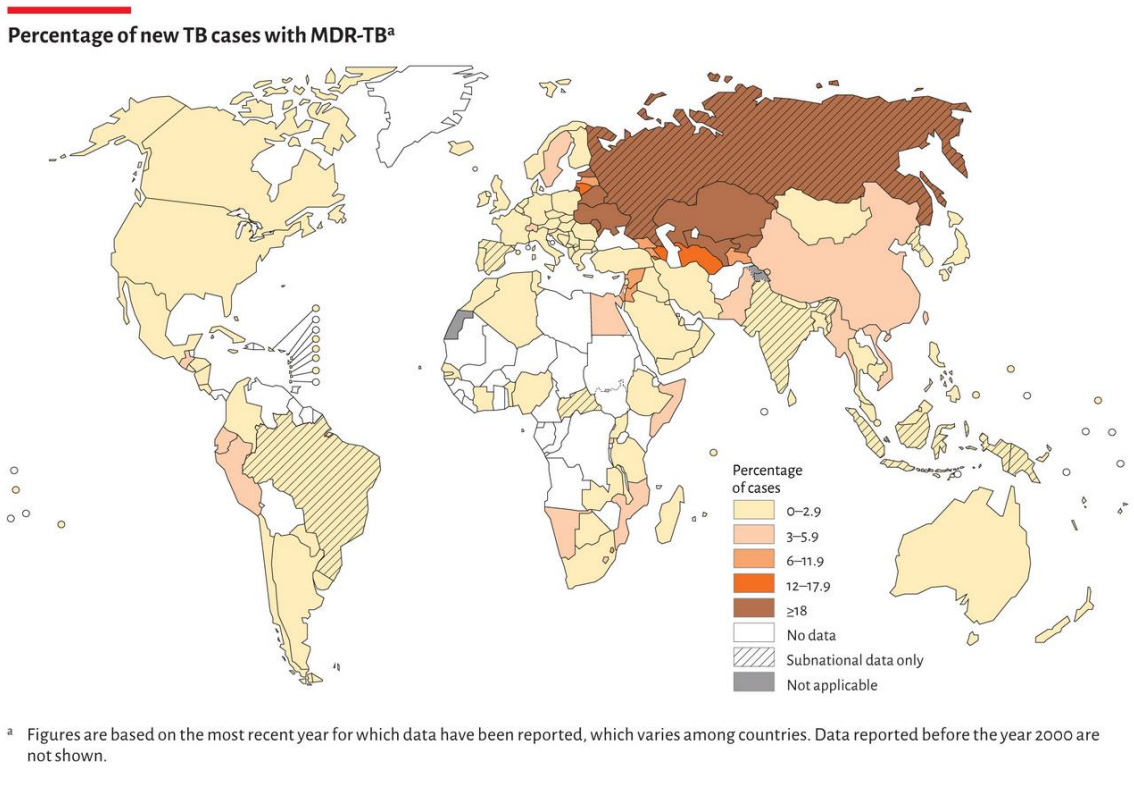

Figure 1. Wold Map and New MDR-TB Cases in Percentage (*adapted from WHO report 2015*).

To decrease resistance numbers surveillance is essential and provides indicators whether common treatment is effective. The Global Project on Anti-TB Drug Resistance Surveillance is the oldest and largest project on surveillance of anti-microbial resistance in the world. Recent innovations in molecular diagnostics are facilitating the shift from periodic surveys to routine surveillance. For example, rapid molecular tests such as Xpert® MTB/RIF for detection of *Mtb* and rifampicin resistance, provide results much faster than conventional methods, do not require sophisticated laboratory infrastructure and decrease cost.

Currently about 1/4 of world's population, besides patients with acute TB, are latently infected, carry a great potential for spreading the disease and developing resistant strains (Houben & Dodd 2016). Risk factors such as malnutrition, smoking or substantial alcohol abuse and social and economic problems are cause for increased infection risk and early disease onset in latent TB infection (Ai et al. 2016, Narasimhan et al. 2013).

The challenges nowadays to fight the pathogen and the resulting disease TB are global, therefore the control and cure strategies have to be orchestrated (Figure 2). Various political, social and economic factors play an important role in causation and control of TB. National and international prevention and education programs have to be improved e.g. with holistic strategies adapted to individual needs (Udwadia & Pinto 2007). Financial support and political commitment is essential for research and development (R&D) and for developing new application methods and technologies. R&D gives us deep insight into the biology of host and pathogen interactions. Understanding molecular mechanisms underlying the infection, disease and resistance are crucial to halter the disease and to up- and downstream network with R&D to find cure and preventions.

However, more detailed knowledge about resistance, disease and biology of *Mtb* is needed and application of novel technologies in diagnosis, treatment and prevention. All challenges have to be accepted and worked out on national and international levels to reach the WHO goal to eliminate TB by 2050 as a public health problem (WHO 2014, Dye & Williams 2008).

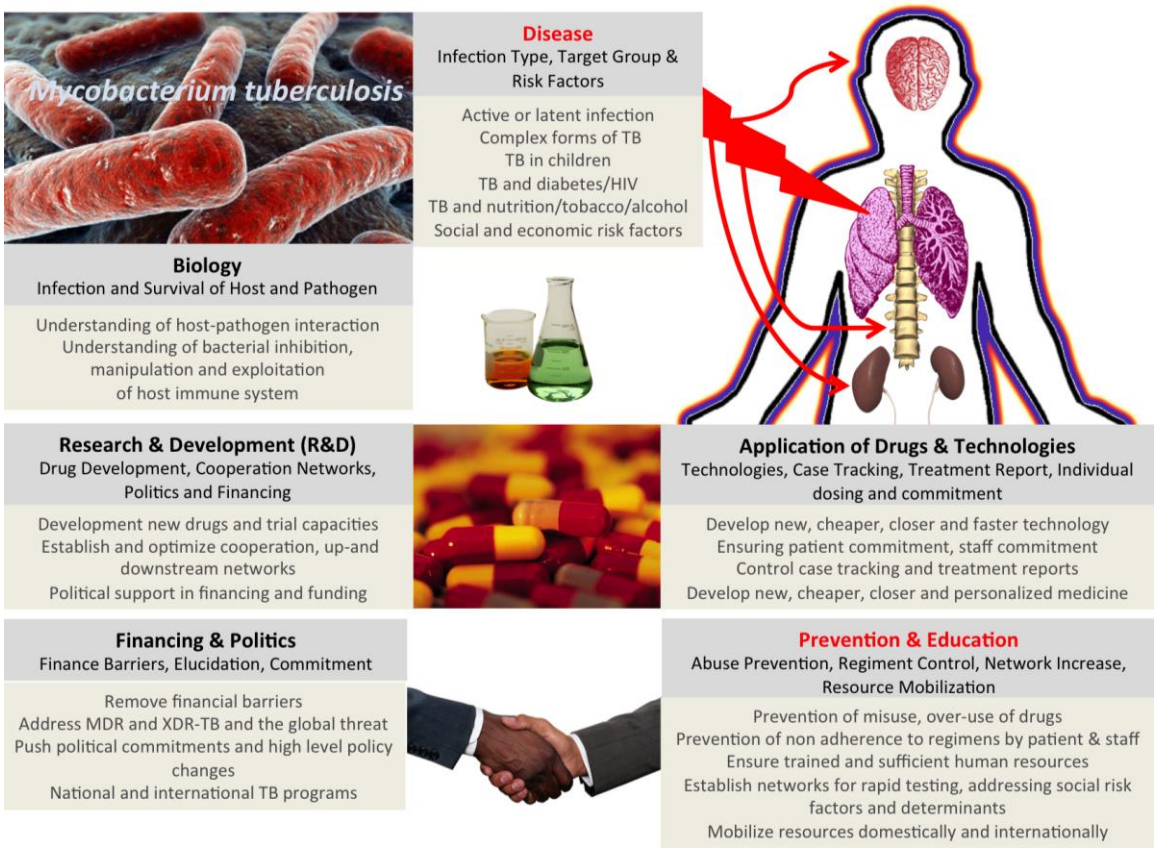

Figure 2. The Global TB Challenges Summarized in Categories.

1.1 THE DISCOVERY OF *MYCOBACTERIUM TUBERCULOSIS*

Mtb is a pathogen without environmental reservoir and humans are the only known host where *Mycobacterium tuberculosis* and *Mycobacterium africanum* can maintain infection cycles and transmission (Smith et al. 2006).

The Mycobacterium genus might have originated about 150 million years ago (Hayman 1984). *Mycobacterium tuberculosis* (*Mtb*) *sensu-stricto* and seven other human-adapted mycobacterial lineages that diverged in different regions of the world, have emerged from a common ancestor and are classified by 99.9% DNA identity as the *Mycobacterium tuberculosis* complex (MTBC) (Brosch et al. 2002, Supply et al. 2013, Brites & Gagneux 2015). So far the oldest reported human case of infection with *Mtb* is dated back 9,000 years from a Neolithic Settlement in the Eastern Mediterranean (Hershkovitz et al. 2008). Throughout all periods of human history TB was a present threat and reached all continents of the world.

During the 18th and 19th century it reached epidemic levels in Europe and North America (Daniel 2006). In 1882, Hermann Heinrich Robert Koch changed the history of tuberculosis

with his presentation *Die Aetiologie der Tuberculose* to the Berlin Physiological Society where he also formulated the Koch-Henle postulates and was awarded the Noble Prize in Medicine or Physiology in 1905 (Koch 1932). Based on Koch's findings in 1907 the Austrian pediatrician Clemens Freiherr von Pirquet developed the tuberculin skin test and used it to demonstrate latent tuberculous infection in asymptomatic children (von Pirquet 1907). In 1921 Albert Calmette and Camille Guérin developed a 'Bacille Calmette-Guérin' (BCG) vaccine based on the attenuated laboratory strain of *Mycobacterium bovis* (Sakula 1983, Daniel 2005). After the Second World War, the BCG vaccine was used in the first international disease control program (International Tuberculosis Campaign) by the WHO based on tuberculin testing followed by BCG vaccination with 30 million tested and 14 million vaccinated in the period between 1948-1951 (Comstock 1994). Together with the discovery of streptomycin in 1944, isoniazid in 1952 and rifamycins in 1957 and their antibacterial activity against *Mtb*, a new era of tuberculosis treatment began (Schatz et al. 1944, Daniel 2006). *Mtb* has the ability to rapidly adapt, resist and develop mechanisms to counteract drugs and treatment. This limits the lifespan of currently used anti-mycobacterial agents and the development of new drugs is of outmost importance.

1.2 THE DISEASE TUBERCULOSIS (TB) - ACTIVE AND LATENT TB INFECTION

Mycobacterium tuberculosis is most commonly transmitted by small infectious droplet nuclei of a person with acute TB and can be inhaled reaching the lung alveoli. One cough or five minutes of talking can produce enough droplet for successful infection and the bacilli may remain airborne for a 30 minutes long period (Loudon & Roberts 1967).

Encountering *Mtb* can result in three possible outcomes. In about 10% of the cases a person (most common in children or immuno-compromised individuals) will develop primary 'active' TB (Young et al. 2009). Most commonly the lungs are affected resulting in active pulmonary TB and symptoms like heavy coughing with cloudy or bloody sputum, fever and night sweats, fatigue, weight loss, short breathe and chest pain are well known indicators. However the majority, about 90% of patients, infected with *Mtb* will develop a contained form of TB with no disease symptoms referred to as a latent tuberculosis infection (LTBI) where bacilli reside in the human lungs over decades causing no active disease. In 10-20% of a LTBI patient's lifetime the infection can be reactivated to active TB ('post-primary' TB, Lillebaek et al. 2002). Disease onset is supported by an immuno-compromised state like HIV infection, diabetes, cancer or drug abuse (Ai et al. 2016). The mechanisms of *Mtb*

transition between latency and reactivation of the disease, the dynamic equilibrium between the human-pathogen crosstalk, which triggers the one or other disease outcome, are still poorly understood (Kondratieva et al. 2014).

1.2.1 The Human Immune Response and Host-Pathogen Interactions

Once *Mtb* is inhaled and on its way to be transported to the alveoli of the lungs it will pass through the human first-line innate defence mechanism – the respiratory mucosa (Figure 3, Middleton et al. 2002). Here *Mtb* encounters the epithelium, a layer of airway epithelial cells (AECs) the lamina propria, a layer of connective tissue and immune cells with lymphocytes and macrophages and a thick mucus layer of airway surface liquid (ASL) (Lugton 1999). AECs present receptors also known as pattern recognition receptors (PRRs). The PRRs include for example Toll-like receptors (TLRs), Dectin-1, C-type lectin receptors (CLRs), nucleotide-binding oligomerization domain-containing protein 2 (NOD2), dendritic cell (DC) and mannose receptors to name just a few (Li et al. 2012). PRRs recognise foreign microbial components, often macromolecules also known as pathogen-associated molecular patterns (PAMPs) that are expressed by *Mtb* (Akira et al. 2001). After PAMPs have been recognized by AECs a first immune response is mounted over presenting antigens to mucosal-associated invariant T cells which triggers the production of cytokines and effector molecules like interferon (IFN)-γ, tumour necrosis factor (TNF)-α and granzyme and as a result the onset of macrophages to initiate a first response to clear the bacterial infection (Harriff et al. 2014, Gold et al. 2010).

1.2.1.1 Host-pathogen Interactions in the Alveoli

In case *Mtb* surpasses the upper airways and reach the alveoli, the bacteria will be exposed to type I and type II alveolar epithelial cells (AECs), alveolar macrophages (AMs), dentritic cells (DCs) and neutrophils as present defenders (Lerner et al. 2015, Figure 3). *Mtb* invades and replicates in both macrophages and epithelial cells, where the latter plays an important role in dissemination of *Mtb* by undergoing necrosis (Li et al. 2012). Type II AECs secret enzymes and hydrolases, together with collectins (e.g. surfactant proteins Sp-A, Sp-D, Kishore et al. 2006) produced in the distal lung airspaces bind *Mtb* and enhance phagocytosis (Ferguson et al. 1999, Gaynor et al. 1995). Upon phagocytosis the activation of TLRs triggers the recruitment of neutrophils (NP), natural killer (NK) cells and T-cells that are part of the early defence against infection (Guirado & Schlesinger 2013). Apoptotic macrophages are phagocytised by DCs, which detect PAMPs and present antigens over Major Histocompatibility Complex class I and II (MHC I and MHC II) to T-cells in the local draining lymph node. This induces the transition from naïve T-cells to effector T-cells forming the link between innate and adaptive immune response (Espinosa-Cueto et al. 2017). In immuno-competent patients the infection will be contained by the formation of granuloma without eradicating *Mtb* completely leading to LTBI infection (Allen et al. 2015).

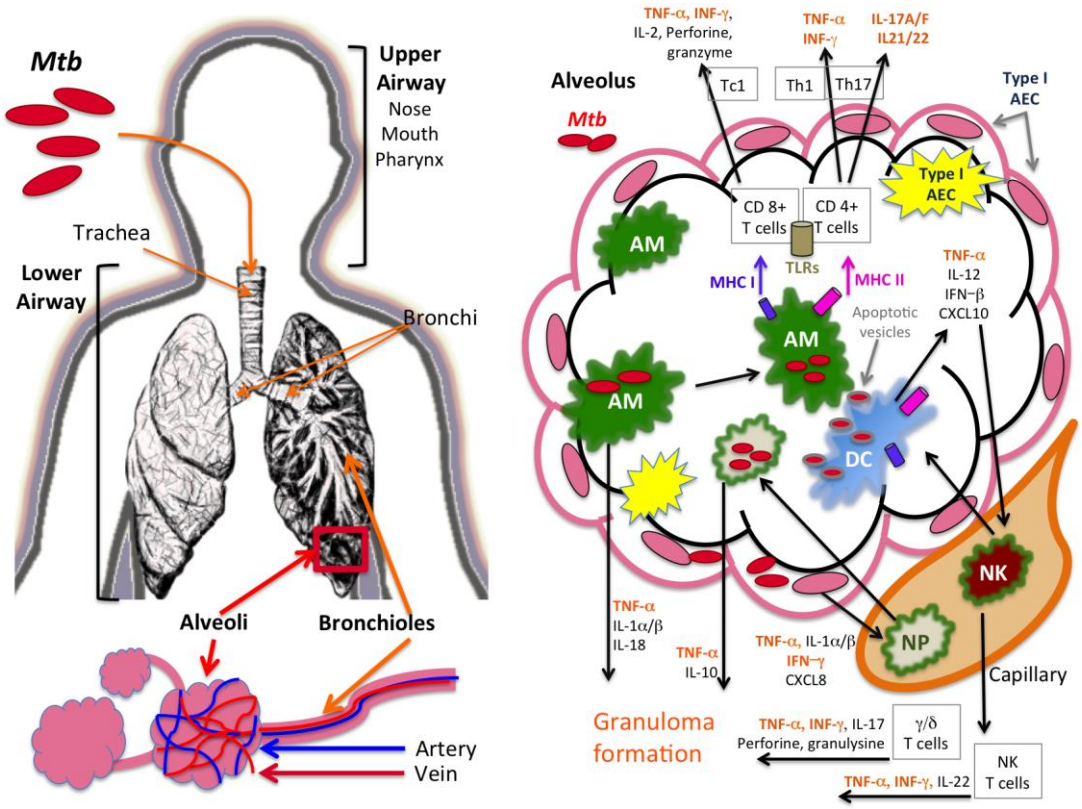

Figure 3. *Mtb* Infection Mechanism in the Human Alveolus.

1.2.1.2 Colonization of Macrophages

Phagocytosis by the alveolar macrophage (AM) can occur via different PRRs (Fc receptor, mannose receptor, complement receptors e.g. CR3) and receptor molecules expressed on the complex *Mtb* cell surface (Hossain & Norazmi 2013). The fate of *Mtb* is dependent on which receptor system for uptake is used. For example phagocytosis over the Fc receptor results in respiratory burst and an inflammatory response where CR3 receptor uptake, dependent on cholesterol presence, prevents lysosome-phagosome fusion and prevents activation of the macrophage (Pieters 2008, Greenberg 1999, Gatfield & Pieters 2000, Peyron 2000, Ernst 1998, Brennan & Nikaido 1995).

Within the AM, *Mtb* has to counteract harsh environmental conditions like low pH, nutrient starvation, hypoxia, reactive oxygen (ROS) and nitrogen species (RNS) (Schnappinger et al. 2003, Gengenbacher & Kaufmann 2012, Martin et al. 2016). As a response the bacilli have to align their metabolism to the environmental changes. The robust impermeable mycobacterial cell envelope is the first shield against any threat from the host. The up-regulation of genes involved in lipid metabolism is crucial (Chang et al. 2009, Nesbitt et al. 2010). Reprogramming mechanisms interfere with the lipid-mediated signalling processes and virulence factors like glycolipid lipoarabinomannan (LAM) and phosphatidylinositol mannoside (PIM) are coordinating the block in Ca^{2+} fluxes that inhibit phagosomal maturation (Rojas et al. 2000, Fratti et al. 2001) and uptake of nutrients by activating a Rab-dependent pathway (Vergne et al. 2004), respectively. Another survival mechanism of *Mtb* is to arrest the process of phagosome acidification by proton pumps to pH 5.0 and keeping a higher pH at pH 6.4 (Gengenbacher & Kaufmann 2012, Sturgill-Koszycki et al. 1994). In the phagolysosome, *Mtb* experiences cationic antimicrobial peptides (CAMPs) e.g. cathelicidin, hepcidin and ubiquitin-related peptides, and the robust cell envelope successfully provides a physical barrier against it (Flannagan et al. 2009b).

The remarkable mycobacterial cell envelope and unique lipid and glycolipid composition play a vital role in immune recognition and processing *Mtb* as an infectious agent (Brennan & Nikaido 1995). It represents a solid physical barrier for defence and loss of cell wall components is correlated with reduced virulence thus playing an important role in immune evasion and intracellular survival (Makinoshima & Glickman 2005).

1.2.1.3 Granuloma Formation and Containment

The granuloma is the histologically defined object that became the hallmark of tuberculosis. By successfully containing the bacilli it also provides *Mtb* a niche to create a microenvironment to survive over long periods. Most important factors for establishment of a granuloma and control bacterial proliferation is a balance between the cytokines IFN-γ and TNF-α which promote granuloma formation and IL-10 which is a negative regulator (Figure 3&4, Cooper et al. 2011, Jo et al. 2007).

Besides the mentioned pro-inflammatory cytokines a complex network of other chemokines and cytokines are involved in cell recruitment mechanisms (CC and CXC chemokines) and maintenance (Miranda et al. 2012). In general there are three different types of granuloma: a) solid granuloma that are formed in LTBI, b) necrotic granuloma, which are typical for active TB infection and c) caseous granuloma, which are specific for severe or end-stage TB (Gengenbacher & Kaufmann 2012).

A usual granuloma has spherical shape and consists of blood-derived macrophages (Mϕ), epithelioid cells (differentiated Mϕ) and multinucleated giant cells (Langhans giant cells), surrounded by lymphocytes, usually $CD4^+$, $CD8^+$, and γ/δ T-cells (Figure 4). Very typical for TB is the appearance of a necrotic centre within the granuloma, also called *caseum* due to the cheese-like appearance. Caseous granulomas are formed by foamy macrophages, epithelioid cells and Langhans giant cells and occasionally NK cells, DCs and neutrophils. Surrounding the necrotic region is a rim of T- and B-cells (Figure 4, Saunders & Cooper 2000, Toossi & Ellner 2001). Other types of granuloma include the solid, non-cavitating, closed granulomas containing a central necrotic area that is fully acellular. Importantly granulomas are heterogeneous, dynamic structures that contain immune cells and viable *Mtb* in various metabolic stages. The downshift from actively dividing to metabolically dormant *Mtb* is proposed to be triggered by the unfavourable conditions (e.g. nutrient and oxygen starvation) inside the granuloma. The DosS/DosT-DosR regulatory complex serves as an important biosensor system and is supposed to govern *Mtb* survival based on NO, CO and oxygen availability and the shift from aerobic to anaerobic metabolism (Boon & Dick 2002, Voskuil et al. 2011, Sivaramakrishnan & Ortiz de Montellano 2013).

Processes involved in the equilibrium between LTBI and replicating *Mtb* remains speculative however an attractive model is that dormant *Mtb* get resuscitated under favourable environmental conditions. Resuscitating-promoting factors (Rpfs) are expected to play a role in the reactivation process (Gengenbacher & Kaufmann 2012).

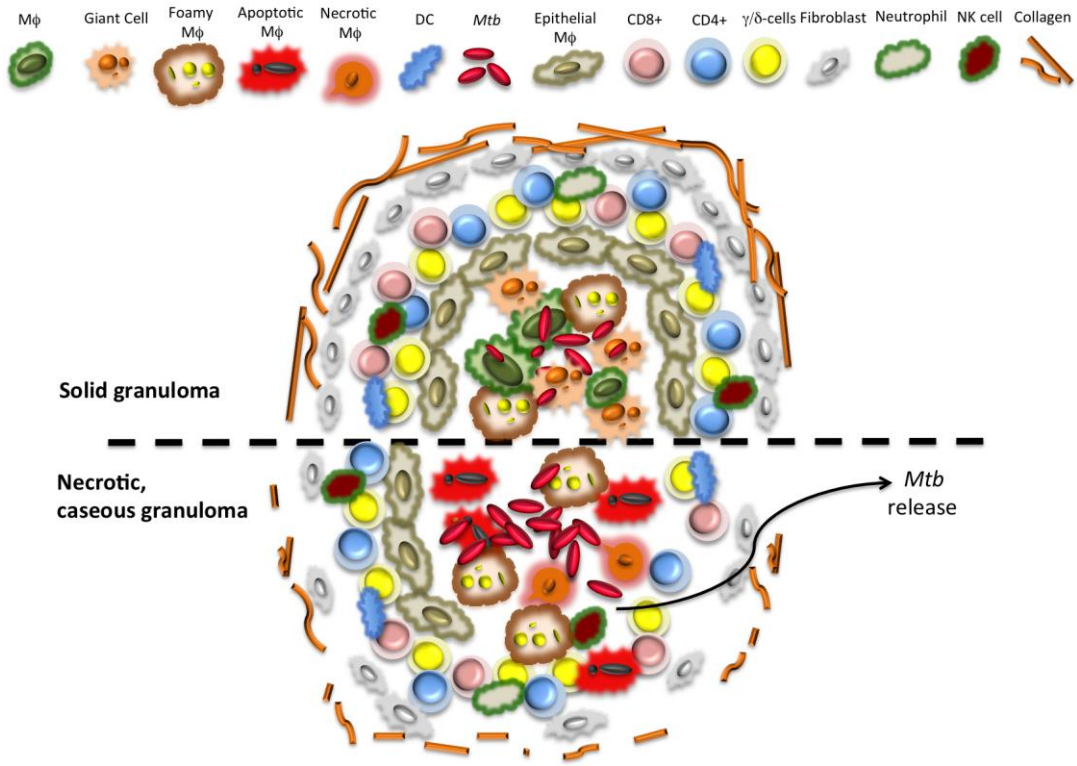

Figure 4. Structural Organization of Different Granuloma Types**.**

1.3 DIAGNOSIS AND TREATMENT - ACTIVE TB, LTBI AND EMERGING DRUG-RESISTANCE

The diagnosis of active TB is based on the usual symptoms (cough, haemoptysis, fever, night sweats, weight loss, chest pain, shortness of breath and fatigue) a Mantoux tuberculin skin test (TST) or TB blood test, chest radiography and testing for presence of acid-fast-bacilli (AFB) in the sputum. The WHO recommends fixed-dose combination (FDCs) anti-TB therapy as the standard regimen for drug-susceptible TB. It includes an intensive phase treatment for 2 month with isoniazid, rifampicin, pyrazinamide, ethambutanol[1] and streptomycine[2] followed by a continuation phase with 4 months of isoniazid and rifampicin, all on a daily dose frequency if applicable (WHO 2010, Table 1).

To monitor the development of multi-drug resistant TB (MDR-TB), which represents TB infection resistant to at least isoniazid and rifampicin, a drug susceptibility testing (DST), is carried out routinely, adaption of treatment is made if necessary and case control is started (WHO 2008). A rare type of MDR-TB is extensively drug-resistant TB (XDR-TB), which

[1] WHO no longer recommends ethambutanol in case of non-cavitary, smear negative TB and HIV-negative patients

[2] Tuberculosis meningitis patients use streptomycine instead ethambutanol

shows resistance to isoniazid and rifampicin, and any fluoroquinolone and at least one of three injectable second-line drugs. Treatment regimens against MDR and XDR-TB are recommended by the WHO and especially for XDR-TB cases have to be designed with great care for each individual patient (WHO 2014, Treatment strategies for MDR-TB and XDR-TB, Table 1).

If a patient from a risk group shows no typical TB symptoms a TST or interferon-gamma release assays (IGRA) indicates that the patient might have developed a LTBI. In case of a positive test result, chest radiography follows to screen for abnormalities. Are there chest abnormalities visible active TB treatment is performed; in case abnormalities are absent the patient receives LTBI adapted treatment. LTBI treatment is recommended with several optional methods: 6-month isoniazid, or 9-month isoniazid, or 3-month regimen of weekly rifapentine plus isoniazid, or 3–4 months isoniazid plus rifampicin, or 3–4 months rifampicin alone. The available LTBI treatment regimens show high efficacy ranging from 60-90% (WHO 2015, Guidelines on the management of latent tuberculosis infection). However also LTBI patients run a high risk in developing MDR-TB.

Drug resistance is one of the major problems in the fight against TB. In 2016 about half a million of new rifampicin-resistant TB (RR-TB) cases or MDR-TB emerged (WHO 2016). To understand the molecular mechanisms causing resistance, for example efflux or hydrolysis of drugs, drug modification (phosphorylation, acetylation, glycosylation etc.), reprogramming bacterial pathways or hitting off-targets (Davies & Davies 2010) and to find new essential targets is necessary to develop new anti-TB drugs with better efficacy.

1.3.1 The Mycobacterial Cell Wall As Target for Antibiotics

Current TB drugs target the mycobacterial cell on the level of RNA-synthesis (rifapentine), DNA-gyrase (fluoroquinilones), protein-synthesis (thioamide, cyclic peptides, aminoglycoside) or energy/ATP production (diarylquinoline). However most commonly whether it is first-line medication or especially second-line treatment against MDR-TB, the mycobacterial cell envelope is the prime target (Table 1). One of the first examples is rifampicin, which we today know, besides RNA polymerase inhibition primarily targets mycolic acid synthesis (Wehrli 1983, Campbell et al. 2001, Slayden et al. 2000). Mycolic acid cyclopropanation is important for the persistence of *Mtb* in mice (Barkan et al. 2012). A plethora of novel inhibitors target the cell wall or biosynthesis pathways of cell wall components (Table 1). An example is the synergistic *in vitro* effects in *Mtb* of the

benzothiazione BTZ043 and ethylenediamide, SQ-109, where the former targets arabinan biosynthesis (target: DprE1) and the latter inhibits mycolic acid incorporation (target: MmpL3), these are used together with bedaquiline an inhibitor of the respiratory ATP-synthase (Lechartier et al. 2012, Tahlan et al. 2012, Reddy et al. 2010).

Table 1. Current TB drugs and their Mechanisms of Action (MOA). Drugs targeting cell wall synthesis are shaded in grey (*table adapted from figures of the NIAID*).

* Development supported by NIAID ** Used in tuberculosis meningitis PE … Potentially Effective E … Effective R … Restistant		*1st Line Drug Susceptible TB*	*MDR-TB 2nd Line Treatment*	*XDR-TB Options*	**Action**
Name	**Orally/Injection**	Key	Key	Key	
Isoniazid	O	E	R		Targets Mycolic Acids
Rifampicin	O	E	R		Inhibits RNA Polymerase
Ethambutanol	O	E	E	PE	Inhibits Cell Wall Synthesis
Pyrazinamide	O	E	E	PE	Target Unclear Disrupts Plasma Membrane
Streptomycin	I	E**	E	PE	Inhibits Protein Synthesis
Thioamides (Ethionamide, Prothionamide)	O		E	PE	Inhibit Cell Wall Synthesis
Diarylquinoline (Bedaquiline TMC-207)	O		E	E, new	Inhibit ATP Synthase
Cyclic Peptides (Capreomycin)	I		E		Inhibit Protein Synthesis
Nitroimidazole (Delamanid OPC-67683)	O		E	E, new	Targets Mycolic Acids
Aminoglycosides (Kanamycin, Amikacin)	I		E		inhibits Protein Synthesis
Cycloserine	O		E	PE	Inhibit Cell Wall Synthesis
Fluoroquinilones (Moxifloxacin, Levofloxacin, Ofloxacin)	O		E	PE	Inhibits DNA Gyrase
Para-aminosolicylic acid (PAS)	O		E		Inhibit Cell Wall Synthesis and Folic Acid Synthesis
Clofazimine	O			PE	Disrupts DNA Template Function
New Candidate TB Drugs in Development					
Name	**Orally/Injection**	**DS-TB**	**MDR-TB**	**XDR-TB**	**Action**
Ethylenediamide SQ-109*	O	PE			Inhibits Cell Wall Synthesis
Meropenem*(together with clavulanate)	I				Inhibits PG Synthesis
Imidazopyridine Amide (Q203)	O				Inhibits Cytochrome Oxidase & ATP synthesis
Benzothiazinone (PBTZ169, BTZ043)	O				Inhibit Cell Wall Synthesis
Oxazolidinones (Sutezolid*, Linezolid*)	O				Inhibit Protein Synthesis
Rifapentine	O				Inhibit RNA Synthesis
Macrolides	O				Inhibit Protein Synthesis
Nitroimidazoles (PA-824*)	O				Inhibits Mycolic Acids and Others

Isoniazid resistance is often caused by the mutation in the promotor region of *inhA* and results in overexpression of the protein (Basso et al. 1998). New inhibitors against enoyl-reductase InhA, a clinically validated target involved in fatty acid biosynthesis and mycolic acid synthesis are available. Novel molecules like 4-hydroxy-2-pyridones when used in combination with isoniazid and rifampicin against MDR-TB, show a great potential and these target the cell envelope (Manjunatha et al. 2015).

Within the mycobacterial cell envelope peptidoglycan (PG) synthesis has recently gained interest as a promising target (Jackson et al. 2013). Cycloserine, inhibiting D-alanine ligase of

the PG peptide chain synthesis (Prosser and de Carvalho 2013), has been long used as a second-line treatment and now also to treat MDR-TB. The importance of targeting the PG metabolism can be underlined by the efficacy of β-lactam-(meropenem or ertapenem)β-lactamase (clavulanate) combinations against replicating and persistent *Mtb* (Hugonnet et al. 2009, Tiberi et al. 2016). Current work on this strategy show promising efficacy against TB and MDR-TB (Hugonnet et al. 2009, England et al. 2012, Dauby et al. 2011, De Lorenzo et al. 2013, Payen et al. 2012) and introduction into standard TB chemotherapy is considered (Jackson et al. 2013).

1.4 THE MYCOBACTERIAL CELL ENVELOPE

The genus *Mycobacterium* shares its evolutionary origin with *Corynebacterium* and *Nocardia* within the *Actinobacteria* phyla, categorized as gram-positive bacteria with high GC-content in their genomic DNA, however the cell wall structure is rather different.

The complex cell envelope present in *Mtb*, a distinctive feature of the *Mycobacterium* genus is composed of multiple layers (Figure 5). This peculiar structure and the constituents are important for the remarkable resistance to environmental stress and low permeability. Extremely long chain fatty acids, so called mycolic acids (MA) and extractable lipids produce an exceptionally thick asymmetric bilayer that is serving as the outer membrane (Figure 5, Brennan & Nikaido 1995). The mycolic acids are covalently linked to arabinogalactan (AG) and that to the innermost peptidoglycan (PG) layer defining the three major sections of the mycobacterial cell wall (Figure 5, Kieser & Rubin 2014). These three main components within the cell envelope referred to as the cell wall core – the mycolyl-arabinogalactan-peptidoglycan (mAGP) complex – essential for *Mtb* viability (Alderwick et al. 2015). In between the two membranes a controlled environment, similar to the periplasmic space of gram-negative bacteria (Daniels et al. 2010) is taking place where the AG and the PG layers are situated (Figure 5).

Nutrients taken up from the surrounding (media or host cell) are passing through porins and channels that ensure a controlled communication with the extracellular space. Since the cell envelope is a protective shield it is also the target of several antibiotics (Table 1, Sarathy et al. 2012). Therefore understanding the cell wall structure, biosynthesis and remodelling are important for the development of future anti-TB therapies. Additionally, classical cell wall components as PG, but also the specific constituents of the mycobacterial cell wall (AG, LAM and LM) are involved in the interaction with the host immune system (Barka et al. 2016).

In the following the mycobacterial cell envelope layers (Figure 5) are described starting from the outermost layer.

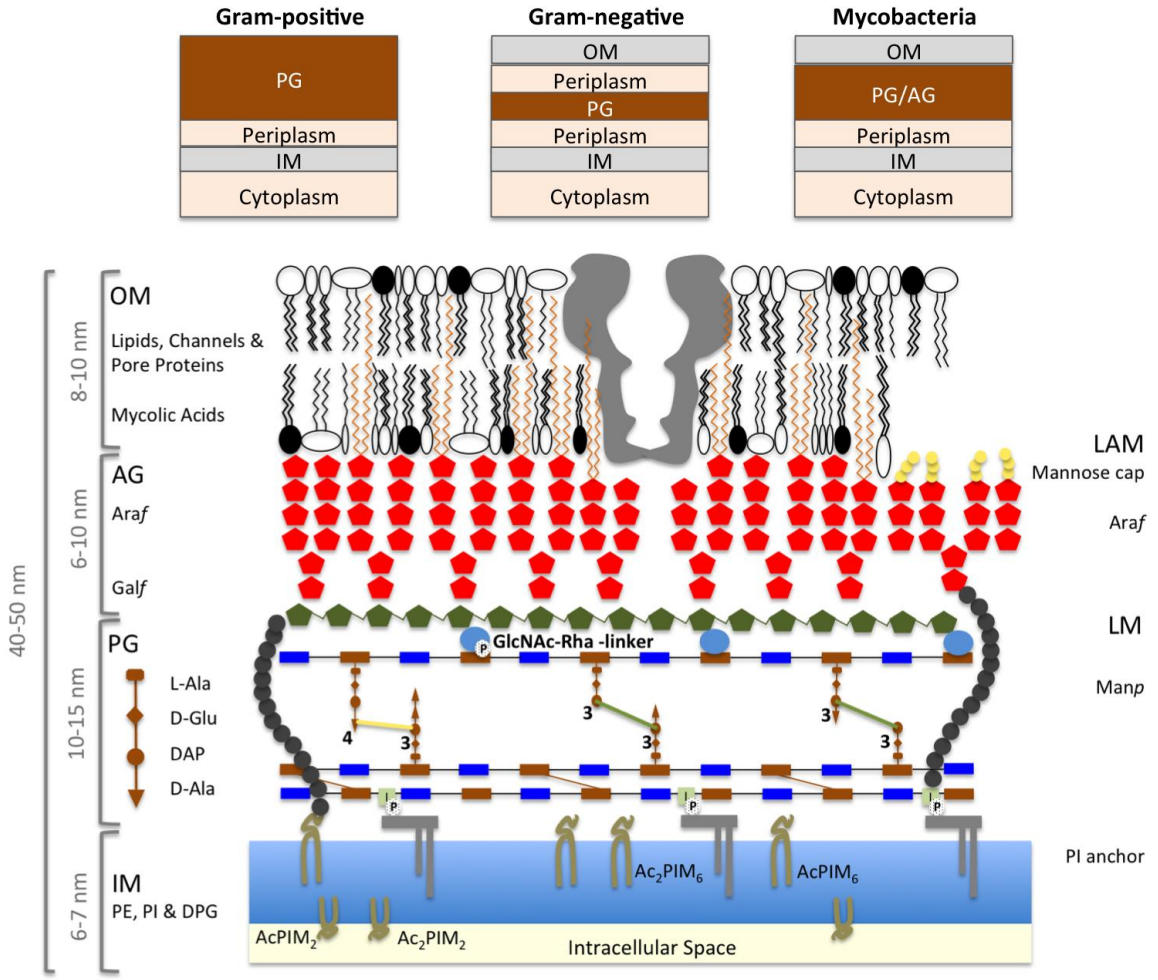

Figure 5. The *Mtb* Cell Envelope. (**Top panel**) Cell envelope architecture is depicted for gram-positive, gram-negative and mycobacteria. (**Bottom panel**) An overview of the mycobacterial cell envelope layers is illustrated. The inner membrane (IM) with its most abundant phospholipids phosphatidylinositol (PI), phosphatidylethanolamine (PE), diphosphatidylglycerol (DPG) and the phosphatidylinositol mannosides (PIMs) are represented. Lipoarabinomannan (LAM) and lipomannan (LM) are covalently attached to the IM and mannose units are in pyranose configuration (Man*p*). The PG, arabinogalactan (AG) and mycolic acids (MA) are forming the cell wall core, where MAs are contributing to the OM. Within the mycobacterial cell envelope arabinan and galactan building blocks are in furanose configuration (Ara*f* and Gal*f*). The AG layer is covalently linked to the muramic acid moieties in the PG via a GlcNAc-Rha-linker (α-l-Rha*p*-(1→3)-α-β-D-GlcNAc-1-P).

1.4.1 The Outer Membrane (OM)

Although Mycobacteria exhibit common evolutionary origin with gram-positive bacteria their cell wall structure is different and the existence of a membrane like structure surrounding the PG-AG cell wall core is well established. Cryo-electron tomography (CET) and cryo-sectioning on *M. bovis* BCG cells suggested a bilayer thickness ≥10 nm (Figure 5, Niederweis et al. 2010, Hoffmann et al. 2008). The main components are free and cell wall bound MAs (70-90 carbon α-mycolates) covalently linked to the arabinose termini of the

mycolyl-arabinogalactan-peptidoglycan (mAGP) cell wall core, and free lipids distributed over the OM like trehalose-based lipooligosaccharides (e.g. diacyl- or pentaacyl trehaloses (DATs, PATs), sulfoglycolipids (SGLs)), phenolic glycolipids (e.g. phthiocerol dimycocerosates (PDIMs)) and glycopeptidolipids (Minnikin et al. 2015). The OM lipid composition was estimated based on reverse micellar solution extraction (RMS) on *M. smegmatis* with mostly anthrone-positive glycopeptidolipids (GPLs), large amounts of triacylglycerols (TAGs), diacyl gycerols (DAGs) and unknown non-polar lipids (Bansal-Mutalik & Nikaido 2014). The *Mtb* genome also encodes for about 140 OM proteins (Niederweis et al. 2010). Due to the high hydrophobicity of the OM, hydrophilic nutrients or drugs require transport through channels and porins. Virulence factors and extracellular materials for capsule and biofilm formation (glycans and glycogens) are proposed to be translocated across the OM, and play a crucial role for intra-host survival and persistence in mice (Sambou et al. 2008).

1.4.2 The Inner Membrane (IM)

The inner membrane (IM), or conventional cytoplasmic membrane of *Mtb* is mostly composed of phospholipids like cardiolipin, phosphatidylinositol (PI), phosphatidylethanolamine (PE) and diphosphatidylglycerol (DPG) (Figure 5). The specific component is the inositol phosphate esterified lipids not present in other prokaryotic cell envelopes (membrane or cell wall) but common in eukaryotes. In mycobacteria most commonly four phosphatidylinositol mannosides (PIMs) are present, where most abundant are diacyl phosphatidyldimannoside (Ac_2PIM_2) with about 40 %, mono phosphatidylinositol dimannosides ($AcPIM_2$) and mono- and diacyl phosphatidylinositol hexamannoside ($AcPIM_6$ and Ac_2PIM_6) (Minnikin et al. 2015, Bansal-Mutalik & Nikaido 2014). The lipoglycans lipomannan (LM) and lipoarabinomannan (LAM) are attached to PIMs, over a manno-phosphatidylinositol (MPI) anchor (Minnikin et al. 2015). The hydrophilic part of lipoglycans is most likely protruding into the periplasmic space of the cell wall moreover protruding through pores within the mAGP reaching through to the OM (Pitarque et al. 2008). LM and LAM are immune-modulatory molecules. Mannose-capped LAM is involved in phagocytosis recognized by host C-lectins and phosphoinositol-capped LAM and LM stimulate the innate immune system through TLR2s, which requires transport of lipoglycans to the outer membrane (Gilleron et al. 2008). Recently, the *Mtb* lipoprotein LprG was identified to bind LAM and controls its distribution in the cell envelope to enhance host interaction (Shukla et al. 2014).

1.4.3 The Mycolyl-Arabinogalactan-Peptidoglycan (mAGP) Cell Wall Core

AG is built of arabinose and galactose units, which are in furanose configuration (Arabinofuranose: Ara*f* and Galactofuranose: Gal*f*) (McNeil et al. 1987, Brennan and Nikaido 1995). The first element is a linear chain of around 30 alternating 1→5 and 1→6 linked Gal*f* units. Three branched arabinan chains are linked to position C5 of galactan. Each arabinan chain is composed of 30 Ara*f* units linked 1→3, 1→5 in 1,2 *trans* and 1→2 in 1,2 *cis* manner and the non-reducing end is free for mycolic acid, succinyl or galactosamine attachment (Alderwick et al. 2015, Abrahams & Besra 2016). Mycolic acids are connected via an ester linkage to the arabinose termini (Minnikin et al. 2015). The root of the branching AG is connected to the O6 of muramic acid in the peptidoglycan (PG) layer using a mycobacterial specific linker (α-l-Rha*p*-(1→3)-α-β-D-GlcNAc-1-P). About 10% of muramic acid residues within the PG layer are connected to AG (McNeil et al. 1987, Barry et al. 2007).

The PG layer forms a continuous meshwork around the cell, also called the sacculus, and is only found in bacterial cells. It is responsible to sustain shape and stability of the cells as well as counteracting turgor pressure (Vollmer et al. 2008, Turner et al. 2014). The model organisms in which the PG structure and composition was studied primarily are *Escherichia coli*, *Bacillus subtilis* and *Staphylococcus aureus* (Turner et al. 2014). In the following the general structure of the bacterial cell wall PG is described and the specific alterations found in *Mtb* are discussed.

The glycan chains of the PG is built by alternating *N*-acetylglucosamine (GlcNAc) and *N*-acetylmuramic acid (MurNAc) that are connected over β(1→4) linkages (Figure 6). In *Mtb* the occurrence of *N*-glycolyl-muramic (MurNGlyc) acid has been reported (replacing MurNAc), which tightens the meshwork (Raymond et al. 2005). Each MurNAc moiety carries a short tetra- or penta-peptide stem that form inter-peptide bridges to the peptide stem of another glycan chain. The sequence of the peptide stems in mycobacterial PG composition is primarily L-Ala-γ-D-Glu-*meso*-DAP-D-Ala-D-Ala in nascent peptidoglycan where the final D-Ala is often removed in the mature PG macromolecule (Vollmer et al. 2008). In *Mtb* the amidation of the carboxylate groups of the *meso*-DAP and D-Glu residues peptide stems account for a specific deviation from the conventional PG structure. Two types of peptide cross-links are found in *Mtb*. The conventional 3-4 peptide cross-link (D-D cross-links) formed between the donor peptide on fourth position D-Ala and the *meso*-diaminopimelic acid (*m*-DAP) on position three of the acceptor peptide stem. And the alternative, so called 3-3 cross-links formed between *m*-DAP residues, hence termed DAP-DAP cross-links (L-D cross-links) occur in spores and stationery phase in gram-positive organisms. In mycobacteria these specific DAP-DAP cross-links (Figure 6) account for about 80% within the PG layer

and these are more abundant in dormant bacteria and probably the relevant type of linkages during intra-host survival in this pathogen (Kumar et al. 2012, Lavollay et al. 2008).
Different models have been proposed for the arrangement of the PG strands including parallel (Vollmer et al. 2008) or perpendicular (Meroueh et al. 2006) arrangement to the cell membrane. The parallel arrangement of glycan strands with the plasma membrane is the model supported by more experimental data. The perpendicular arrangement is not compatible with the long glycan strands >5 µM present in *B. subtilis*, however in other gram-positive bacteria perpendicular PG arrangement might be possible (Turner et al. 2014). Establishment of the PG strand arrangement within the sacculus needs further investigation by new high resolution imaging technologies or combinatory approaches e.g. fluorescent probes in combination with super-resolution imaging techniques (Turner et al. 2014, Abrahams & Besra 2016, Minnikin et al. 2015).

1.4.3.1 Peptidoglycan (PG) Synthesis in Mtb

The carbon skeleton for PG synthesis comes from glycolysis where fructose-6-P is converted into glucosamine-6-P by the glucosamine-6-phosphate synthase GlmS and phosphoglucosamine mutase GlmM to form glucosamine-1-P (GlcN-1-P). The first committed step, the formation of the PG building block branch, starts from GlcN-1-P and GlmU (acetyltransferase and uridyltransferase activity) using acetyl coenzyme A (acetyl-CoA), where first the acyl group and as a second step uridine-5'-monophosphate from UTP is transferred, to form uridine diphosphate-*N*-acetylglucosamine (UDP-GlcNAc) (Figure 6). In the next steps cytoplasmic synthesis of UDP-*N*-acetylmuramic acid (UDP-MurNAc)-penta-peptide (also known as Park's nucleotide), is performed by enzymes of the Mur family (MurA-F) that successively incorporate the amino acids L-Ala, D-*iso*-Glu, *m*-DAP and D-alanyl-D-Ala added by the ligase Ddl (Kurosu et al. 2007, Barreteau et al. 2008, Abrahams & Besra 2016). The members MurC, MurD, MurE and MurF catalyze ATP-dependent non-ribosomal peptide bond formation by adding peptide moieties to the PG building block. They are essential for mycobacterial survival and represent validated targets for developing new anti-mycobacterial drugs (Kouidmi et al. 2014).

An important step within building up the PG units involves UDP-*N*-acetylmuramic acid hydroxylase, NamH, which modifies a fraction of UDP-MurNAc to UDP-*N*-glycolylmuramic acid (UDP-MurNAc/Glyc) (Mahapatra et al. 2005a, Abrahams & Besra 2016). This

modification is unique to mycobacterial cells, decreases lysozyme susceptibility and tightens the intrinsic PG strength (Raymond et al. 2005).

The first membrane anchored PG precursor is generated by MurX, which couples the Park's nucleotide to decaprenyl phosphate (C_{50}-P) forming Lipid I (Kurosu et al. 2007). The last intracellular step is the β(1→4) linkage between UDP-GlcNAc and MurNAc/Glyc carried out by the glycosyltransferase MurG, which results in generation of Lipid II, the monomeric PG building block (Mengin-Lecreulx et al. 1991). Two enzymes, MurJ and/or FtsW, are suggested to translocate Lipid II across the IM (Ruiz 2015). Recently the structure of MurJ in *Thermosipho africanus* was solved and providing first insights into multidrug/oligosaccharidyl-lipid/polysaccharide (MOP) transporter superfamily function and translocation of PG-units (Kuk et al. 2017). After translocation the mono or bifunctional penicillin-binding-proteins (PBPs) are polymerizing the PG units releasing them from Lipid II (Sauvage et al. 2008).

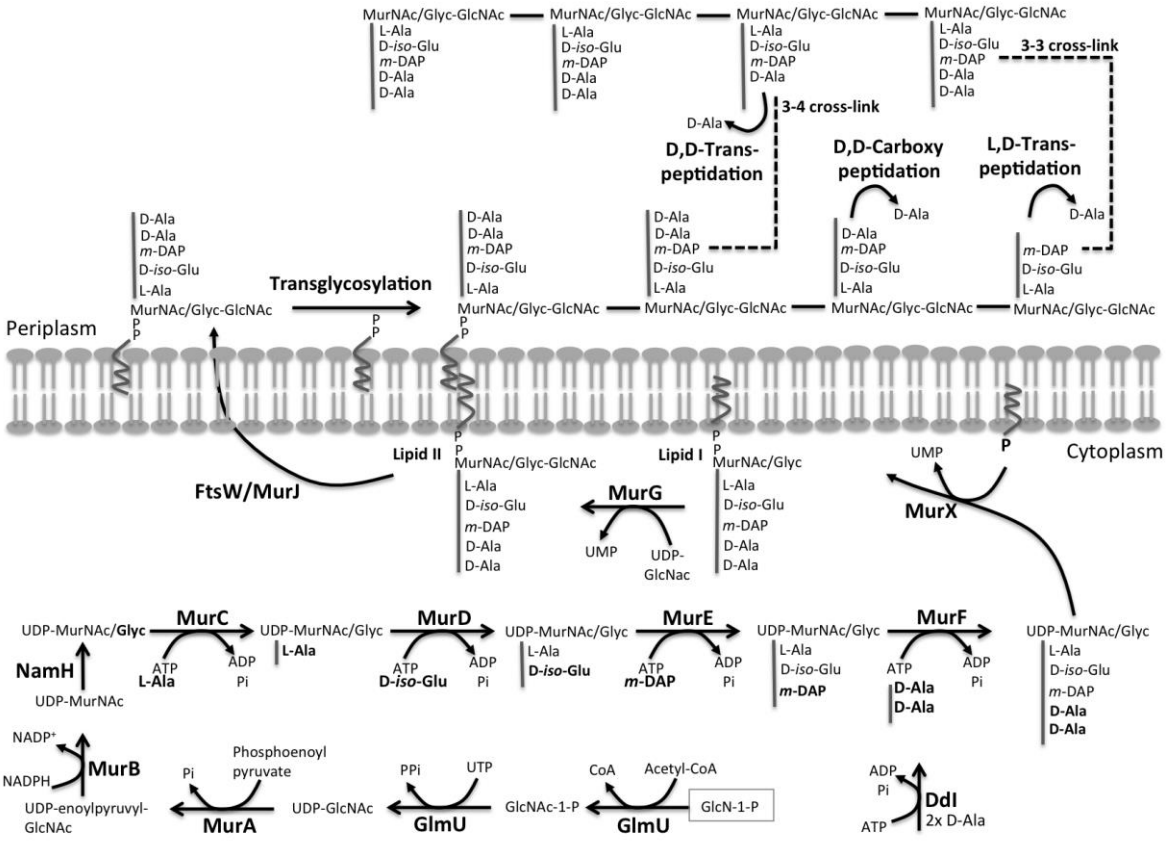

Figure 6. Cytoplasmic Synthesis and Periplasmic Assembly of PG. Key enzymes involved in cytosolic and periplasmic PG synthesis.

1.4.3.2 PG Polymerization

Mycobacteria possess several PG synthases that polymerize Lipid II and cross-link the peptide stems to a multi-layered PG meshwork (Figure 6&7). The most prominent polymerizing enzyme group is the PBPs, usually membrane-bound proteins (SxxK D,D-acyltransferase group I) classified into Class A (glycosyltransferase domain fused to SxxK acetlytransferase of class A) and Class B (protein recognition module fused to SxxK acetyltransferase of class B). The reason for the name Penicillin Binding Protein (PBP) is that their transpeptidase (TP) domain is covalently modified and inhibited by penicillin and other β-lactam antibiotics (Goffin & Ghuysen 2002). Bifunctional PBPs of Class A, like PonA1 and PonA2 (PBP1 and PBP2 in *E. coli*), carry out transglycosylation (TG domain) and transpeptidation (TP domain), for linking the disaccharide building blocks of Lipid II to existing glycan chains and catalyze conventional 3-4 peptide cross-links between *m*-DAP and D-Ala of the adjacent penta-peptide chains, with the cleavage of the terminal D-Ala (Figure 7). Class B PBPs have a TP domain and a non-catalytic domain for enzyme positioning or promoting protein-protein interactions. Monofunctional PBPs carry out D,D-transpeptidation (TP), D,D-carboxypeptidation (CP) with the release of a D-Ala or can even break 4-3 cross-links by D,D-endopeptidase activity (EP) (Egan & Vollmer 2015, Goffin & Ghuysen 2002).

PBPs are the classical targets for the β-lactam antibiotics. For a long time the β-lactam antibiotics were not considered as potential treatment against TB since most of them are inactivated by the β-lactamase BlaC (Hugonnet & Blanchard 2007). Combination of clavulanic acid, which irreversibly inhibits BlaC with carbapenems (imipinem and meropenem) however, shows promising results in *Mtb*-infected macrophages or against XDR-TB *in vitro* (England et al. 2012, Hugonnet et al. 2009). Using β-lactams and targeting Ldts and the process of the predominant 3-3 cross-link and PG biosynthesis can represent a novel strategy in TB therapy (England et al. 2012, Hugonnet et al. 2009, Kumar et al. 2017, Steiner et al. 2017).

However the majority of the peptide cross-links (about 80%) in the *Mtb* PG are of 3-3 type. Their formation includes the release of D-Ala at the fourth position and is carried out by the L,D-transpeptidases (Ldts) Ldt_{Mt1}-Ldt_{Mt5} (Figure 7, Kumar et al. 2012). The L,D-transpeptidases are not related to the D,D-transpeptidases present in PBPs, represent a different protein fold and active site architecture. For instance an invariant catalytic cysteine residue instead of a serine found in PBPs (Mainardi et al. 2005).

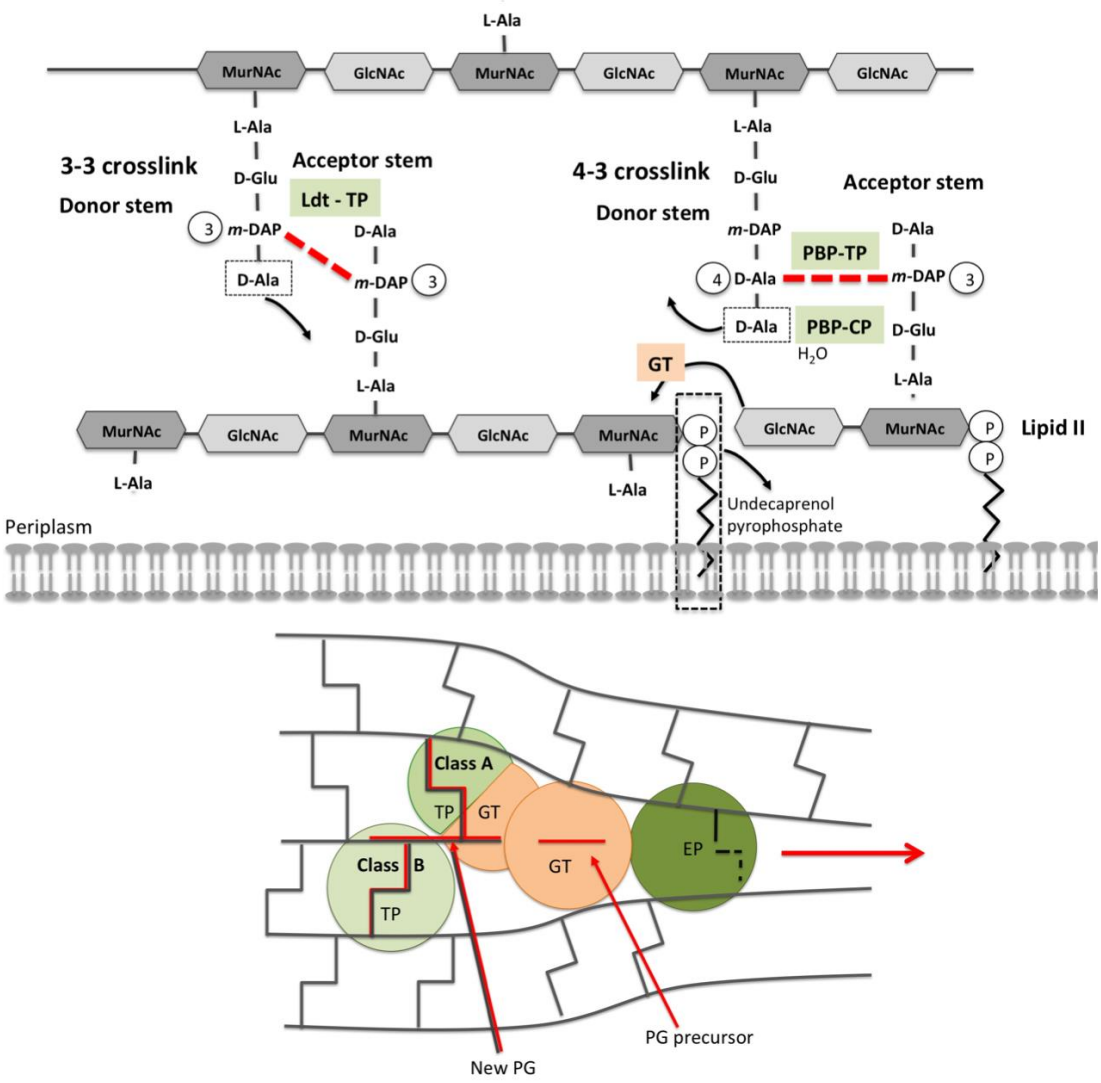

Figure 7. (**Top panel**) PG polymerization processes in *Mtb*. Lipid II is attached to an existing glycan-peptide chain by glycosyltransferase (GT) action and the undecaprenol pyrophosphate anchor is released. Inter-peptide stem cross-links are formed by D,D-transpeptidases using the transpeptidase domain (TP) catalyzed by PBPs (PonA1 and PonA2) forming conventional 4-3 cross-links. Some PBPs can hydrolyze the D-Ala of the penta-peptide stem or the 4-3 cross-link through D,D-carboxypeptidase (CP) or endopeptidase activity (EP), respectively. The predominant 3-3 cross-links specific for mycobacteria are catalyzed by the L,D-transpeptidases (Ldts). (**Bottom panel**) The PG growth is illustrated in a simple model involving the necessary enzyme activities (EP, GT, TP). The GT activity from class A PBPs is inserting Lipid II (PG precursor) into the existing PG network together with the TP activity of class A and class B PBPs. The EP cleaves the cross-links within the PG layer to allow insertion of new material in between the existing PG chains (*figure adapted from Pazos et al. 2017*).

1.4.3.3 The L,D-Transpeptidases (Ldts) in Mtb

In the *Mtb* H37Rv genome five homologs of Ldts can be found (Figure 8A) representing short (Rv0116c, Rv1433 and Rv0192) and long (Rv2518c and Rv0483) variants reflecting the domain organization e.g. two or three domain proteins. The common features of these are the catalytic transpeptidase domain in C-terminal position preceded by one or two spacer domains of the Ig-fold-type (Böth et al 2013). They are all required for cell wall stability and gene knock-out studies showed that each results in alteration of cell size, stability and increased susceptibility to β-lactam antibiotics (e.g. amoxicillin, imipinem) (Gupta et al. 2010, Schoonmaker et al. 2014, Sanders et al. 2014). The overall sequence identity is moderate with about 30–35%, where the two paralogs Ldt_{Mt2} and Ldt_{Mt5} are in closest relationship. High sequence conservation can be observed for all Ldts in *Mtb* when comparing the catalytic transpeptidase domain (C) and also suggests the presence of at least one N-terminal module (Ig domain) for all homologs (Figure 8A). However, until now structural information is only available for three of the five homologs, Ldt_{Mt1}, Ldt_{Mt2} and Ldt_{Mt5} (Figure 8B) (Correale et al. 2013, Böth et al. 2013, Li et al. 2013, Basta et al. 2015).

The L,D-transpeptidase-2 (Ldt_{Mt2}, Rv2518c) in *Mtb*, responsible for the predominant 3-3 cross-links during all growth stages in *Mtb*, was shown to be essential for infectivity in mouse model of acute TB infection and exhibits the highest expression level (Gupta et al. 2010). The Ldt_{Mt2} consists of a catalytic domain with the characteristic ErfK/YbiS/YhnG (EYY) fold and two consecutive domains belonging to the immunoglobulin (IgG) fold family (*paper I* - Böth et al. 2013, Erdemli et al. 2012, Kim et al. 2013, Li et al. 2013). Besides the PBPs as the main target, the Ldt_{Mt2} was shown to be targeted by β-lactam antibiotics, primarily by the carbapenem-type. The covalent binding of β-lactams and inactivation kinetics were investigated by biochemical and structural methods (*paper I and paper II* - Böth et al. 2013, Erdemli et al. 2012, Kim et al. 2013, Li et al. 2013, Steiner et al. 2017).

The paralog of Ldt_{Mt2}, Ldt_{Mt1} (Rv0116c) is an example for the short two-domain variant was also found to be inactivated by carbapenems (Correale et al. 2013) and thought to play a critical role in peptidoglycan adaptation to the non-replicative state of *Mtb* (Lavollay et al. 2008, Dubée et al. 2012). Structural comparison of the two structures shows good overall similarity with an r.m.s.d. of 1.5 Å (over all Cα atoms) (Correale et al. 2013).

A

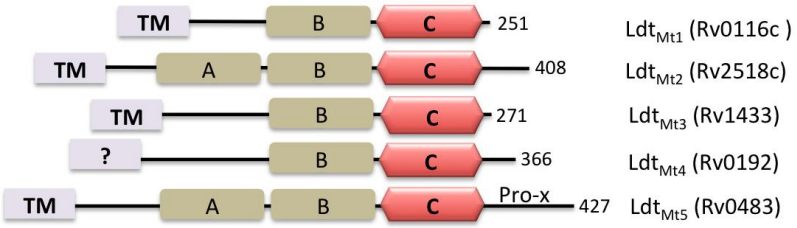
TM
B
C
251
Ldt$_{Mt1}$ (Rv0116c)
TM
A
B
C
408
Ldt$_{Mt2}$ (Rv2518c)
TM
B
C
271
Ldt$_{Mt3}$ (Rv1433)
?
B
C
366
Ldt$_{Mt4}$ (Rv0192)
TM
A
B
C
Pro-x
427
Ldt$_{Mt5}$ (Rv0483)

B

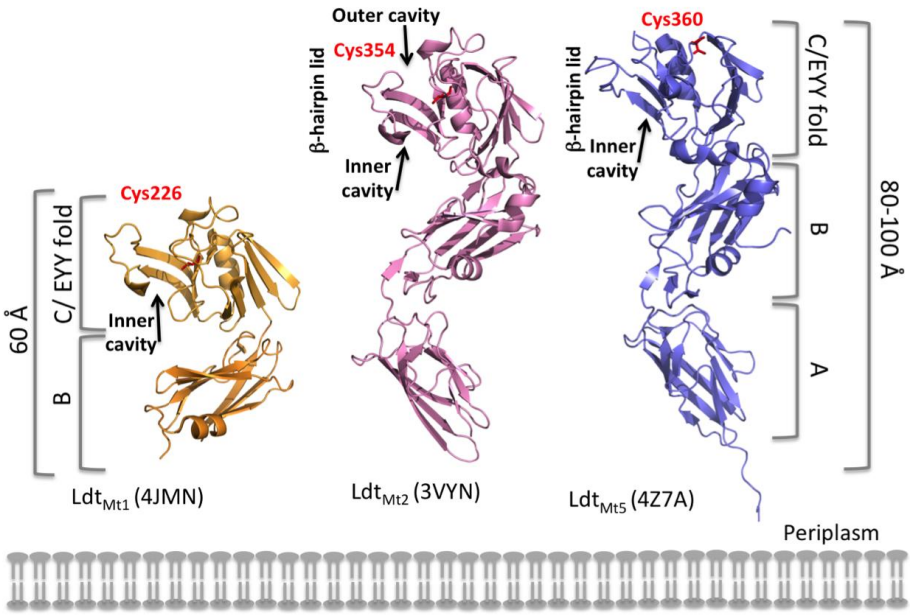
Outer cavity
Cys354
β-hairpin lid
Inner cavity
Cys360
β-hairpin lid
Inner cavity
C/EYY fold
B
A
80-100 Å
Cys226
C/ EYY fold
Inner cavity
B
60 Å
Ldt$_{Mt1}$ (4JMN)
Ldt$_{Mt2}$ (3VYN)
Ldt$_{Mt5}$ (4Z7A)
Periplasm

C

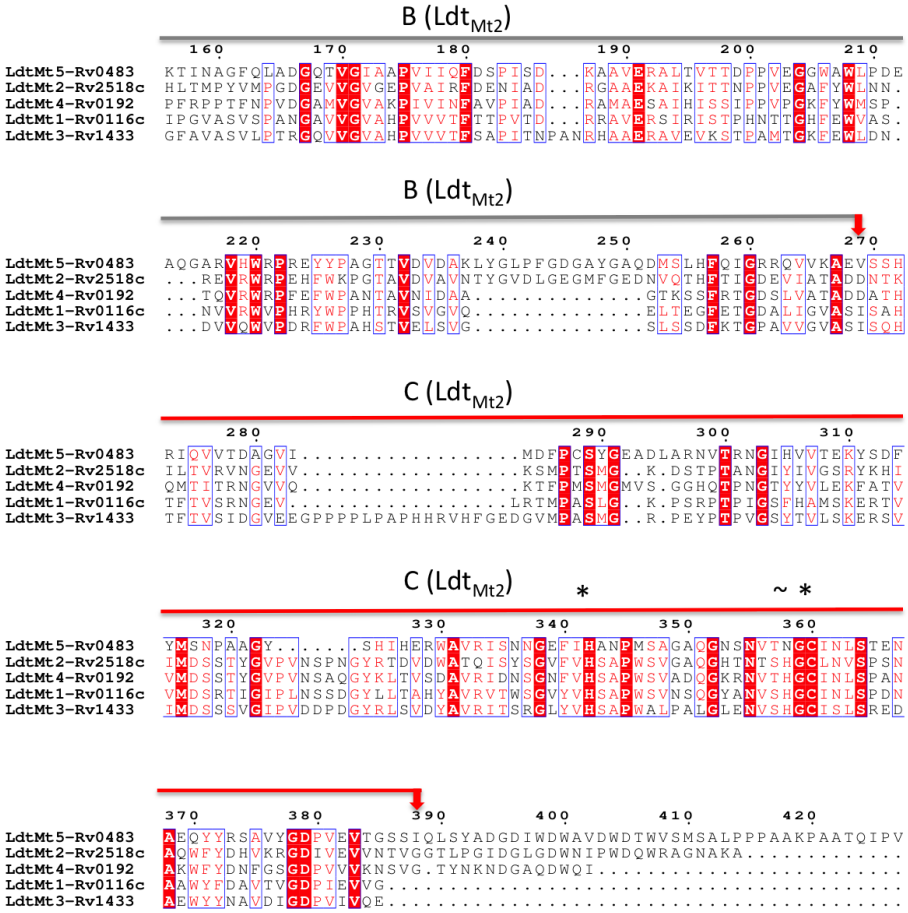
B (Ldt$_{Mt2}$)
160 170 180 190 200 210
LdtMt5-Rv0483 KTINAGFQLADGQTVGIAAPVIIQFDSPISD...KAAVERALTVTTDPPVEGGWAWLPDE
LdtMt2-Rv2518c HLTMPYVMPGDGEVVGVGEPVAIRFDENIAD...RGAAEKAIKITTNPPVEGAFYWLNN.
LdtMt4-Rv0192 PFRPPTFNPVDGAMVGVAKPIVINFAVPIAD...RAMAESAIHISSIPPVPGKFYWMSP.
LdtMt1-Rv0116c IPGVASVSPANGAVVGVAHPVVVTFTTPVTD...RRAVERSIRISTPHNTTGHFEWVAS.
LdtMt3-Rv1433 GFAVASVLPTRGQVVGVAHPVVVTFSAPITNPANRHAAERAVEVKSTPAMTGKFEWLDN.
B (Ldt$_{Mt2}$)
220 230 240 250 260 270
LdtMt5-Rv0483 AQGARVHWRPREYYPAGTTVDVDAKLYGLPFGDGAYGAQDMSLHFQIGRRQVVKAEVSSH
LdtMt2-Rv2518c ...REVRWRPEHFWKPGTAVDVAVNTYGVDLGEGMFGEDNVQTHFTIGDEVIATADDNTK
LdtMt4-Rv0192 ...TQVRWRPFEFWPANTAVNIDAA.....GTKSSERTGDSLVATADDATH
LdtMt1-Rv0116c ...NVVRWVPHRYWPHTRVSVGVQ.....ELTEGFETGDALIGVASISAH
LdtMt3-Rv1433 ...DVVQWVPDRFWPAHSTVELSVG.....SLSSDFKTGPAVVGVASISQH
C (Ldt$_{Mt2}$)
280 290 300 310
LdtMt5-Rv0483 RIQVVTDAGVI.....MDFPCSYGEADLARNVTRNGIHVVTEKYSDF
LdtMt2-Rv2518c ILTVRVNGEVV.....KSMPTSMG..K.DSTPTANGIYIVGSRYKHI
LdtMt4-Rv0192 QMTITRNGVVQ.....KTFPMSMGMVS.GGHQTPNGTYYVLEKFATV
LdtMt1-Rv0116c TFTVSRNGEV.....LRTMPASLG..K.PSRPTPIGSFHAMSKERTV
LdtMt3-Rv1433 TFTVSIDGVEEGPPPPLPAPHHRVHFGEDGVMPASMG..R.PEYPTPVGSYTVLSKERSV
C (Ldt$_{Mt2}$) * ~ *
320 330 340 350 360
LdtMt5-Rv0483 YMSNPAAGY.....SHIHERWAVRISNNGEFIHANPMSAGAQGNSNVTNGGINLSTEN
LdtMt2-Rv2518c IMDSSTYGVPVNSPNGYRTDVDWATQISYSGVFVHSAPWSVGAQGHTNTSHGGLNVSPSN
LdtMt4-Rv0192 VMDSSTYGVPVNSAQGYKLTVSDAVRIDNSGNFVHSAPWSVADQGKRNVTHGGINLSPAN
LdtMt1-Rv0116c VMDSRTIGIPLNSSDGYLLTAHYAVRVTWSGVYVHSAPWSVNSQGYANVSHGGINLSPDN
LdtMt3-Rv1433 IMDSSSVGIPVDDPDGYRLSVDYAVRITSRGLYVHSAPWALPALGLENVSHGGISLSRED
370 380 390 400 410 420
LdtMt5-Rv0483 AEQYYRSAVYGDPVEVTGSSIQLSYADGDIWDWAVDWDTWVSMSALPPPAAKPAATQIPV
LdtMt2-Rv2518c AQWFYDHVKRGDIVEVVNTVGGTLPGIDGLGDWNIPWDQWRAGNAKA.....
LdtMt4-Rv0192 AKWFYDNFGSGDPVVVKNSVG.TYNKNDGAQDWQI.....
LdtMt1-Rv0116c AAWYFDAVTVGDPIEVVG.....
LdtMt3-Rv1433 AEWYYNAVDIGDPVIVQE.....

Figure 8. L,D-transpeptidase (Ldt) Homologs in *Mtb* H37Rv. (**A**) Domain arrangement of the five Ldt homologs. The conserved catalytic domain (C) with its characteristic ErfK/YbiS/YhnG (EYY) fold (red box), the domains belonging to the immunoglobulin (Ig) fold family (brown box) and the transmembrane regions (TM, purple box) are represented. The genetic location is given as Rv codes in brackets (**B**) Structural comparison of the three crystal structures available for Ldt_{Mt1} (PDB: 4JMN), Ldt_{Mt2} (PDB: 3VYN) and Ldt_{Mt5} (PDB: 4Z7A). Images were made using MacPyMol. The *Mtb* Ldt homologs show different distance of the catalytic active site cysteine residues (red sticks) to the IM therefore reaching to different levels (60 Å and 80–100 Å) in the PG layer. (**C**) Multiple sequence alignment of Ldt_{Mt1}-Ldt_{Mt5} using Clustal Omega (Sievers et al. 2011) and ESPript 3.0 (Robert & Gouet 2014). Strictly conserved residues are highlighted with a red box. The active site residues His336, His352 and Cys354 of Ldt_{Mt2} are highlighted with star and tilde symbols. The B and C domain region of Ldt_{Mt2} are indicated with a grey and red bar respectively.

1.4.3.4 Cell Wall Growth and Division in Mycobacteria

PG forms a net-like, continuous macromolecule of polymerized glycan strands and cross-linked peptides, called the sacculus, surrounding the cytoplasmic membrane. A bacterial cell needs to increase the surface of its sacculus in order to grow and divide. The sacculus growth and division during daughter cell separation is a challenging balance between rebuilding and simultaneously degrading PG and has to be well-controlled to avoid accumulation of defects within the cell wall causing increased susceptibility to antibiotics and cell lysis (Egan & Vollmer 2015). Most studies on cell elongation and division were carried out on *Escherichia coli* and gram-positive *Bacillus subtilis*, *Staphylococcus aureus* and *Streptococcus pneumoniae,* demonstrating the arrangement of protein complexes and interactions between PG synthases, hydrolases, regulatory proteins, and cytoskeletal elements (Typas et al. 2012, Egan & Vollmer 2013). The concept of the divisosome and elongasome was born including the above constituents contributing to these large membrane-linked machineries (Egan & Vollmer 2015, Kieser & Rubin 2014).

These multi-protein complexes carry out the cell elongation, septum formation and daughter cell separation synchronized with the genome replication and chromosome segregation (Szwedziak & Lowe 2013). Both complexes have common features and subunits consisting of enzymes required for the incorporation of new subunits into the growing PG sacculus, as well as proteins, like Wag31 and FtsZ, acting as scaffold platforms for large cell elongation and division complexes (Figure 9, Kieser & Rubin 2014, Favini-Stabile et al. 2013). The elongation complex involves the PBPs and PG hydrolases responsible for PG synthesis and hydrolysis. The activity of these proteins have to be strictly regulated and are guided to the

cell poles by the scaffold protein Wag31, the *Mtb* homolog of the better investigated DivIVA in *B. subtilis* (Typas et al. 2012, Hett & Rubin 2008, Plocinski et al. 2012). The CrgA–CwsA (cell wall synthesis protein A) complex is interacting with Wag31, which is involved in peptidoglycan synthesis and cell shape determination (Plocinski et al. 2012). As the PG layer is highly cross-linked during all growth stages also Ldts might be recruited to the elongation complex, substituting for PBPA (Figure 9, Kieser & Rubin 2014).

Possible interaction and cross-talk between the elongation machinery and the cell division complex might move PG synthesis to the mid-cell. Very specific for mycobacterial cell division is asymmetric septation (daughter cell separation). The reason for this is unknown but variation in size between daughter cells increases population heterogeneity (Kieser & Rubin 2014). After PG degradation the two daughter cells appear as V-shaped object, maybe resulting from asymmetric splitting or from unbalanced levels of AG and MA layers that are proposed to stay intact during the whole mycobacterial cell separation (Hett & Rubin 2008, Kieser & Rubin 2014).

After septum synthesis is finished daughter cells have to be separated. Daughter cell separation is dependent on RipA an NlpC/P60-type endopeptidase enzyme (Gao et al 2006, Hett et al. 2007) localized at the septum of dividing cells. Mycobacteria encode for several PG hydrolases, where the most prominent candidates are the individually non-essential hydrolases RipA and RipB (Martinelli & Pavelka 2016) and RipC (Parthasarathy et al. 2012). RipA also interacts with other PG hydrolase, the resuscitation promotion factor B (RpfB) containing a lysozyme-like domain. The two enzymes are proposed to synergistically cleave peptide and glycoside bonds in the PG (Hett et al. 2007). PonA1 was also found to form a complex with RipA probably competing for binding with RpfB (Hett et al. 2010). Here, the balance between PonA1-RipA and RpfB-RipA interactions might regulate that synthesis is carried out before degradation of the septum (Kieser & Rubin 2014). Another crucial PG hydrolase is RipC shown to interact with FtsX and needed for *Mtb*s full virulence (Parthasarathy et al. 2012, Mavrici et al. 2014).

Septation in *E. coli* or in *S. pneumoniae* requires amidases like, AmiA/B/C or LytA respectively that cleave the PG in between the MurNac and the peptide stem. In *Mtb* this process was clearly linked to the endopeptidase RipA however, the role of amidases is poorly understood in mycobacteria (Priyadarshini et al. 2007, Mellroth et al. 2012). Recently the discovery of a *N*-acetylmuramyl-L-alanine amidase (Rv3717) from *Mtb* points to a role in recycling of degraded PG fragments (Prigozhin et al. 2013).

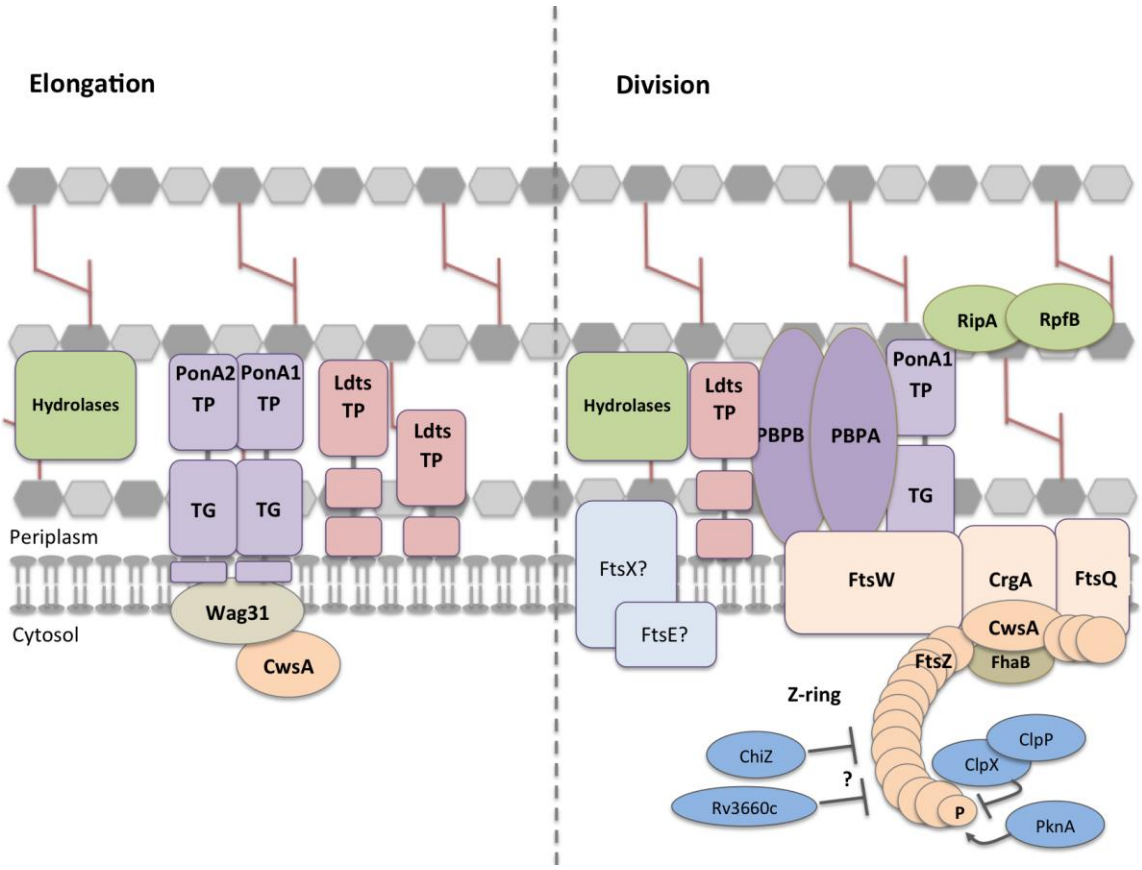

Figure 9. The Elongation and Division Complex in Mycobacteria. The complexes are built up of PG synthases (purple), hydrolases (green), scaffold proteins regulating structure (beige), regulatory proteins (blue) involved in cell elongation and separation. The elongation complex is anchored by Wag31, which itself is stabilized by CwsA. New PG is incorporated by PonA1 produced by cell wall hydrolases, which also loosen the structure for insertion of new material. PonA2 together with the Ldts are cross-linking and further polymerizing the PG meshwork (**left panel**). Cell division is initiated by polymerization of FtsZ and Z-ring formation is regulated by regulatory proteins e.g. PknA, ClpX or Rv3660c. Structural proteins FtsW/Q, CrgA and CwsA are joining to assemble the divisome and together with PBPA/B, PonA1 and Ldts form the septal disc. In a dynamic network, the hydrolysases RipA and RpfB, a synergy of peptide and glycoside cleavage, facilitated by FtsE and FtsX, the daughter cells are separated without losing integrity (**right panel**, *figure adapted from Kieser & Rubin 2014*).

1.4.3.5 The PG Hydrolases of the Rip Family

PG remodelling at the septum and daughter cell separation in *Mtb* was found to be dependent on the NlpC/P60 domain containing endopeptidase RipA (Anantharaman & Aravind 2003, Gao et al. 2006). The *Mtb* genome encodes for five proteins with such an NlpC/P60 (**NlpC/P60**: **n**ew **l**ipo**p**rotein **C** from *E. coli* and a **60** kDa extracellular **p**rotein from *Listera monocytogenes*) domain: Rv0024, RipA (Rv1477), RipB (Rv1478), RipC (Rv2190c) and RipD (Rv1566c) (Figure 10). Rv0024 lacks export signal sequence, hence it is likely

intracellular but uncharacterized. The catalytic NlpC/P60 hydrolase domain contains a catalytic site analogous to the papain-like peptidases (Anantharaman & Aravind 2003) based on a cysteine, in the conserved motif 'DCSG', a histidine and glutamate (Parthasarathy et al. 2012). These PG hydrolases contain an additional domain or shorter modules in N-terminal position (RipA, RipB, RipC), or C-terminal extensions (RipD) attached to the catalytic domain. Loss of either RipA or RipB causes increased susceptibility to antibiotics however the mutant phenotype can partially be rescued by RipD (Martinelli & Pavelka 2016).

RipA is the best characterised member of the Rip-family (Figure 10) and was shown to interact with the resuscitation promoting factors RpfB (Rv1009), RpfE (Rv2450c) and with PonA1 (Hett et al. 2007, Hett & Rubin 2008). The catalytic activity regarding PG degradation has been established for RipA and RipB indicating a pH optimum of 5-6, and the cleavage position in between the D-Glu/*m*-DAP residues. The PG degradation activity and PG binding properties were characterized (Böth et al 2011, Ruggiero et al. 2010). The N-terminal module of RipA remains unknown, however it was proposed to be an inhibitory module regulating the catalytic activity (Ruggiero et al. 2010, Botella et al. 2017). This N-terminal module occurring in RipA and RipC shows 35 % sequence identity (RipA residues 39-255, RipC residues 38-212). It was proposed to mediate the interactions between RipC and FtsX (Mavrici et al. 2014). The structure of this domain was solved by X-ray crystallography and the results from small angle X-ray scattering (SAXS) allowed to model the domain-arrangement of the whole periplasmic part of RipA including the N-terminal domain and the catalytic domain (*paper IV*).

RipC is expected to carry out similar catalytic activity, as RipA based on sequence homology, although otherwise remains uncharacterized. From genetic analysis it appears to be necessary for virulence (Parthasarathy et al. 2012).

RipD represents an exception, a non-catalytic variant of the NlpC/P60 hydrolase family. The cysteine (Cys383 in RipA and Cys152 in RipB) of the catalytic triad is replaced by an alanine and the histidine (His432 in RipA and His201 in RipB) by a serine residue. Another peculiar feature of RipD is the 61 residues long repeat sequence attached to the NlpC/P60 domain in C-terminal position containing the PVQQA motif (*paper III*, Böth et al. 2014). The function of RipD is so far unknown but might be involved in protecting PG cleavage sites and/or recruiting other cell wall remodelling proteins.

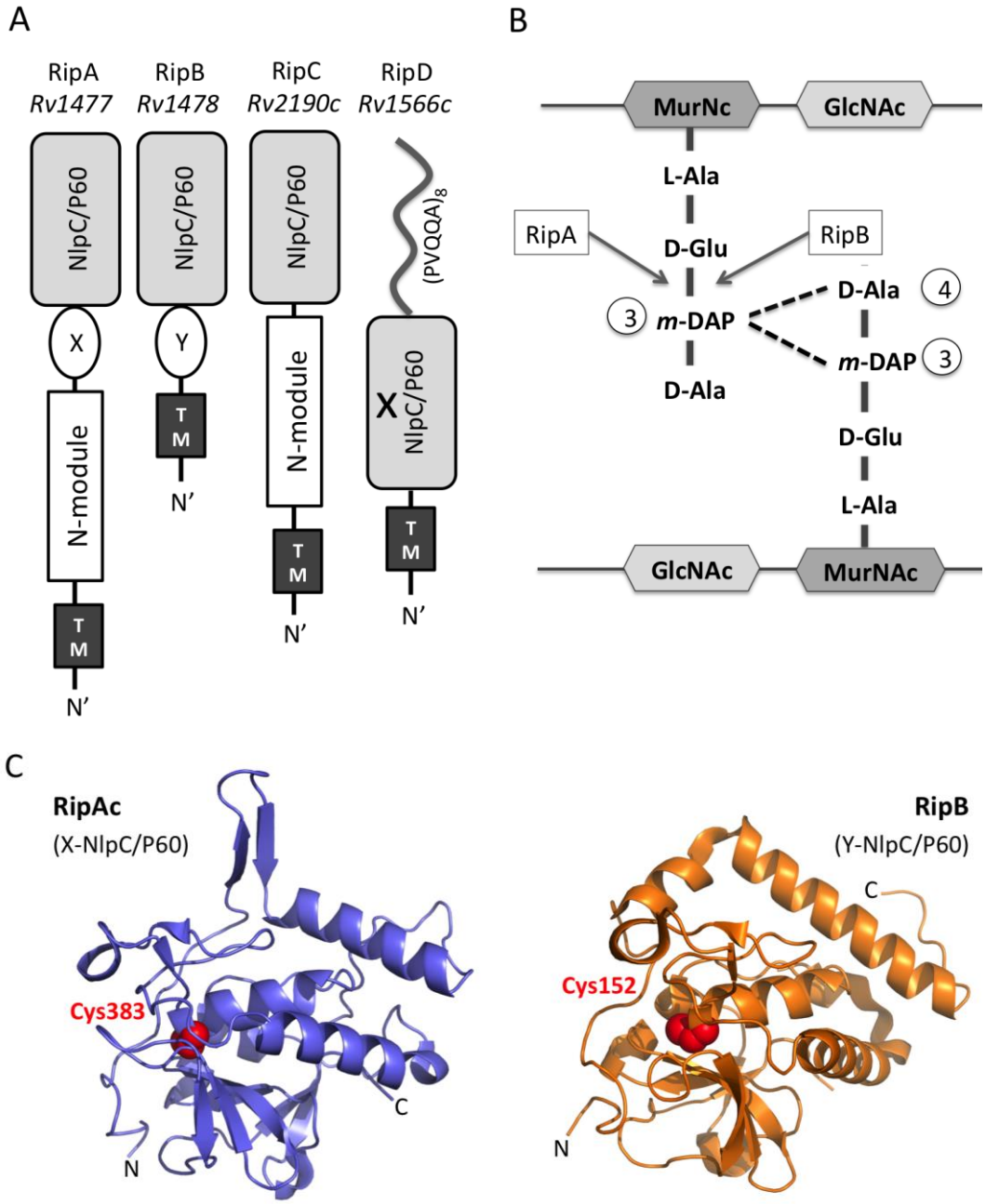

Figure 10. The Four Periplasmic NlpC/P60 Hydrolases in *Mtb*. (**A**) The *Mtb* genome encodes for at least five homologous NlpC/P60 proteins, where RipA, RipB, RipC and RipD have a predicted signal sequence indicating localization into the PG periplasm (TM). RipA and RipB carry an additional lid-module covering the catalytic doman labelled with X and Y respectively. RipA and RipC also feature an additional N-terminal module (approx. 200 residue-long). In RipD, the NlpC/P60 domain is non-catalytic (cross) and carries a 61 residue long PVQQA-repeat at its terminus (*paper III*). (**B**) Enzymatic activity and cleavage position within the PG layer of RipA and RipB hydrolases. Dashed lines indicate the two potential cross-link types present in the PG of *Mtb*. (**C**) Structure of RipAc (blue, residues 260-472, PDB: 3PBC) and RipB (orange, residues 30-241, PDB: 3PBI). The catalytic cysteine of RipA and RipB are highlighted in red.

1.4.4 Inhibitors Targeting PG Synthesis in *Mtb*

PG is unique to bacterial cells and therefore enzymes involved in metabolism and synthesis are targeted by antibacterial compounds but also promising targets for the development of novel antibiotics (Table 2). There are few essential proteins in bacterial genomes, and not all of these can be used as a target because of close homology to human enzymes. The first example at the beginning of PG synthesis is GlmU with acetyltransferase and uridyltransferase activity forming UDP-GlcNAc (Figure 6). Due to the close homology of the GlmU uridyltransferase domain to human enzymes only the acetyltransferase domain represents a potential target and currently inhibitors and substrate analogs of GlcN-1-P are under development (Tran et al. 2013, Abrahams & Besra 2016).

Table 2. Inhibition of PG synthesis.

Target Protein	***Inhibitor***	***Mode of Action***
GlmU	Substrate analogs of GlcN-1-P	Acetyltransferase activity
MurB	Dioxopyrazolidines	UDP-*N* -acetylenolpyruvylglucosamine reductase
Ddl	D-cycloserine (D-Ala analogue)	D-alanine ligase
MurX (MraY)	Natural products e.g. muraymycin, liposidomycin, caprazamycin and capuramycin SQ641 (preclinical development)	Translocase I
MurG	Ramoplanin (lipoglycodepsipeptide) Transition state mimics	Binding Lipid I and Lipid II Preventing MurG action and polymerization
Lipid II	Lantibiotics (Nisin) Ramoplanin	Interaction with pyrophosphate moiety
Pentapeptide stem	Vancomycin, Teicoplanin (glycopeptides)	D-Ala-D-Ala binding, Inhibition of PG polymerization
PBPs	Moenomycin (natural product glycolipid) β-lactams	Transglycosylase activity
Ldts	β-lactams	Transpeptidase activity

The following Mur ligases build up the peptide chain linked onto UDP-MurNAc/Glyc (Figure 6). Despite their distinct peptide selectivity Mur C-F ligases share a common ATP binding domain, and small molecule inhibitors are identified (Barreteau et al. 2008, Hrast et al. 2014, Abrahams & Besra 2016). The next validated target represents, Ddl, which is

inhibited by D-cycloserine, acting as D-Ala analogue, currently used against MDR-TB and XDR-TB (Prosser & de Carvalho 2013a,b).

Several nucleoside-based natural products inhibit membrane anchoring of the Lipid I precursor by MurX (Table 2, Abrahams & Besra 2016). Capuramycin shows killing of non-replicating TB *in vitro* and *in vivo*, which is not common for most of PG synthesis inhibitors (Siricilla et al. 2015).

Compounds mimicking the transition state during enzyme catalysis targeting MurG from *E. coli* are now tested on *Mtb* MurG, and successfully inhibited the generation of Lipid II, the final intracellular step of PG synthesis (Trunkfield et al. 2010).

The polymerization of Lipid II in the periplasm is carried out by PBPs (mono- and bifunctional) and L,D-transpeptidases (Ldts). The β-lactam antibiotics, mainly targeting the PBPs, experience a revival as potential anti-TB treatment; particularly the carbapenems class show also inhibition against Ldts (*paper I* - Böth et al. 2013, Erdemli et al. 2012, Kim et al. 2013, Li et al. 2013, Mainardi et al. 2007, Dubée et al. 2012, Lecoq et al. 2012). Combination treatment of β-lactams and β-lactamase inhibitors against BlaC in *Mtb* show promising efficacy in both non-replicating and active TB and clinical trials are currently ongoing (Hugonnet et al. 2009, Rullas et al. 2015). Another class, the penem-type of β-lactams appeared in the field as faropenem was found to be the most effective even in the absence of clavulanic acid against *Mtb* in culture but also inside macrophages (*paper II*, Dhar et al. 2015). Considering the favorable properties of faropenem (stable and oral bioavailability) and the above fact it has been proposed as a good candidate for TB chemotherapy (Dhar et al. 2015, Steiner et al. 2017, Hoagland et al. 2016, WHO 2017 Executive Summary).

2 AIMS OF THE THESIS

Paper I and Paper II – 'Structure of Ldt_{Mt2}, an L,D-transpeptidase from *Mycobacterium tuberculosis*' and 'Binding and processing of β-lactam antibiotics by the transpeptidase Ldt_{Mt2} from *Mycobacterium tuberculosis*'.

- Structural characterization of the essential transpeptidase Ldt_{Mt2} using X-ray crystallography, give insights to the transpeptidation by the five mycobacterial homologues.
- Comparison of the action of different β-lactam antibiotics using enzyme kinetics, mass spectrometry and X-ray crystallography. Analysis of the adducts and the events following the acylation reaction.
- Identification of the most efficient β-lactam compound and explain the mechanism of action in detail.

Paper III - RipD (Rv1566c) from *Mycobacterium tuberculosis*: Adaptation of an NlpC/P60 Domain to a Non-catalytic Peptidoglycan-binding Function.

- Structural investigation of the NlpC/P60 domain of RipD (Rv1566c).
- Biophysical characterization of the 61-residues long penta-peptide (PVQQA) repeat sequence in C-terminal position.

Paper IV - Structure of the N-terminal Module of the Cell Wall Hydrolase RipA and its Role in Regulating Catalytic Activity.

- Structural characterization of the N-terminal module of the NlpC/P60 hydrolase RipA using X-ray crystallography and small-angle X-ray scattering (SAXS).
- Investigation of the role of the N-terminal module and the inter-domain linker with regards to active site access.

3 RESULTS AND DISCUSSION

3.1 *PAPER I:* STRUCTURE OF LDT_{MT2}, AN L,D-TRANSPEPTIDASE FROM *MYCOBACTERIUM TUBERCULOSIS*

The L,D-transpeptidase 2 from *Mtb* (Ltd_{Mt2}) catalyzes the formation of the predominant 3-3 cross-links within the PG layer and was shown to be essential for virulence in *Mtb.* Among the five homologues within the *Mtb* genome Ltd_{Mt2} is expressed at the highest level (Gupta et al. 2010). Inactivation of the Ldt_{Mt2} gene *lppS* (*rv2518c)* led to an attenuated phenotype and to increased susceptibility to clavulanate-amoxicillin treatment *in vitro* and in a mouse TB model (Gupta et al., 2010). The essentiality of Ldt_{Mt2} for virulence makes it a potential target for antibiotic development. The targeting of L,D-transpeptidases in *Mtb* by β-lactam antibiotics has been exemplified by several examples (*paper I and paper II*, Dubée et al. 2012, Erdemi et al 2012, Böth et al. 2013, Kim et al. 2013, Li et al. 2013, Bianchet et al. 2017). Promising results were obtained by combination therapy of clavulanic acid and carbapenems (imipinem and meropenem) in *Mtb*-infected macrophages or against XDR-TB *in vitro.* Inhibition of the 3-3 cross-link formation and PG biosynthesis represents a promising strategy in anti-TB therapy (England et al. 2012, Hugonnet et al. 2009, Dhar et al. 2015, Hoagland et al. 2016).

The gene of Ldt_{Mt2} encodes for an enzyme with 408 amino acids. A short intracellular segment (residue 1-17), a trans-membrane domain (residue 18-34) and a large periplasmic part (residue 35-408) was predicted and potential domain organization for the extramembrane part was investigated by sequence comparisons and domain prediction algorithms. The catalytic domain (domain C, residues 250-408) and an adjacent domain (domain B: residues 150-250) was defined by sequence similarity to other Ldt_{Mt2} homologs in *Mtb* and *Corynebacteria* genomes (Figure 8&11A, *paper I*). We have predicted an additional domain (domain A, residues 34-150) based on domain-border analysis (http://www.tuat.ac.jp/~domserv/cgi-bin/DLP-SVM.cgi; Ebina et al. 2009) and secondary-structure prediction using JPred (Cole et al. 2008). The N-terminal starting point of this domain was suggested by the predicted lipoprotein-attachment site (position 35) (Rahman et al. 2008) or the start of the predicted

secondary-structure domain element at position 55. The collective results from the bioinformatics analysis for the periplasmic part of Ldt_{Mt2} defined three domains: two smaller domains **A** (residues 34/55-146) and **B** (residues 149-250) and a catalytic domain (**C**, residues 240-408) belonging to the EYY-fold family (Figure 8&11, Bielnicki et al. 2006). Based on the above analysis three constructs were investigated: a full-length periplasmic construct (residues 34-408), the **AB** module (residues 55-250) and the **BC** module (residues 149-408). These were expressed in *E. coli* and purified to homogeneity. All these constructs are in a monomeric state in solution according to size-exclusion chromatography results. Crystallization trials of the full-length construct did not result in crystal formation, however crystallization screening of the AB and BC-domain resulted in well-diffracting crystals.

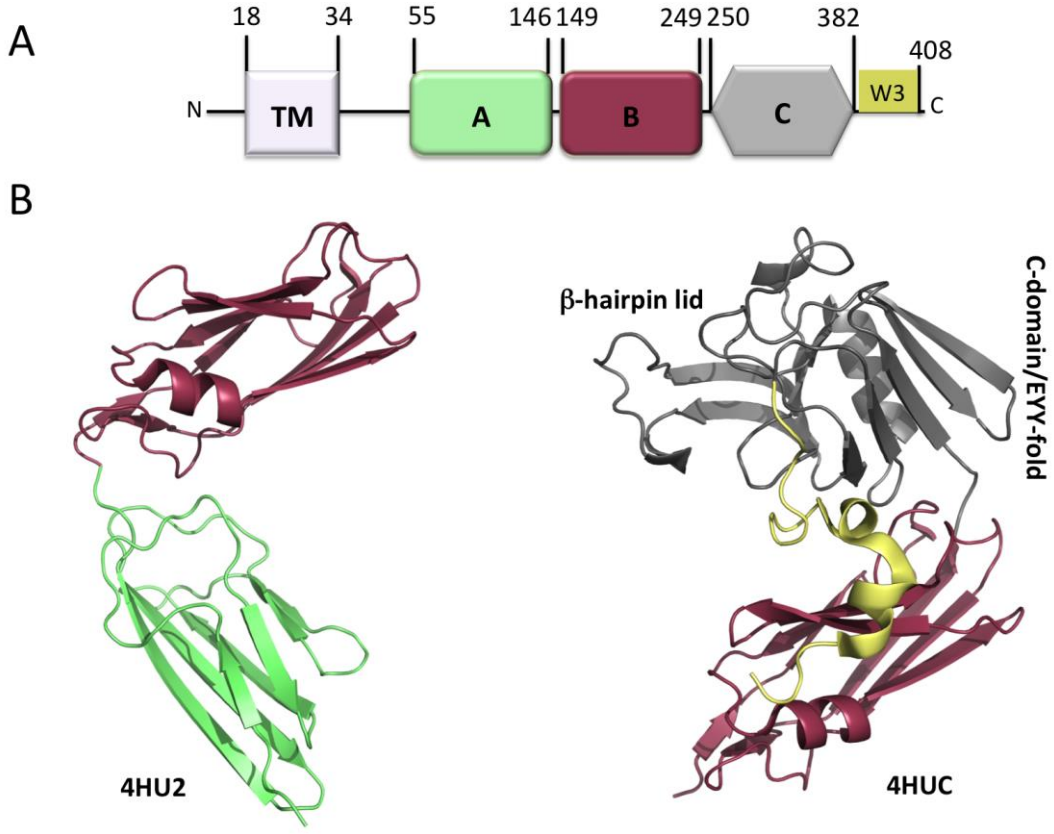

Figure 11. Domain Organization and the X-ray Structure of Ldt_{Mt2}. (**A**) Domain arrangement of Ldt_{Mt2} indicating the A, B, C domain with residues involved. The predicted trans-membrane (TM) region, the two immunoglobulin-like (Ig) domains A and B, the catalytic transpeptidase domain (C) and the C-terminal extension (W3) are illustrated. (**B**) Cartoon representation of the AB (PDB: 4HU2) module and BC (PDB: 4HUC) module in cartoon representation, colors as in panel-A.

The crystal structure of Ldt_{Mt2} was solved in two fragments comprising the AB and the BC domains. The structure of the BC module (PDB: 4HUC) was solved to 1.86 Å using Se-SAD phasing. Domain B unexpectedly revealed an immunoglobulin-like (Ig) fold, while domain C comprising the catalytic center belongs to the ErfK/YbiS/YbnG fold family. The structure of the AB-module (PDB: 4HU2) was solved by molecular replacement to 1.45 Å, using the B-module from the BC structure as search model. Despite the low sequence similarity (12%) the A domain reveals an Ig-like fold very similar to the B domain. The combination of both structures provides a view on the full-length periplasmic three-domain Ldt_{Mt2} protein (residues 55–408), which is in contrast to the two-domain model of Ldt_{Mt2} proposed involving only one Ig-like domain (domain B) by an earlier publication Erdemli et al. 2012.

The full periplasmic Ldt_{Mt2} structure is extending about 80-100 Å into the PG layer and defines the approximate distance at which the 3-3 cross-links are formed by this transpeptidase (Böth et al. 2013). Mycobacterial transpeptidases contain one or two Ig-like domains that likely play a spacer role for positioning the active site to the appropriate location where cross-link formation is performed (*paper I*, Böth et al. 2013). The proposed domain arrangements for the short and longer Ldt homologues (Figure 8) were shortly after confirmed by the structures of the two domain Ldt_{Mt1} (Correale et al. 2013) and the three-domain Ldt_{Mt2} (Li et al. 2013) and Ldt_{Mt5} (Basta et al. 2015).

3.1.1 The Catalytic Domain of Ldt_{Mt2}

The crystal structure of the BC module was solved to 1.86 Å resolution by Se-SAD phasing from crystals of selenomethionine-substituted protein. Two polypeptide chains (residues 149–408) are defined in the asymmetric unit. The refined model contains also 480 water molecules and 12 acetate ions, where two of the acetate ions are situated in the active site of domain C. Each polypeptide chain contains a bound metal-ion, which based on electron density, typical metal-ligand distances and coordination sphere was modeled as Na^+ ion.

Structural comparison of domain C using the DALI algorithm (Holm & Rosenström 2010) identified the transpeptidase domain of related proteins from *Enterococcus faecium* (PDB: 1ZAT, Biarotte-Sorin et al. 2006, Z-score of 19.3 and a Cα r.m.s.d of 1.9 Å for 120 residue-long alignment) and a homologue in *B. subtilis* (PDB: 1Y7M, Bielnicki et al. 2006, Z-score of 17.7 and Cα r.m.s.d. of 1.6 Å for 109 residue-long alignment). The key residues of the catalytic site, Cys354 and His336, correspond to Cys442 and His421 in the *E. faecium* homologue. In Ldt_{Mt2} the active site is located under β-hairpin lid (residues 298–324), which limits the access to the active site (Figure 11B&12). The β-hairpin lid is not present in the *B. subtilis* protein and part of the lid is disordered in the X-ray structure of the *E. faecium* homologue.

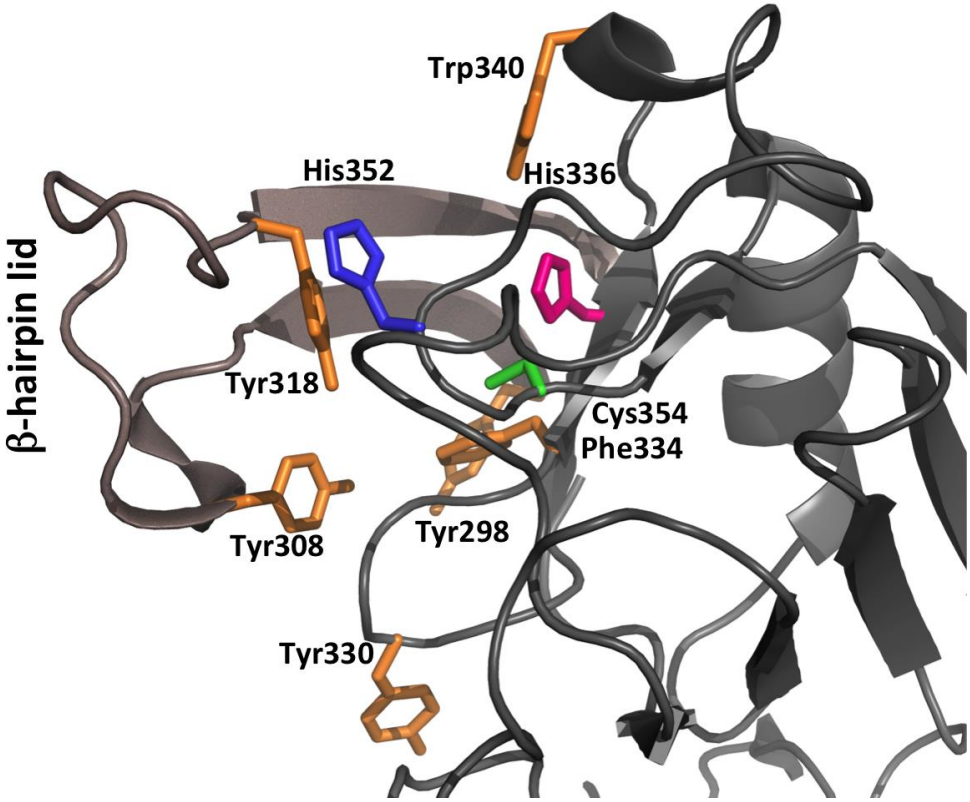

Figure 12. The Active Site of Ldt_{Mt2}. The β-hairpin lid (residues 298-324, light brown) presents large hydrophobic residues (Tyr298, Tyr308 and Tyr318, orange sticks) and together with residues close to the active site entrance (Tyr330, Phe334 and Trp340, orange sticks) they are expected to regulate active site accessibility. The active site residues Cys354 (green stick), His336 and His352 are highlighted in pink and blue, respectively.

In the Ldt_{Mt2} lid, large hydrophobic residues (Tyr298, Tyr308 and Tyr318) and the residues surrounding the entrance to the active site (Tyr330, Phe334 and Trp340) contribute to closure of the active site and exclusion of solvent, which might be important during catalysis (Figure 12). At the C-terminal end an extension comprising residues 382-408 (W3, Figure 11) can be found in Ldt_{Mt2}. The W3 extension runs along the domain C and forms contacts with domain B stabilizing the relative orientation of domains B and C (Figure 11). In the W3 extension a pattern of tryptophan residues (Trp394, Trp398 and Trp401 in Ldt_{Mt2}), present in Ldt_{Mt5} (Rv0483) as well forms stacking interactions at the domain interface.

3.1.2 The AB-module as a Spacer in Ldt_{Mt2}

The structure of the AB module including A and B domains (57-250) was solved to 1.45 Å resolution by molecular replacement using the B domain from the BC module structure (residues 149–250) as search model. The two domains appear in a V-shaped arrangement; each of them is built up by a β-sandwich of two antiparallel β-sheets (Figure 13). Both domains belong to the c-type Ig-fold, with strand orders a–b–e–d and c–f–g in the two antiparallel β-sheets (Figure 13A, Bork et al. 1994).

Comparison of the two domains A and B structures (sequence identity 12%) results in a Cα r.m.s.d. of 2.7 Å over 85 aligned residues (Figure 13B). The major differences between the two structures are an additional short α-helix (residues 180–187 in domain B, between β-strands β2 and β3) and the loop connecting β6 and β7, which is longer domain B (Figure 13B). The size of the A and B domain interface (350 $Å^2$), the short linker (Ala149-His150) and the fact that B factors of the linker residues are in the range 18–22 $Å^2$, comparable to the remaining part of the structure, suggests that the linker is not flexible, i.e. the V-shaped arrangement appears rather rigid (Figure 11C). Superposition of the B domain from the AB and BC module shows high similarity over the full-length sequence (r.m.s.d. of 0.4 Å over 101 residues). The relative orientation of these domains retains this arrangement in the three-domain structure (Li et al. 2013).

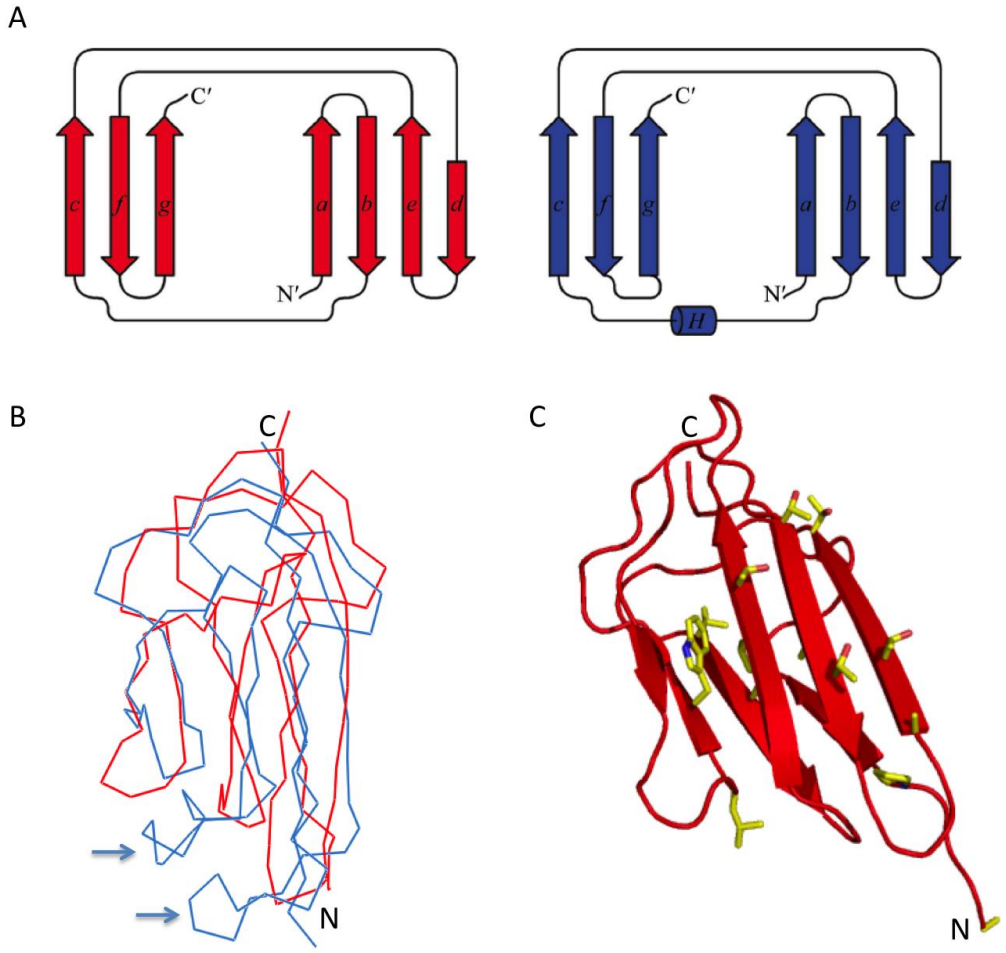

Figure 13. The Ig-like Domains A and B of Ldt_{Mt2}. (**A**) Domain topology diagram of domain A (red) and domain B (blue). (**B**) Superposition of the Cα-trace of domain A (red) and B (blue). The major differences, the short α-helix (residues 180-187) inserted between β2 and β3 and a longer loop connecting β6 and β7 are indicated with arrows on domain B. (**C**) The comparison of domain A and the Ig-like domains from other polysaccharide specific enzyme (endo-β-1,4-mannanase from *C. fimi*, PDB: 2X2Y) reveals the conserved residues shown as sticks (yellow) in domain A (red cartoon).

Structural homologs of the two Ig-like domains using the DALI server were identified in *Pseudomonas syringae* (a periplasmic copper-resistance protein, PDB entry 2C9R, Zhang et al. 2006, Z-score of 10.2 and Cα r.m.s.d. of 2.4 Å), *Halothermothrix orenii* (N-terminal domain of amylase, PDB: 3BC9, Tan et al. 2008) and a similar domain of the endo-β-1, 4-mannanase from *Cellulomonas fimi* (PDB: 2X2Y, Hekmat et al., 2010) with similar Z-scores (6.0–10.1) and r.m.s.d. values (Cα 2.6–3.1 Å). Additionally, the cell-wall-located S-layer protein from *Geobacillus stearothermophilus* (PDB: 2RA1, Pavkov et al. 2008) shows reasonable Z-score of

7.8 and a Cα r.m.s.d. value of 3.2 Å. Interestingly the non-catalytic Ig-like domains of the amylase from *H. orenii* have been shown to mediate enzyme activity within the high-molecular-weight (HMW) substrate (Tan et al. 2008).

Similar sequences are present in enzymes processing high-molecular-weight polysaccharides. The domains of the mannanase in *C. fimi* (sequence identity 18.5%) and a glucodextranase from *Arthrobacter globiformis* (sequence identity 15.2%) could potentially be relevant for Ldt_{Mt2}, as the substrate is a modified oligosaccharide chain. The conserved residues in domain A and the Ig-like domain from mannanase and glucodextranase contain a set of conserved Thr residues exposed on β-sheet surface (Figure 13C).

3.1.3 The Periplasmic Ldt_{Mt2}

The superposition of the B-domains in the AB and BC module structures, allows modeling the three-domain periplasmic Ldt_{Mt2} structure (Figure 14). This model is in good agreement with the three-domain structure solved later (PDB: 3VYN, Li et al. 2013) indicated by the structural superimposition using DALI light server (Hasegawa & Holm 2009) resulting in a Cα r.m.s.d. value of 0.8 Å over 347 aligned residues. The three-domain Ldt_{Mt2} protein extends about 80-100 Å (including sequence 34-54) from the inner membrane. Compared to the other four Ldt_{Mt} homologs in *Mtb* H37Rv genome there are variations in sequence length and predicted domains (Figure 8&14). The candidates Rv0116c (Ldt_{Mt1} with 45% sequence identity) and Rv1433 (Ldt_{Mt3} with 38% sequence identity) also encode for a trans-membrane domain but the extra-membrane sequence is one domain shorter (Figure 8A). The homologs Rv0483 (Ldt_{Mt5}, 35% identity) and Rv0192 (Ldt_{Mt4}, 18% identity) were likely to contain three domains. The five Ldt homologs in *Mtb* therefore can be grouped into transpeptidases with one or two Ig-like domains positioning the catalytic center at different levels/height in the PG layer. Such an arrangement of the PG-production line (transpeptidases) supports the parallel multi-layered PG model (see chapter 1.4.3.3) within the mycobacterial cell wall. The Ig-like domains seem to act as spacer units and define the distance of catalytic action from the membrane. It appears that the 3-3 cross-link formation can occur at two levels carried out by long (Rv2518c, Rv0483 and Rv0192) and short (Rv0116c and Rv1433) transpeptidase variants (Figure 8B&14).

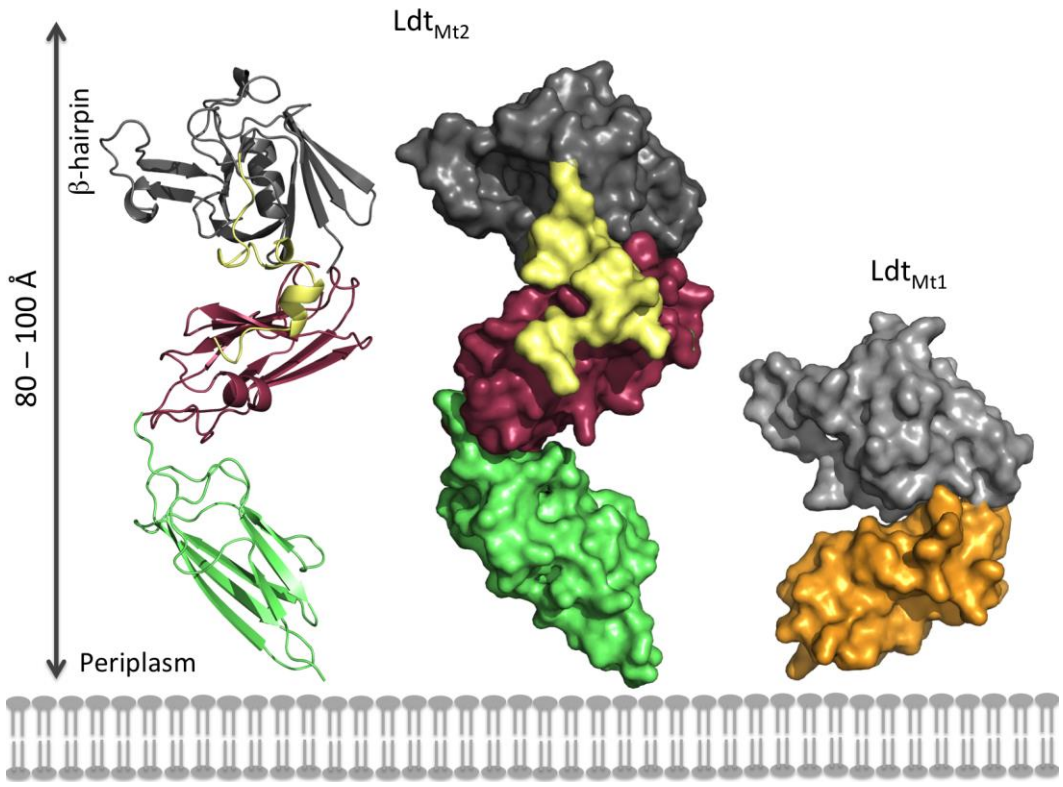

Figure 14. The Model of the Periplasmic Ldt$_{Mt2}$. Superposition of domain B common in structure AB and BC results in the full-length Ldt$_{Mt2}$ model. The catalytic center is placed at a maximal distance of 80–100 Å from the inner membrane. The structure of Ldt$_{Mt1}$ (PDB: 4JMN, to the right) is shown as an example for the mycobacterial two-domain (short) Ldt. The differences in the placement of the active sites suggest that the formation of 3-3 cross-links may happen at two different levels within the peptidoglycan of *Mtb*.

3.1.4 Covalent Adduct Formation with β-lactam Antibiotics

The inhibitory action of β-lactam antibiotics is based on the formation of a covalent complex between the transpeptidase active site and the antibiotic. The active site serine residues in D,D-transpeptidases are the primary targets but the cysteine residues in L,D-transpeptidases in *B. subtilis* (Lecoq et al. 2012) and the Ldt$_{Mt2}$ (Rv0116c, Dubée et al. 2012) were also shown to be targeted by β-lactams. Covalent adduct formation could be observed with the BC module and the ABC construct (residues 34-408) of Ldt$_{Mt2}$ with imipinem (299.3 Da, cabapenem) and ampicillin (349.4 Da, penam class) using ESI-MS (*paper I*, Böth et al. 2013). The observed covalent mass differences correspond to the exact mass of the respective antibiotic. Together with the observation from imipinem and meropenem binding to Ldt$_{Mt2}$ using ITC (Erdemli et al. 2012) and the crystal structures of meropenem-bound Ldt$_{Mt2}$ (Li et al. 2013, Kim et al. 2013) the data

indicates that Ldt_{Mt2} is targeted by various β-lactam antibiotics. However, a systematic analysis is necessary to identify the best candidates. Ldt_{Mt2} is one of the few validated targets in *Mtb* (Gupta at al. 2010) and as a periplasmic (extracellular) target presents high potential for future TB-therapy.

3.2 *PAPER II:* BINDING AND PROCESSING OF β-LACTAM ANTIBIOTICS BY THE TRANSPEPTIDASE LDT_{MT2} FROM *MYCOBACTERIUM TUBERCULOSIS*

The use of β-lactam antibiotics represents a novel way of anti-TB therapy (Rullas et al. 2015, Hoagland et al. 2016). The L,D-transpeptidases were shown to bind β-lactams, specifically carbapenems, resulting in a covalent modification of the active site cysteine by forming an acyl-enzyme adduct in the process referred to as acylation. We investigated a cohort of 16 β-lactam antibiotics, from the penem, penam and carbapenem group, and characterized their action of inhibition by kinetics, mass spectrometry and X-ray crystallography on the essential Ldt_{Mt2} transpeptidase. Most compounds from the carbapenems class showed fast acylation kinetics but faropenem, a penem-type antibiotic, outperforms these by a 2–3 fold faster rate in adduct formation. Mass spectrometry results indicated that carbapenems antibiotics might undergo decarboxylation. Faropenem is also decomposing after the acylation step resulting in a 87 Da β-OH-butyryl adduct bound at the active site cysteine. The co-crystal structure of Ldt_{Mt2} with this faropenem fragment bound was solved to 1.54 Å resolution, and shows that the protein completely shields the cysteine-adduct from the solvent. The complex representing the inactivated state of the enzyme shows high stability in biochemical assays.

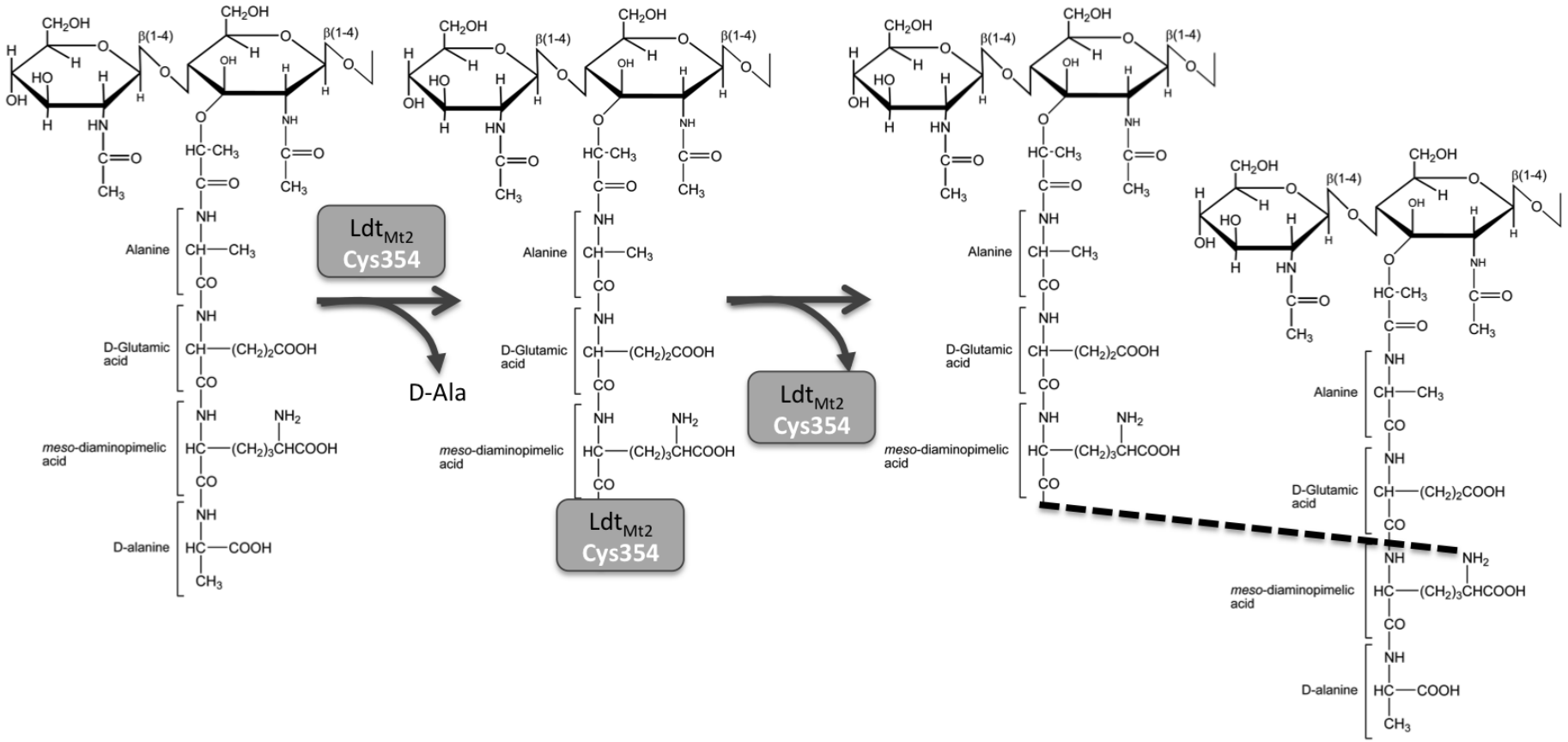

Figure 15. The 3-3 cross-link (DAP-DAP, dashed line) formation catalyzed by Ldt_{Mt2}.

3.2.1 Adduct Formation at the Active Site Cys354 by β-lactams

The mechanism of peptide cross-link formation by Ldts includes a covalent intermediate formed between the donor peptide and the active site cysteine. This reaction intermediate is resolved by the amino group of the acceptor peptide (Figure 15). The action of β-lactams relays on mimicking the donor peptide substrate hence, covalent binding of β-lactam antibiotics starts with the nucleophilic attack of the catalytic Cys354 on the carbonyl carbon of the lactam ring leading to an enzyme-acyl adduct formation. This way the mechanism of action is similar to the inhibition of D,D-transpeptidases. The Ldt_{Mt2} construct used, namely the BC module (residues 149-408, Figure 11), contains a single cysteine residue, located in the active site. This opens the possibility to follow the acylation reaction by monitoring the covalent modification of Cys354 using dithio-nitrobenzoate (DTNB) spectrophotometrically at 412nm (Figure 16A).

The fraction of free cysteine was monitored after exposure to β-lactams (7 min) by DTNB-derivatization and reactivity of the compounds, seven penam (PA), two penem (PE), six carbapenems (CA) and one cephem (CE), was ranked (Figure 16B). Fast Cys354 modification was observed for the carbapenems tepipenem (TEBI), meropenem (MERO), ertapenem (ERTA), doripenem (DORI) and biapenem (BIA), for the two penem-type antibiotics faropenem (FARO) and faropenem daloxate (FAROdal) and three of the penams 6-amino penicillanic acid (APA), piperacillin (PIP) and penicillin-G (PEN) (Figure 16B). The kinetic constants of the acylation reaction was measured and compared for the selected compounds, revealing that faropenem outperforms all other tested β-lactams (Figure 16C).

Electrospray ionization mass spectrometric (ESI-MS) analysis was used to confirm complex formation between the Ldt_{Mt2} and the selected β-lactam compounds. Covalent complex formation with the expected m/z value (unmodified adduct mass) was detected as the main peak with thio-nitrobenzoate (TNB), tebipenem (TEBI), biapenem (BIA), carbenicillin (CAR) and piperacillin (PIP).

The carbapenems MERO, ERTA and DORI adducts were detected with the expected unmodified masses however a peak corresponding to a 40–47 Da smaller mass were also detected (Figure 17). The mass difference could result from a decarboxylation reaction (44 Da) on the β-lactam ring, which has been observed in previous studies (Brown et al. 1996) and is in accordance with the error of the method (3–4 Da) in the mass-range monitored (30 kDa). The faropenem derived adduct was detected as a 87 Da fragment, and indicated the decomposition of the bound antibiotic after the acylation step.

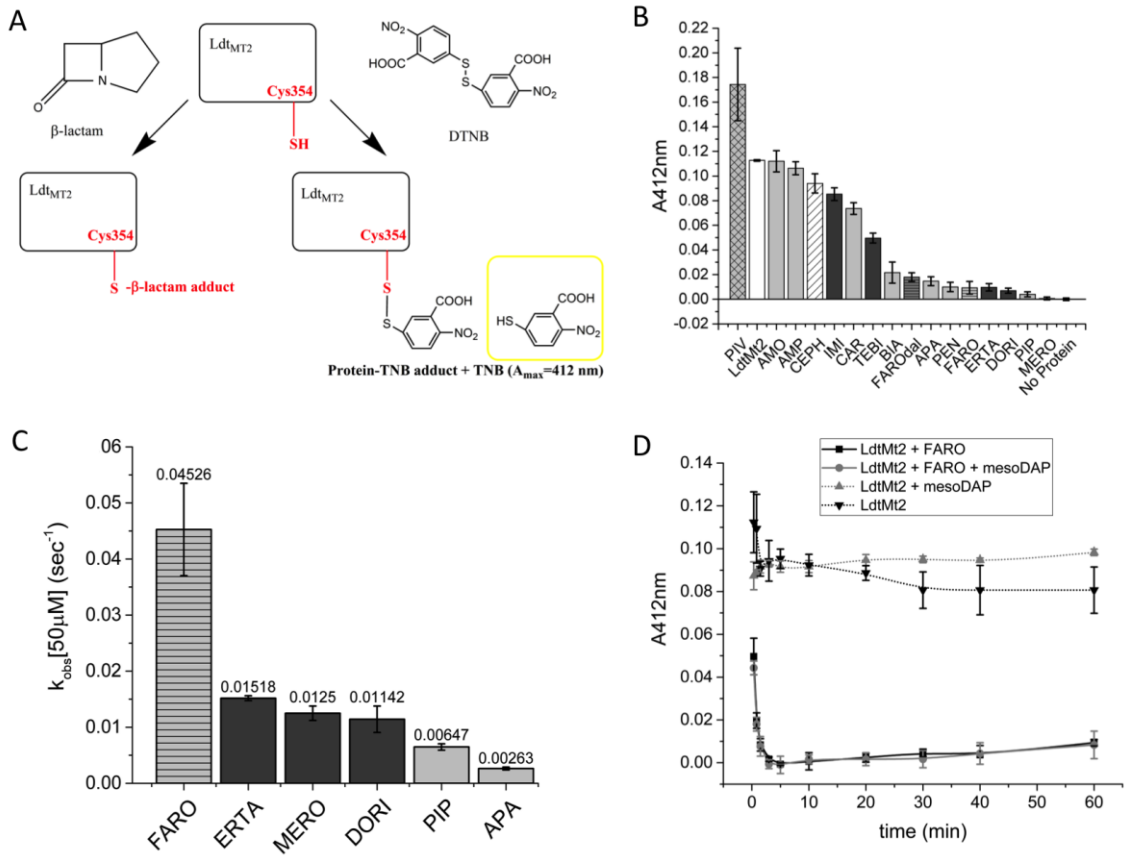

Figure 16. Investigation of β-lactam Binding Based on Enzyme-acyl Formation at the Ldt_{Mt2} Active Site. (**A**) The presence of free Cys354 was monitored by 5,5'-dithio-bis-2-nitrobenzoic acid (DTNB) which leads to the formation of a cysteine-TNB adduct. A stoichiometric amount of TNB is released that can be followed spectrophotometrically at 412 nm. Enzyme-antibiotic adduct formation blocks the active site cysteine residue leading to a proportionally decreased spectrophotometric signal. (**B**) The comparison of the 16 different β-lactam compounds (abbreviated names are used) regarding their reactivity in the acylation reaction. The Ldt_{Mt2} BC-module was exposed to 1 mM of antibiotic for 7 min followed by DTNB derivatization. Ranking of the compounds was possible based on comparison in acylation kinetics. (**C**) The acylation rate constants (k_{obs}) at 50 µM antibiotic concentration are shown for the six fastest β-lactam compounds. The faropenem (FARO)-driven reaction is about 2–3 times faster than the carbapenems (ERTA, MERO, DORI), 7 times faster than piperacillin (PIP) and 17 times faster than 6-aminopenicillanicacid (APA). Error bars indicate the standard deviation for three independent measurements. (**D**) The adduct formation with faropenem and the adduct stability monitored in the presence of 2 mM acyl acceptor *meso*-DAP investigated by DTNB derivatization. Fast modification of the enzyme sulfhydryl group can be observed with FARO (black) and in the presence of *meso*-DAP (grey), and no difference in the adduct stability is observed. As a reference the reaction of the native protein (black dashed line) and the protein in presence of *meso*-DAP (grey dashed line) are given.

The structure of this enzyme-adduct was investigated (Figure 18D) and the faropenem derived fragment was identified as a β-OH-butyryl adduct (87 Da) bound at the active site

cysteine. The adduct resembles to the acyl-enzyme reaction intermediate formed during the catalytic cycle (Figure 15), hence the question arises if the acceptor peptide may react with this adduct releasing it, and consequently the unmodified enzyme. Therefore, the preformed adduct was challenged by potential acceptor substrates (L-alanine, L-lysine, L-aminopimelate, D-aminopimelate) and the likely natural acceptor substrate *meso*-DAP, and the adduct stability was monitored by DTNB or by mass-spectrometry but no release of the free cysteine was observed. We also monitored the formation and stability of the adduct in the presence of the likely natural acceptor substrate *meso*-DAP, however neither the acylation kinetics nor the adduct stability was affected (Figure 16D). Consequently, faropenem was identified as the most efficient in binding kinetics, and the resulting adduct that represents the inactivated form of Ldt_{Mt2} shows a long-term stability.

Beta-lactam	Ligand MW (Da)	Mass Detected (Da)	Mass Bound (Da)	Mass Deviation (Da)	Conclusion
Faropenem (PE) FARO	285.1	28571.1	87.4	-197.7	Fragment bound
Doripenem (CA) DORI	420.5	28863.61 28907.41	379.9 423.7	-40.6 +3.2	Decarboxylated Full mass bound
Tebipenem (CA) TEBI	497.6	28978.29	494.6	-3.0	Full mass bound
6-Aminopenicillanic acid (PA) APA and APA dimer	216.3 432.6	28919.57	435.9	+3.4	APA dimer bound

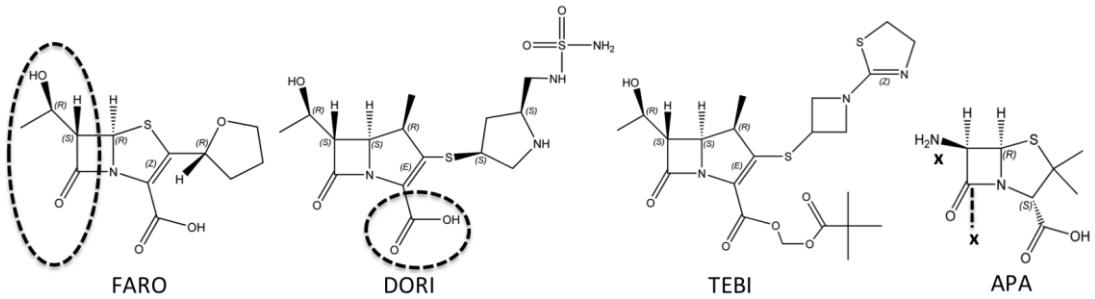

Figure 17. Representative Selection of β-lactam Driven Adduct Formation on the Ldt_{Mt2} Investigated by Mass Spectrometry. (**Upper panel**) Compounds selected come from the penem (PE), carbapenems (CA) and penam (PA) group. (**Lower panel**) Chemical structures are presented of the selected β-lactam antibiotics and modifications by the Ldt_{Mt2} are highlighted in bold dashed lines and crosses.

3.2.2 Structures of Covalent Adducts at the Ldt_{Mt2} Active Site

As part of the assay validation BC-module of Ldt_{Mt2} was crystallized with the bound TNB adduct. The 1.55 Å resolution structure clearly shows the TNB-adduct covalently bound to the Cys354 in the active site in both chains of the asymmetric unit. The catalytic site lays on a β-sheet platform covered by a β-hairpin loop called the lid (residues 300-323) adapting to ligand-dependent changes exposing or covering the active site (Figure 18A).

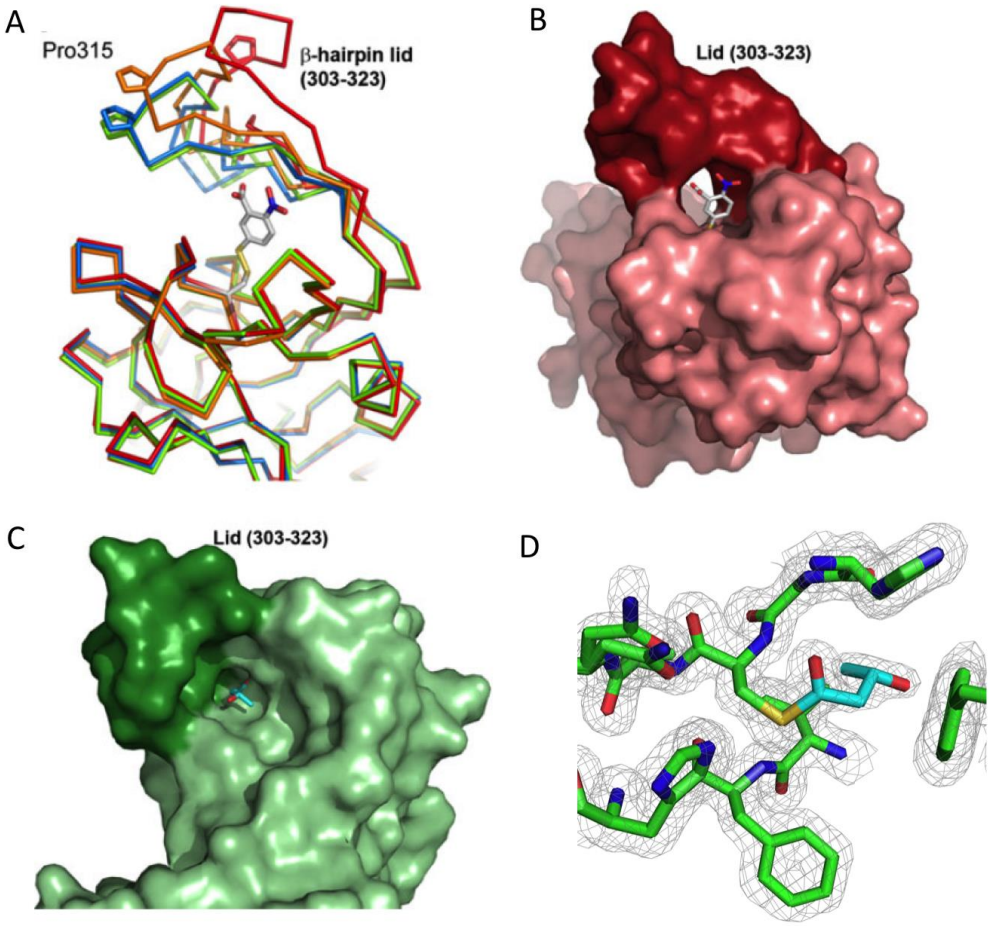

Figure 18. Structures of Ldt_{Mt2} and Covalent Adducts Formed at the Cys354. (**A**) The Cα backbone trace representation of the *apo*-Ldt_{Mt2} (blue, 4HUC), in complex with the FARO-derived adduct (green, 5LBG), the Ldt_{Mt2}-meropenem complex (orange, 4GSU) and the TNB-adduct (red, 5LB1) are superimposed to highlight the lid mobility. The Pro315 residue within the β-hairpin loop is represented as stick model as a reference point. (**B**) The Ldt_{Mt2}-TNB adduct structure in surface representation. The lid (residues 303-323, dark red) above the TNB adduct (stick model) within the active site is in open conformation. (**C**) Surface representation of the Ldt_{Mt2} with the faropenem-derived adduct (light blue, stick model) in the active site. The lid is in a closed conformation comparable to the *apo*-Ldt_{Mt2} structure. (**D**) Active site map (stick model) of the Ldt_{Mt2} structure with the β-OH-butyryl adduct (light blue) bound to Cys354 (yellow) within the active site cleft (residues as green sticks). The $2F_o$-F_c electron density map contoured at 1σ is depicted as a grey mesh.

When the TNB adduct is bound, the lid is moved out with a displacement at the tip (Pro315) of 12.0 Å compared to the ligand free Ldt_{Mt2} structure (PDB: 4HUC, Figure 18A&B). The accessible surface area (ASA) for the Cys354-linked sulfur atom is 4.7 $Å^2$.

The faropenem derived adduct detected earlier by mass spectrometry (Figure 17) was captured in the crystals of Ldt_{Mt2} by soaking the crystals in 4mM faropenem. The 1.54 Å resolution crystal structure shows additional density covalently linked to the Cys354 in one of the polypeptide chains of the asymmetric unit. The size and shape corresponds to the β-OH-butyryl (87 Da) fragment observed in mass spectrometry and was modeled with satisfying refinement parameters. The lid is in a closed conformation comparable to the ligand free structure. Compared to the TNB adduct the FARO-derived adduct seems to be inaccessible with an ASA of 0.1 $Å^2$ for the carbon atom of the carbonyl group that is in connection with Cys354. This is in line with the high stability of the β-OH-butyryl adduct observed in biochemical assays (Figure 16D). As this adduct represents the inactivated state of the target protein, the above structure is an important piece of information in establishing the mechanism of action.

3.2.3 Faropenem as the Most Efficient β-lactam Targeting *Mtb*

Faropenem was shown to be the most efficient β-lactam killing *Mtb* in culture and inside macrophages (Dhar et al. 2015). This work gives insights to the mechanism of action of this β-lactam compound on a validated target in *Mtb* and establishes some relevant points that may reveal the reason behind its success. The fast kinetics in inactivation of Ldt_{Mt2} and the high stability of the formed adduct that is protected by the enzyme are these relevant points. The same adducts formed by faropenem in targeting Ldt_{Mt1} and Ldt_{Mt2} were observed by other scientists, and the first steps of designing improved β-lactam antibiotics based on these results have been taken (Kumar et al. 2017).

3.3 *PAPER III*: RIPD (RV1566C) FROM *MYCOBACTERIUM TUBERCULOSIS*: ADAPTATION OF AN NLPC/P60 DOMAIN TO A NON-CATALYTIC PEPTIDOGLYCAN-BINDING FUNCTION

RipD (Rv1566c) from *Mtb* is, like RipA and RipB, a member of the enzyme family carrying an NlpC/P60 domain. However, alterations in the NlpC/P60 catalytic triad and a peculiar C-terminal penta-peptide repeat extension distinguish RipD from the other previously characterized members of this enzyme family. A bioinformatics analysis revealed that RipD homologs containing these specific features occur in 11 mycobacterial genomes and similar penta-peptide repeats can be found in proteins from mycobacteriophage and other bacterial species with periplasmic localization. In contrast to RipA or RipB, RipD does not show PG hydrolase activity, which is in agreement with the residue alteration within the active site. However, PG binding of the NlpC/P60 core is retained, presenting the first non-catalytic NlpC/P60 protein with PG-binding function. CD-spectroscopy indicated the C-terminal repeat sequence is most likely a random coil in solution, a common feature of protein repeats. The unstructured character is also in agreement with the crystallographic analysis based on the 1.17 Å crystal structure carrying two penta-peptide repeat units.

3.3.1 Structure of the Non-catalytic NlpC/P60 Hydrolase RipD (1566c) and $RipDR_2$

The RipD full-length protein consists of 230 amino acids encoding for a short N-terminal signal sequence (residue 1-30), a NlpC/P60 core domain, sharing about 50% sequence similarity with RipA and RipB, followed by a 61 residue C-terminal penta-peptide ($PVQQA_n$) repeat sequence (Figure 10A&19A). Three protein constructs were produced in *E. coli*; a full-length RipD (residues 38–230, lacking signal sequence), a RipD-core (residues 38-169, NlpC/P60 domain) and the $RipDR_2$ (residues 38-182, NlpC/P60 domain plus P^{173}VQQA-PVQPA^{182}) including two penta-peptide repeat units (Figure 19A).

The crystal structure of the RipD-core was determined by molecular replacement using the structure of the homologous protein from *Mycobacterium avium* (PDB: 3GT2) to 1.56 Å resolution. The structure of the core domain reflects an NlpC/P60 fold built up by five antiparallel β-sheets and three α-helices (Figure 19B). Superimposition of the RipD-core with structures of the NlpC/P60 domain of RipA and RipB results in an r.m.s.d. of 0.8 Å and 0.9 Å (over 130 Cα atoms) respectively. The RipD-core contains a PG-binding groove also present in the catalytically active homologues RipA and RipB (Böth et al. 2011, Figure 19C&D). The

main difference is that in the RipD-active site the cysteine and histidine residues are replaced by an alanine and serine, respectively (Figure 19D). Two acetate ions are bound within the groove, one in the center of the groove and another at the funnel entry (Figure 19D).

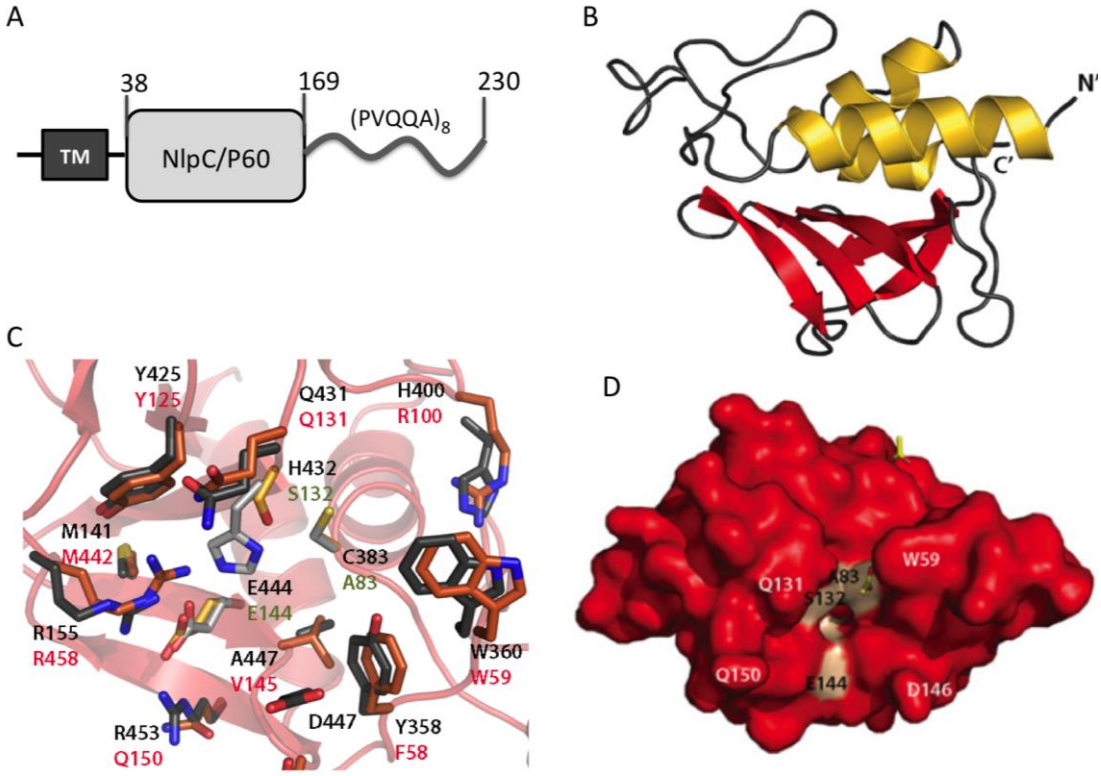

Figure 19. RipD, a Catalytically Inactive Member of the NlpC/P60 Family. (**A**) Domain organization of RipD (Rv1566c) in *Mtb* and crystal structure of the RipD-core domain. The transmembrane region (TM) the core domain (NlpC/P60 domain) and the repeat sequence (residues 169-230) in C-terminal position indicating the sequence of the repeat unit PVQQA. (**B**) The 1.56 Å resolution crystal structure of the RipD-core is presented (cartoon) built by a five-stranded antiparallel β-sheets (red) and three α-helices (yellow). (**C**) The peptide binding groove of RipD is superimposed with the catalytic active site of RipA. Residues forming the groove are represented as orange sticks for RipD and black sticks for RipA. Active site residues of RipA (grey sticks) and the corresponding amino acids in RipD (gold sticks) are highlighted. The polypeptide chain of the RipD-core (red cartoon) is presented. (**D**) Surface representation of the RipD-core domain to illustrate the peptide binding groove. The two acetate ions bound at the proteins surface are shown as yellow sticks. Alterations in the catalytic triad (A83, S132, E144) are shaded in beige and surrounding residues Trp59, Gln131 and Asp146 are highlighted as a reference points.

The crystal structure of the RipD construct including two penta-peptide repeat units, $RipDR_2$, was solved to 1.17 Å (Figure 20A). The electron density map allowed modeling of the core domain and the second repeat segment (residues $P^{178}VQPA^{182}$). Eight residues connecting the modeled repeat were disordered in the crystal. The PVQPA-repeat is bound in an extended

conformation at the interface of the symmetry related molecule (Figure 20A&B). The interaction at the interface is based on three hydrogen bonds and hydrophobic interactions (Figure 20B). The solution state of the RipD constructs used is monomeric according to size-exclusion chromatography.

3.3.2 The Penta-peptide Repeat

The CD spectroscopy of the full-length RipD (residues 38-230) compared to the RipD-core domain (residues 38-169) demonstrates that the C-terminal tail adds an increased amount of random coiled regions, suggesting that the C-terminal repeat sequence does not adopt a specific secondary structure in solution, which is common for peptide repeat sequences.

Table 3. RipD-like Proteins and Their Repeat Sequences in Mycobacterial Homologs.

Species (strain)	**Functional annotation**	**UniProt ID**	**Length (aa)**	**Repeat character N/L**
Mycobacterium tuberculosis (H37Rv)	Invasion-associated	O06624	230	10/5
Mycobacterium tuberculosis (H37Ra)*	Putative invasion protein	A5U2S3	230	10/5
Mycobacterium bovis (BCG and AF2122/97)	Putative invasion protein	Q7VEY5	230	10/5
Mycobacterium ulcerans (Agy99)	Invasion protein	A0PNZ9	259	16/5
Mycobacterium marinum (ATCC BAA-535)	Invasion protein	B2HQ87	259	16/5
Mycobacterium avium (k10)	Hypothetical protein	Q740S0	316	19/5 and 3/4
Mycobacterium avium (104)	NlpC/P60 protein	A0QHK2	289	21/5 and 3/4
Mycobacterium leprae (TN)	Secreted P60 protein	Q9CC67	212	1/5
aa, amino acid; L, length of one repeat unit; N, number of repeats.				
*Other *M. tuberculosis* strains: RGTB327, RGTB423, F11, CDC1551, Haarlem (draft) and strain C.				

The RipD-like proteins can be found in 21 mycobacterial genomes and closely related species (e.g. *Segniliparus rotundus*), however RipD variants containing a PVQQA-type repeat sequence can only be found in a few mycobacterial species (Table 3). Similar peptide repeat sequences can be also found in other cell wall or periplasmic proteins e.g. in the *Thiorhodococcus drewsii* flagellar assembly protein FliH (UniProt ID G2E335; $PXRQS_8$), *Yersinia pseudotuberculosis* haem exporter protein D (UniProt ID: Q668U1; $PXQQX_2$ and $PLHQX_5$) and the mycobacteriophage Pixie gp99 protein (UniProt ID: G1D508; $PVQXX_6$) (Pope et al. 2011).

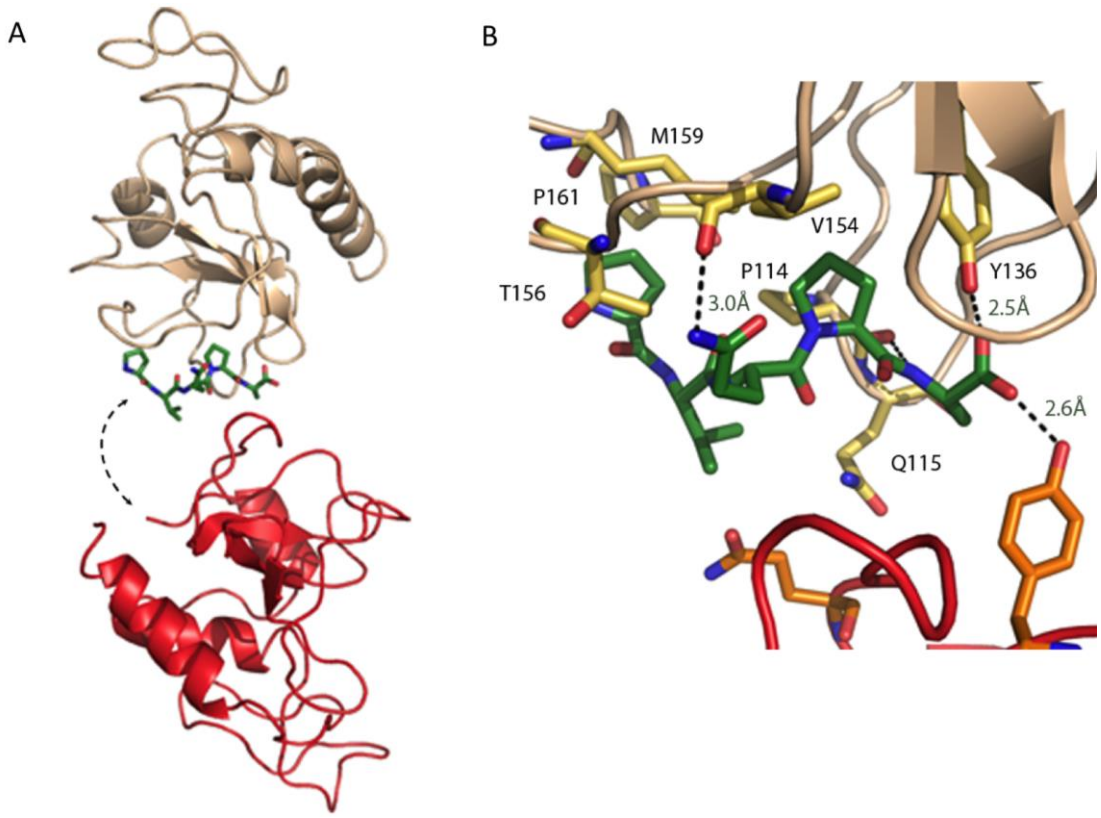

Figure 20. (**A**) The penta-peptide repeat unit resolved in the RipDR$_2$ crystal structure, PVQPA (green sticks), forms intermolecular contacts with a symmetry-related molecule in the crystal. (**B**) The PVQPA-repeat interactions at the intermolecular interface within the crystal lattice. Hydrogen bonds are illustrated with dashed lines, distances indicated.

3.3.3 The Biochemical Properties of RipD

The enzyme assay based on *o*-phthalaldehyde (*o*-PA) derivatization established for RipA and RipB (Böth et al. 2011) was used to detect peptidase activity with the dipeptide iE-DAP and the tripeptide tri-DAP as substrates using the catalytic RipAc domain as a positive control. According the expectations, the RipD-core domain did not show peptidase activity on the substrates tested. The RipD-core domain shows alterations at the corresponding residues where the cysteine is replaced by alanine (Ala83) and the histidine by a serine (Ser132) explaining the lack of peptidase activity (Figure 19D). The structures of the RipD, RipA and RipB PG binding grooves however are very similar and suggest PG binding for all three enzymes.

To investigate a potential RipD PG binding activity we used PG from *B. subtilis* in a PG-binding assay since the peptide stem has an identical peptide composition as PG from *Mtb*. Lysozyme and BSA were used as positive and negative controls, respectively. The RipD-core showed binding to high-molecular-weight (HMW)-PG demonstrating binding ability. The

presence of the C-terminal penta-peptide repeat however significantly lowered the binding to HMW-PG. Therefore we used mycobacterial cell wall extract (CWCx), including PG and arabinogalactan, to examine whether the full-length RipD is capable of binding other cell wall components. The RipD-core and the full-length RipD showed similar behavior in binding to CWCx as to HMW-PG and the presence of the C-terminal repeat seems to interfere with RipD-core PG-binding. Based on the ability of RipD to bind PG, we suggested for this non-catalytic variant a role in cell wall stabilization, serving as a shield to protect the peptide stems from cleavage by other hydrolases.

3.4 *PAPER IV* (*MANUSCRIPT IN PREPARATION*): THE STRUCTURE OF THE N-TERMINAL MODULE OF THE CELL WALL HYDROLASE RIPA AND ITS ROLE IN REGULATING CATALYTIC ACTIVITY

RipA is the mycobacterial NlpC/P60 hydrolase that has been most thoroughly investigated. The PG degrading activity based on the NlpC/P60 domain is potentially harmful therefore regulatory control is important. The N-terminal domain of RipA has been proposed to play an inhibitory role by blocking the C-terminal catalytic domain (Ruggerio et al. 2010, Botella et al. 2017). Active site accessibility is however not limited by the presence of the N-terminal domain, but by the lid-module of the inter-domain linker, that is situated in the PG binding groove of the catalytic domain. The N-terminal domain structure was solved to 2.25 Å resolution by Se-SAD phasing revealing an all-α-fold with two long antiparallel α-helices. Dimerization of this domain was observed in size exclusion chromatography and in SAXS experiments. Using SAXS data the periplasmic two-domain RipA structure was investigated and modeled presenting a rigid hairpin-like module and the catalytic domain connected by flexible linker (24 residues). This linker limits the movement of the catalytic domain and allows for a defined range of catalytic action and PG degradation.

3.4.1 The Inter-Domain Linker Regulates Active Site Accessibility in RipA

The RipA polypeptide chain contains an N-terminal signal sequence (TM, residues 1-39) predicted by the SignalP server (Petersen et al. 2011). The whole periplasmic RipA protein (RipApp, residues 39-472) contains a single cysteine residue, the catalytic Cys383, situated in the NlpC/P60 domain (Figure 21A). This fortunate condition gives the possibility to monitor active site accessibility using the sulfhydryl-specific DTNB derivatization assay (Figure 21B). We monitored the cysteine accessibility in RipApp, the catalytic domain

RipAc including a lid-module (X), the catalytic domain without the lid-module (RipActr) and a Cys383Ala mutant of RipActr, denoted as RipActr(C383A) (Figure 21B). The catalytic Cys383 was not exposed in the two-domain construct RipApp (residues 39-472) and not in the RipAc construct either. Cys383 only becomes accessible when the lid-module (X) is not present indicating that it is the lid-module of the inter-domain linker (residues 260-321) and not the N-terminal domain, which regulate the active site accessibility. This implies also that the N-terminal domain may have another function.

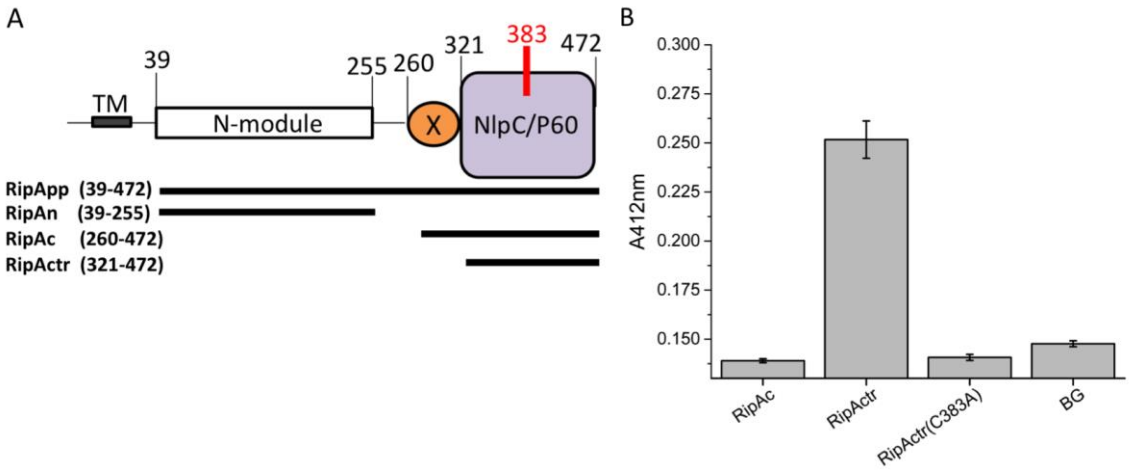

Figure 21. (**A**) The domain structure of RipA and the constructs used in the study are shown with the residue range indicated by horizontal bars with respect to the domain structure. The catalytic Cys383 in the active site is highlighted in red, the lid-module (X) connecting the catalytic and N-terminal domain is coloured in orange. (**B**) The RipA active site accessibility is monitored at 412nm using DTNB derivatization of the catalytic Cys383 present in construct RipApp, RipAc and RipActr. The construct with the Cys383 mutated to alanine RipActr(C383A), was used as negative control. The columns represent the average of three independent measurements and standard deviation is indicated with error bars.

3.4.2 Characterization and Structure of the N-terminal Domain of RipA: RipAn

The N-terminal domain of RipA (RipAn, residues 39-255) was investigated by circular dichroism (CD) spectroscopy indicating an all α-protein (minima at 222 and 208 nm and maximum at 202 nm). Analytical size exclusion chromatography (SEC) indicated the formation of dimers in solution. The catalytic module RipAc (residues 260-472) is a monomer in solution based on SEC, while the two-domain construct RipApp (residues 39-472) representing the periplasmic RipA protein eluted in a single peak suggesting a size in between monomer and dimer (RipApp MW of 46 kDa).

The 2.25 Å resolution structure of RipAn was determined by Se-SAD phasing. It reveals an all-α-fold in agreement with the CD-spectroscopy data. The asymmetric unit contains a single polypeptide chain folded in two long helices with 92 (helix α1: D40-S131) and 103 (helix α2: P138-E240) residues (Figure 22A). The two helices are connected by a 6-residue long loop (132-YLSASS-137).

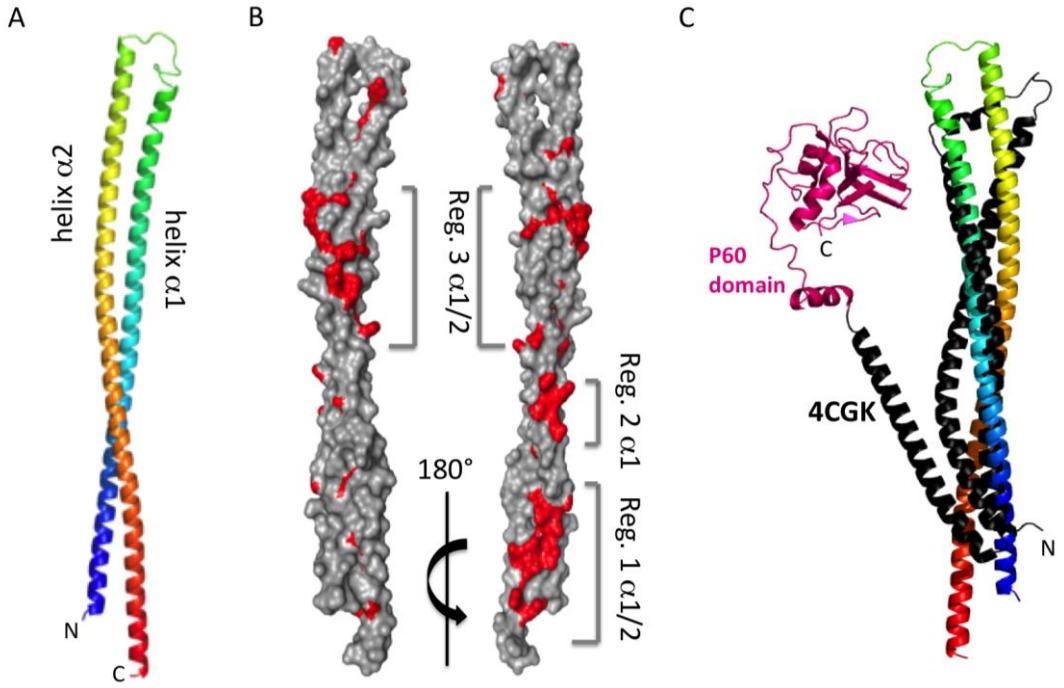

Figure 22. The Crystal Structure of the N-terminal Domain from RipA: RipAn. (**A**) Cartoon of RipAn presenting an all α-fold with two long α-helices (helix α1and helix α2) in rainbow color scheme. N- and C-termini are indicated. (**B**) Surface exposed conserved residues highlighted in red are grouped into three regions, region-1 and region-3 involve both helices, and region-2 only contains residues from helix α1. (**C**) PcsB (PDB: 4CGK) from *S. pneumoniae* is a peptidoglycan hydrolase involved in cell separation consisting of an N-terminal domain (black) and an NlpC/P60 domain (pink). Superimposition of RipAn (rainbow) and PcsB based on the helical domains is presented.

Sequence alignments with RipA homologues from mycobacterial and Rhodococcus genomes (Figure 22B) indicate 42% sequence identity in the area of this two-helix module. Several of the residues are responsible for connecting the two α-helices, and are not surface exposed. The conserved sequences on the surface are grouped into three regions: region-1 and region-3 including regions in both helices, while region-2 contains residues from α1 only (Figure 22B).

Structural comparisons of RipAn with other proteins from the PDB using the DALI algorithm (Holm & Rosenström 2010) result in a list of α-helical proteins with the most significant hit being PcsB, a PG remodeling protein from *S. pneumoniae* (Figure 22C).

PcsB contains a helical N-terminal domain and an NlpC/P60-like catalytic module, thereby it is a functional analogue of RipA (Bartual et al. 2014). The structural comparison of the N-terminal domain results in 13% sequence identity (over 141 residues) with Cα r.m.s.d. of 3.4 Å and Z score of 6.3.

3.4.3 Solution Structures from SAXS

Small-angle X-ray scattering (SAXS) was used to investigate the solution state of RipAn (23.2 kDa), the N-terminal module of RipA, and RipApp (46.0 kDa), the two-domain construct representing the periplasmic segment. SAXS data was collected at pH 5.0-8.0 for RipAn and Guinier- and indirect Fourier transformation (IFT) analyses were performed to obtain information on oligomerization state of the proteins. At pH 5.0 RipAn is suggested a monomer as the dominant species with a small amount of dimers present. At pH 6.0-8.0 the calculated average molecular mass from IFT was 57.1 kDa yielding a monomer multiple of 2.46. This points to the formation of dimers and perhaps coexistence of higher-order oligomers in all higher pH samples. Rigid-body refinement was performed using the online version of SASREF (Petoukhov et al. 2005, https://www.embl-hamburg.de/biosaxs/atsas-online) with P2 symmetry constraints. Every run came out with very similar 3D structures with a dimer crossed about one quarter from the ends at an angle of ~120° (Figure 23A). The Aarhus in-house rigid-body refinement program, WLSQ_SYMXV1 was used along with SASREF on all samples to obtain complementary fits and resulting 3D structures almost identical (with SAXS resolution) and the crossed dimer motif is reproduced across runs, confirming again the robustness of the obtained structure.

The scattering data from the RipApp sample at pH 8.0 was also evaluated by Guinier- and IFT analyses estimating the two-domain RipApp construct being a monomer with a small dimer fraction. The model of the complete two-domain construct was prepared from the X-ray crystal structures of the RipAn domain (representing residues 40-240), the C-terminal NlpC/P60 domain (representing residues 265-472), and the 24 residue long inter-domain linker that was modeled using I-TASSER (Roy et al. 2010). No dimer structures consistent with the RipAn dimers could be fitted to the SAXS data. The best fits for the periplasmic segment of RipA were achieved with a monomer, where the linker and the catalytic domain flex back alongside the stalk but not collapsing onto it (Figure 23B).

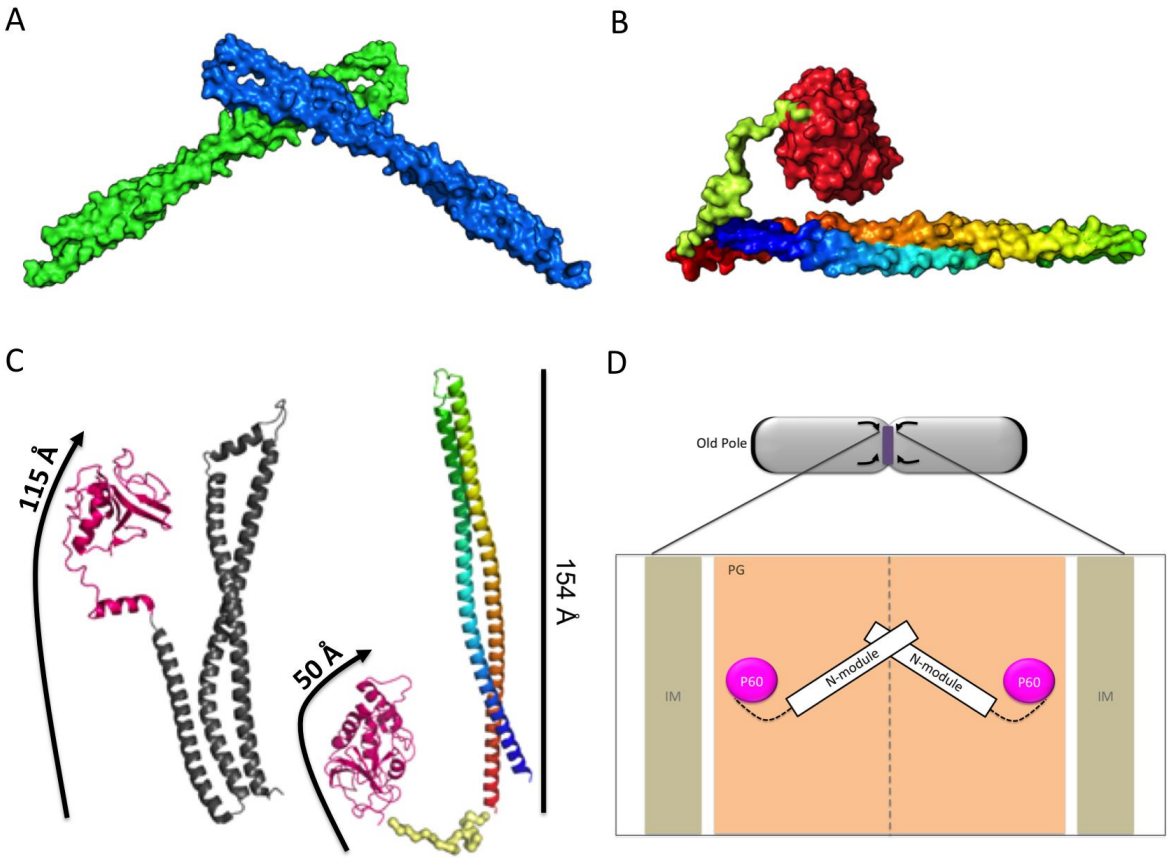

Figure 23. Model of the Periplasmic RipA Based on X-ray Structures and SAXS Solution Structures. (**A**) SAXS solution structure of RipAn derived from SASREF rigid-body refinement of P2 dimers based on the RipAn crystal structure. (**B**) The SAXS solution structure of RipApp results from WLSQ_SYMXV1 rigid-body refinement of linked structures of RipAn-Linker-RipAc. The model of the two domain structure is based on the crystal structure of RipAn (residues 40-240) colored as rainbow, the inter-domain linker (residues 241- 264) in green and RipAc (residues 265-472) in red. (**C**) The PcsB structure (grey, PDB: 4CGK, left) and the two-domain structure of the RipA derived from SAXS data and the X-ray structures of the individual domains of RipA. Arrows are indicating the proposed range of movement of the catalytic domain and peptide bond cleavage within the thicker or thinner PG layer in *S. pneumoniae* and *Mtb* respectively. (**D**) A model for cell wall degradation by RipA is depicted suggesting a dimer at the septum of two daughter cells.

3.4.4 Model of the Periplasmic RipA

PcsB from *S. pneumoniae* was identified as the most relevant hit among structural homologues. It is also a functional analogue of RipA, displaying an NlpC/P60 domain, involved in cell division and contains a α-helical domain at N-terminal position (Bartual et al. 2014). Comparison of RipA and its functional analogue PcsB, reveals that PcsB has a third helical segment (47 residues) connecting the two helix module to the catalytic domain (Figure 23C). In RipA, the catalytic domain is connected to the two-helix module via a

shorter (24 residue) linker. The typical gram-positive PG layer is ranging from 200–400 Å (Giesbrecht et al. 1998, Bartual et al. 2014) while in *Mtb* the corresponding layer is thinner with 100–150 Å (Hett et al. 2008). Combinations of the catalytic domains with longer (PcsB) or shorter (RipA) structural spacers enable positioning of the catalytic hydrolase domain so it can work on thicker (*S. pneumoniae*) or thinner (*Mtb*) PG layer in the respective organism (Figure 23C, top). The observed dimerization of RipAn (SEC and SAXS) might position RipA proteins also as a dimer between the separating daughter cells combining a cleavage and tethering/locating function (Figure 23D, bottom).

4 CONCLUSIONS

Paper I describes the crystal structure of the essential Ldt_{Mt2} transpeptidase in *Mtb* responsible for 3-3 cross-link formations. The periplasmic protein consists of three domains, two smaller Ig-like domains attached to a transpeptidase domain at the C-terminus. The full-length structure was solved in two fragments and the combination of the two provides a view of the complete three-domain periplasmic Ldt_{Mt2} protein that extends about 80–100 Å from the inner membrane. The Ig-like domains might serve as spacer positioning the catalytic transpeptidase domain at the appropriate site within the PG layer, which defines the maximal distance for 3-3 cross-link formation by Ldt_{Mt2}. The model also supports a complementary role for the longer three-domain and the shorter two-domain L,D-transpeptidases (e.g. Ldt_{Mt1}) in carrying out the transpeptidation at two different levels in the multi-layered peptidoglycan. In paper I we also indicate that the Ldt_{Mt2} is targeted by β-lactam antibiotics, suggesting a potential for the design of Ldt_{Mt2} specific inhibitors.

In ***paper II*** a cohort of 16 β-lactam antibiotics were investigated by binding kinetics, mass spectrometry, and X-ray crystallography to identify efficient compounds and study their action the Ldt_{Mt2}. We gained insight into β-lactam processing by the Ldt_{Mt2}, where some carbapenem-type antibiotics seem to undergo decarboxylation and 6-aminopenicillanic acid can be coupled to a dimer by Ldt_{Mt2}. We highlight faropenem, a penem-type β-lactam, exhibiting the fastest binding kinetics and show that it is decomposed to a small 87 Da fragment that is stably bound to the active site of Ldt_{Mt2}.The 1.54Å resolution crystal structure of this enzyme-adduct complex represents the inhibited state and has implications for the mechanism of action of faropenem.

In ***paper III*** we show that RipD (Rv1566c) contains an NlpC/P60 domain that lacks catalytic activity, but retains PG binding *in vitro*. The RipD-core shows strong binding to high molecular weight PG and purified cell wall complex (CWCx) of *M. smegmatis*. RipD therefore represents the first example of a non-catalytic NlpC/P60 domain protein with PG-binding function, an adaptation maybe specific for mycobacterium genus. RipD contains a 61-residue-long unstructured C-terminal penta-peptide ($PVQQA_8$) repeat sequence that interferes with PG binding *in vitro*. RipD most probably has a role in cell wall stabilization or in protecting the peptide linkages from hydrolysis by other catalytically active proteins.

Paper IV (*Manuscript in progress*) investigates the structure and role of the N-terminal domain of RipA. We show that the presence of the N-terminal domain does not affect active site accessibility, however the lid-module covering the peptide-binding groove of the catalytic domain does. The X-ray structure of the N-terminal domain reveals an all-α-fold with two long α-helices that form a dimer in solution. SAXS data in combination with X-ray structures of both RipA domains were used to model the two-domain RipA consisting of a rigid hairpin-like module and the catalytic domain connected by a 24 residue long flexible linker. We propose that the linker limits the movement of the catalytic domain within the PG meshwork as part of the spatiotemporal control of peptidoglycan degradation.

5 ACKNOWLEDGEMENTS

I started a PhD because after working on my master thesis for 1.5 years in an RNA lab I felt that's not enough. I wanted to know and understand more. I became curious about proteins and was particularly fascinated by crystallography and the projects of Gunter's group.

I want to express my sincere gratitude to you **Gunter**, for making it possible to start my PhD life in a crystallography group, even if there was no open position when I applied. You gave me the chance to develop and learn how magical crystallography can be! The beautiful mixture of experience, luck and belly feeling, working with precise hands and on big acceleration rings that let you see as small as atoms. **Ylva**, you always have been my idol, an outstanding researcher and passionate and successful woman in science. I wished I could have learned much more from your immense crystallographic knowledge. Thank you so much for your supporting words when my little PhD problems seemed so big.

Dear **Robert**, I am one of the lucky students with not only one but two understanding, supporting, inspiring and inventive bosses that guided me through this period of life in science. Thank you for not throwing me out of your office when I came the 1000st time with a new crazy experimental idea, 'scientific breakthrough' or thought, for listening, your jokes and your recommendations and for being the coolest PhD father someone can imagine. I hope you will supervise many PhD students because I am convinced you are a researcher and teacher future science needs. **Gabriella**, thank you for the family support, all the first-hand kids knowledge and for being an inspiration in 'how to live with a husband in science'.

I want to say thank you to my dearest friends on the PhD road. **Dominic** I am very lucky to have learned from you. To get the opportunity to follow a mature PhD student at the beginning of a PhD is so precious. Working with you showed me how efficient projects can be, how to delegate and follow, how to design experiments and how much can be done and achieved in a good team. We were working hard, educating students, laughing and crying together. You became one of my closest friends. **Micha**, 'unser Finanzminister', you know so much, and you saved me a couple of times with a healthy dose of rude direct reality and warnings. I miss you two so much and hope our paths will meet again! My **K8**. We met late in our PhD periods and grew close together. Thank you for opening your heart and letting me in. Without you I would not have met my future husband and not experienced the magic of dancehall. Your warm rays of a critical and positive mind are inspiring and I know we can always count on each other, listen to and support each other - the perfect fundament for a life-long friendship. **Francesca**, with you I can share everything. You are my dancing and stretching queen. We are sharing and changing our lives together and I really hope we continue to meet and care. **Iuliia**, I am glad I met you in the ethics course and since then we always stayed connected. Thank you for the 'fikas' together, about sharing dreams and wishes and getting to know a real Ukrainian woman who loves her country and people! **Laura** you are my idol of preciseness, organization and of keeping a cool head in all situations. I am so happy we shared precious moments while cycling around the Vättern or seeing the Northern Lights in Kiruna. Now we are both mamas here in Sweden and our little girls are our new focus and precious.

I send big warm hugs to the former lab couples and members. **Berni and Doreen, Jodie and Magnus, Eddie, Dominik and Maria, Selma, Ming-Wei, Ömer, Jason, Peter, Ahmad, Victoria** and so many more. You always showed us PhD newbies the way! Every one of you was so supportive with us on synchrotron trips, in the lab and in unforgettable meetings and kitchen moments.

Big thanks to the students I was working with. **Kristina, Iryna, Philip and Daniela**. You trusted me and gave me the opportunity to share my knowledge and passion for science. We were working hard and good and some things we even published in a paper together. I want to thank **Katja**. You are a young and very successful woman in science. You are focused and know what you want, managing the split between challenging science and family projects! You brought fresh wind with **Hampus, Ileana, Judith, Lorenzo, Luca** and all your crew and I am a bit sad there was not enough time to get to know you better guys. Dear **Helena, Tomas, Martin and PSF members**. Your support and facility is amazing. Thank you for instructions, help on all ends and making crystallography more efficient! Thank you **Lionel, Joseph, Madhu and Fatma** for protein purification and crystallography help, for cycling trips and all the parties, get-togethers and being around throughout my PhD.

I am so grateful to have shared many adventures, parties and lovely moments with good friends like **Shiromi, Håkan, Sifiso, Timofey, Irina and Marcus, Armando and Cindy, BigAleksey and Conran**. We all grew up a bit together and I really hope we will stay in touch or find back to each other one day. I was very lucky to have met two wonderful landlords, **Khaled and Jozefina**. You not only gave your wonderful place to live but also lots of support and an open-hearted friendship! Jozefina I am looking forward to our future long talking-walks and send Ana, Elliot and you big hugs!

I am thankful to have **Bettina** in my life. You are like a sister and we are not only the best tennis double that Austria knows but also so honest and supportive to each other. I wish to stay friends forever and imagine us at 80-years of age on the tennis court still playing and talking about our husbands and twenty grandchildren. Meine **Nora**fee. Together we are 'Hormonella' and 'Emotionella'. We shared unforgettable moments, crying and laughing, dancing in the rain in our 'hot-lab' coats. I also wish we will never loose each other.

My precious and big **family** in Austria, in my heart I know I always can count on every one of you. I am so thankful for having my **grandparents** close. You are my heroes. Your incredible stories and experiences make me remember what is really important in life. In our today's society I feel we are puffed in pillows of wealth and forget what our family fundament has been gone through so we can enjoy a safe life. You experienced hunger and real rough life and are the example that we can endure much more than our mind can imagine. I wish we will continue to hike, cook and talk together for long time. My beloved **Mama,** I thank you for being so warm-hearted and supportive. For always caring about me, my sister and two brothers and that I can still come to you to cry my eyes out. Thank you my other part of heart, **Katrin**, for being in my life. My sister I miss you every minute! **Papa**, you are my advisor, my biggest fan and strictest reviewer. You always encouraged me, questioned me and are the reason of my curiosity. You made me work hard in school, in sports and in the forest cutting trees. I am so happy you offered me an open-minded childhood and taught me how to help myself. 'A healthy mind lives in a healthy body', I will always remember!

My husbee, my **Алёша**, моё всё! You are the miracle in my life! You give me peace and strength, are my island of fun, craziness, creativity and happiness. I am so proud of what we do and that we chose to walk the way together. Thank you for **Annika**, a **little sister** on the way and a wonderful warm-hearted **Ukrainian-Russian family** that supports me like I am their own.

6 REFERENCES

Abrahams KA & Besra GS (2016) Mycobacterial cell wall biosynthesis: a multifaceted antibiotic target. *Parasitology*, 1–18.

Ai JW, Ruan QL, Liu QH & Zhang WH (2016) Updates on the risk factors for latent tuberculosis reactivation and their managements. *Emerging Microbes & Infections* **5**(2):e10.

Akira S, Takeda K & Kaisho T (2001) Toll-like receptors: critical proteins linking innate and acquired immunity. *Nat Immunol* **2**(8), 675–680.

Alderwick LJ, Harrison J, Lloyd GS & Birch HL (2015) The Mycobacterial Cell Wall—Peptidoglycan and Arabinogalactan. *Cold Spring Harbor Persp in Med* **5**(8):a021113.

Allen M, Bailey C, Cahatol I, et al. (2015) Mechanisms of Control of *Mycobacterium tuberculosis* by NK Cells: Role of Glutathione. *Front Immunol* **6**:508.

Anantharaman V & Aravind L (2003) Evolutionary history, structural features and biochemical diversity of the NlpC/P60 superfamily of enzymes. *Genome Biol* **4**(2), R11.

Bansal-Mutalik R & Nikaido H (2014) Mycobacterial outer membrane is a lipid bilayer and the inner membrane is unusually rich in diacyl phosphatidylinositol dimannosides. *PNAS* **111**(13), 4958–4963.

Barka EA, Vatsa P, Sanchez L, et al. (2016) Taxonomy, Physiology, and Natural Products of Actinobacteria. *Microbiol and Mol Biol Reviews* **80**(1), 1–43.

Barkan D, Hedhli D, Yan H-G, Huygen K & Glickman MS (2012) *Mycobacterium tuberculosis* Lacking All Mycolic Acid Cyclopropanation Is Viable but Highly Attenuated and Hyperinflammatory in Mice. Flynn JL, ed. *Infection and Immunity* **80**(6), 1958–1968.

Barreteau H, Kovac A, Boniface A, Sova M, Gobec S & Blanot D (2008) Cytoplasmic steps of peptidoglycan biosynthesis. *FEMS Microbiol Rev* **32**, 168–207.

Barry CE, Crick DC & McNeil MR (2007) Targeting the Formation of the Cell Wall Core of *M. tuberculosis*. *Infect dis drug targets* **7**(2), 182–202.

Bartual SG, Straume D, Stamsas GA, et al. (2014) Structural Basis of Pcsb-Mediated Cell Separation in *Streptococcus Pneumoniae*. *Nat Commun* **5**:3842.

Basso LA, Zheng R, Musser JM, et al. (1998) Mechanisms of isoniazid resistance in *Mycobacterium tuberculosis*: enzymatic characterization of enoyl reductase mutants identified in isoniazid-resistant clinical isolates. *J Infect Dis* **178**(3), 769–75.

Basta LAB, Ghosh A, Pan Y, et al. (2015) Loss of a functionally and structurally distinct L,D-transpeptidase, Ldt_{Mt5}, compromises cell wall integrity in *Mycobacterium tuberculosis*. *J Biol Chem.* doi: 10.1074/jbc.M115.660753.

Bianchet MA, Pan YH, Brammer Basta LA, et al. (2017) Structural insight into the inactivation of *Mycobacterium tuberculosis* non-classical transpeptidase Ldt_{Mt2} by biapenem and tebipenem. *MC Biochem* **18**(8). https://doi.org/10.1186/s12858-017-0082-4.

Biarrotte-Sorin S, Hugonnet JE, Delfosse V et al. (2006) Crystal structure of a novel beta-lactam-insensitive peptidoglycan transpeptidase. *J Mol Biol* **359**, 533–538.

Brites D & Gagneux S (2015) Co-evolution of *Mycobacterium tuberculosis* and *Homo sapiens*. *Immunol Rev* **264**(1), 6–24.

Bielnicki J, Devedjiev Y, Derewenda U, et al. (2006*) B. subtilis* ykuD protein at 2.0 Å resolution: Insights into the structure and function of a novel, ubiquitous family of bacterial enzymes. *Proteins* **62**, 144–151.

Boon C & Dick T (2002) *Mycobacterium bovis* BCG response regulator essential for hypoxic dormancy. *J Bacteriol* **184**, 6760–6767.

Bork P, Holm L & Sander C (1994) The immunoglobulin fold. Structural classification, sequence patterns and common core. *J Mol Biol* **242**, 309–320.

Botella H, Vaubourgeix J, Lee MH, et al. (2017) *Mycobacterium tuberculosis* protease MarP activates a peptidoglycan hydrolase during acid stress. *EMBO J* **36**, 536–548.

Brennan PJ & Nikaido H (1995) The envelope of mycobacteria. *Annu Rev Biochem* **64**, 29–63.

Brosch R, Gordon SV, Marmiesse M, et al. (2002) A new evolutionary scenario for the *Mycobacterium tuberculosis* complex. *PNAS* **99**(6), 3684–3689.

Brown RP, Aplin RT & Schofield CJ (1996) Inhibition of TEM-2 beta-lactamase from *Escherichia coli* by clavulanic acid: observation of intermediates by electrospray ionization mass spectrometry. *Biochemistry* **35**, 12421–12432.

Böth D, Schneider G & Schnell R (2011) Peptidoglycan Remodeling in *Mycobacterium tuberculosis*: Comparison of Structures and Catalytic Activities of RipA and RipB. *J of Mol Biol* **413**(1), 247–260.

Böth D, Steiner EM, Stadler D, Lindqvist Y, Schnell R & Schneider G (2013) Structure of Ldt_{Mt2}, an L,D-transpeptidase from *Mycobacterium tuberculosis*. *Acta Crystallogr D* **69**(Pt 3), 432–441.

Böth D, Steiner EM, Izumi A, Schneider G & Schnell R (2014) RipD (Rv1566c) from *Mycobacterium tuberculosis*: adaptation of an NlpC/p60 domain to a non-catalytic peptidoglycan-binding function. *Biochem J* **457**(1), 33–41.

Campbell EA, Korzheva N, Mustaev A, et al. (2001) Structural Mechanism for Rifampicin Inhibition of Bacterial RNA Polymerase. *Cell* **104**(6), 901–912.

Chang JC, Miner MD, Pandey AK, et al. (2009) igr Genes and *Mycobacterium tuberculosis* cholesterol metabolism. *J Bacteriol* **191**, 5232–5239.

Cole C, Barber JD & Barton GJ (2008) The Jpred 3 secondary structure prediction server. *Nucl Acids Res* **35**, W197–W201.

Comstock GW (1994) The International Tuberculosis Campaign: A Pioneering Venture in Mass Vaccination and Research. *Clin Infect Dis* **19**, 528–40.

Cooper AM, Mayer-Barber KD & Sher A (2011) Role of innate cytokines in mycobacterial infection. *Mucosal Immunol* **4**(3), 252–260.

Correale S, Ruggiero A, Capparelli R, Pedonea E & Berisioa R (2013) Structures of free and inhibited forms of the L,D-transpeptidase Ldt_{Mt1} from *Mycobacterium tuberculosis*. *Acta Crystallogr D* **69**(Pt9), 1697–1706.

Daniels R, Mellroth P, Bernsel A, et al. (2010) Disulfide Bond Formation and Cysteine Exclusion in Gram-positive Bacteria. *J of Biol Chemistry* **285**(5), 3300–3309.

Daniel TM (2005) Leon Charles Albert Calmette and BCG vaccine. *Int J Tuberc Lung Dis* **9**, 205–206.

Daniel TM (2006) The history of tuberculosis. *Resp Med* **100**(11), 1862–1870.

Dauby N, Muylle I, Mouchet F, Sergysels R & Payen MC (2011) Meropenem/clavulanate and linezolid treatment for extensively drug-resistant tuberculosis. *Pediatr Infect Dis J* **30**, 812–813.

Davies J & Davies D (2010) Origins and Evolution of Antibiotic Resistance. *Microbiol Mol Biol Rev* **74**(3), 417–433.

De Lorenzo S, Alffenaar JW, Sotgiu G, et al. (2013) Efficacy and safety of meropenem-clavulanate added to linezolid-containing regimens in the treatment of MDR-/XDR-TB. *Eur Respir J* **41**, 1386–1392.

Dhar N, Dubée V, Ballell L, et al. (2015) Rapid cytolysis of *Mycobacterium tuberculosis* by faropenem, an orally bioavailable β-lactam antibiotic. *Antimicrob Agents Chemother* **59**, 1308–1319.

Dubée V, Triboulet S, Mainardi JL, et al. (2012) Inactivation of *Mycobacterium tuberculosis* l,d-Transpeptidase Ldt_{Mt1} by Carbapenems and Cephalosporins. *Antimicrob Agents and Chemother* **56**(8), 4189–4195.

Dye C & Williams BG (2008) Eliminating human tuberculosis in the twenty-first century. *J Soc Interface* **5**, 653–62.

Ebina T, Toh H & Kuroda Y (2009) Loop-Length-Dependent SVM Prediction of Domain Linkers for High-Throughput Structural Proteomics. *Biopolymers* **92**, 1–8.

Egan AJF & Vollmer W (2013) The physiology of bacterial cell division. *Ann NY Acad Sci* **1277**, 8–28.

Egan AJF & Vollmer W (2015) The stoichiometric divisome: a hypothesis. *Front Microbiol* **12**, https://doi.org/10.3389/fmicb.2015.00455.

England K, Boshoff HI, Arora K, et al. (2012) Meropenem-clavulanic acid shows activity against *Mycobacterium tuberculosis in vivo*. *Antimicrob Agents Chemother* **56**, 3384–3387.

Erdemli SB, Gupta R, Bishai WR, et al. (2012) Targeting the cell wall of *Mycobacterium tuberculosis*: structure and mechanism of L,D-transpeptidase 2. *Structure* **20**, 2103–2115.

Ernst JD (1998) Macrophage receptors for *Mycobacterium tuberculosis*. *Infect Immun* **66**, 1277–1281.

Espinosa-Cueto P, Magallanes-Puebla A, Castellanos C & Mancilla R (2017) Dendritic cells that phagocytose apoptotic macrophages loaded with mycobacterial antigens activate CD8 T cells via cross-presentation. *PLOS ONE* **12**(8): e0182126.

Favini-Stabile S, Contreras-Martel C, Thielens N & Dessen A (2013) MreB and MurG as scaffolds for the cytoplasmic steps of peptidoglycan biosynthesis. *Environ Microbiol* **15**(12), 3218–28.

Ferguson JS, Voelker DR, McCormack FX & Schlesinger LS (1999) Surfactant protein D binds to *Mycobacterium tuberculosis* bacilli and lipoarabinomannan via carbohydrate-lectin interactions resulting in reduced phagocytosis of the bacteria by macrophages. *J Immunol* **163**, 312–321.

Flannagan RS, Cosio G & Grinstein S (2009b) Antimicrobial mechanisms of phagocytes and bacterial evasion strategies. *Nat Rev Microbiol* **7**, 355–366.

Fratti RA, Backer JM, Gruenberg J, Corvera S & Deretic V (2001) Role of phosphatidylinositol 3-kinase and Rab5 effectors in phagosomal biogenesis and mycobacterial phagosome maturation arrest. *J Cell Biol* **154**, 631–44.

Gao LY, Pak M, Kish R, Kajihara K & Brown EJ (2006) A mycobacterial operon essential for virulence *in vivo* and invasion and intracellular persistence in macrophages. *Infect Immun* **74**(3), 1757–1767.

Gatfield J & Pieters J (2000) Essential role for cholesterol in entry of mycobacteria into macrophages. *Science* **288**, 1647–1650.

Gaynor CD, McCormack FX, Voelker DR, McGowan SE & Schlesinger LS (1995) Pulmonary surfactant protein A mediates enhanced phagocytosis of *Mycobacterium tuberculosis* by a direct interaction with human macrophages. *J Immunol* **155**, 5343–5351.

Gengenbacher M & Kaufmann SHE (2012) *Mycobacterium tuberculosis*: success through dormancy. *FEMS Microbiol Rev* **36**(3), 514–532.

Giesbrecht P, Kersten T, Maidhof H & Wecke J (1998) Staphylococcal cell wall: morphogenesis and fatal variations in the presence of penicillin. *Microbiol Mol Biol Rev* **62**, 1371–1414.

Gilleron M, Jackson M, Nigou J & Puzo G (2008) Structure, biosynthesis, and activities of the phosphatidyl-*myo*-inositol-based lipoglycans. In: Daffé M, Reyrat JM, editors. The Mycobacterial Cell Envelope. *ASM Press*, 75–105.

Goffin, C & Ghuysen, JM (2002) Biochemistry and comparative genomics of SxxK superfamily acyltransferases offer a clue to the mycobacterial paradox: presence of penicillin-susceptible target proteins versus lack of efficiency of penicillin as therapeutic agent. *Microbiol and Mol Biol Rev* **66**, 702–738.

Gold MC, Cerri S, Smyk-Pearson S, et al. (2010) Human mucosal associated invariant T cells detect bacterially infected cells. *PLOS Biol* **8**: e1000407.

Greenberg S (1999) Fc receptor mediated phagocytosis. S. Gordon (Ed.), Phagocytosis: the host, *JAI Press*, 149–191.

Guirado E & Schlesinger LS (2013) Modeling the *Mycobacterium tuberculosis* granuloma – the critical battlefield in host immunity and disease. *Front Immunol* **4**:98.

Gupta R, Lavollay M, Mainardi JL, et al. (2010) The *Mycobacterium tuberculosis* protein Ldt_{Mt2} is a nonclassical transpeptidase required for virulence and resistance to amoxicillin. *Nat Med* **16**(4), 466–469.

Harriff MJ, Cansler ME, Toren KG, et al. (2014) Human lung epithelial cells contain *Mycobacterium tuberculosis* in a late endosomal vacuole and are efficiently recognized by CD8+ T cells. *PLOS ONE* **9**: e97515.

Hasegawa H & Holm L (2009) Advances and pitfalls of protein structural alignment. *Curr Opin Struct Biol* **19**, 341–348.

Hayman J (1984) *Mycobacterium ulcerans*: an infection from Jurassic time? *Lancet* **2**, 1015–1016.

Hekmat O, Lo Leggio L, Rosengren A, et al. (2010) Rational engineering of mannosyl binding in the distal glycone subsites of *Cellulomonas fimi* endo-beta-1,4-mannanase: mannosyl binding promoted at subsite -2 and demoted at subsite -3. *Biochemistry* **49**, 4884–4896.

Hershkovitz I, Donoghue HD, Minnikin DE, et al. (2008) Detection and Molecular Characterization of 9000-Year-Old *Mycobacterium tuberculosis* from a Neolithic Settlement in the Eastern Mediterranean. *PLOS ONE* **3**(10):e3426.

Hett EC Chao MC, Steyn AJ, Fortune SM, Deng LL & Rubin EJ (2007) A partner for the resuscitation promoting factors of *Mycobacterium tuberculosis*. *Mol Microbiol* **66**, 658–668.

Hett EC & Rubin EJ (2008) Bacterial growth and cell division: a mycobacterial perspective. *Microbiol Mol Biol Rev* **72**, 126–156.

Hett EC, Chao MC & Rubin EJ (2010) Interaction and modulation of two antagonistic cell wall enzymes of mycobacteria. *PLOS Pathogens* **6**:e1001020.

Hoagland DT, Liu J, Lee RB & Lee RE (2016) New agents for the treatment of drug-resistant *Mycobacterium tuberculosis*. *Adv Drug Deliv Rev* **102**, 55–72.

Hoffmann C, Leis A, Niederweis M, Plitzko JM & Engelhardt H (2008) Disclosure of the mycobacterial outer membrane: Cryo-electron tomography and vitreous sections reveal the lipid bilayer structure. *PNAS* **105**(10), 3963–7.

Holm L & Rosenström P (2010) Dali server: conservation mapping in 3D. *Nucl Acids Res* **38**, W545–549.

Hossain MM & Norazmi MN (2013) Pattern Recognition Receptors and Cytokines in *Mycobacterium tuberculosis* Infection—The Double-Edged Sword? *BioMed Res Intern* 2013:179174.

Houben RMGJ & Dodd PJ (2016) The Global Burden of Latent Tuberculosis Infection: A Re-estimation Using Mathematical Modelling. Metcalfe JZ, ed. *PLOS Medicine* **13**(10):e1002152.

Hrast M, Sosic I, Sink R & Gobec S (2014) Inhibitors of the peptidoglycan biosynthesis enzymes MurA-F. *Bioorg Chem* **55**, 2–15.

Hugonnet JE & Blanchard JS (2007) Irreversible Inhibition of the *Mycobacterium tuberculosis* β-lactamase by Clavulanate. *Biochemistry* **46**(43), 11998–12004.

Hugonnet JE, Tremblay LW, Boshoff HI, Barry CE, 3rd & Blanchard JS (2009) Meropenemclavulanate is effective against extensively drug-resistant *Mycobacterium tuberculosis*. *Science* **323**(5918), 1215–1218.

Jackson M, McNeil MR & Brennan PJ (2013) Progress in targeting cell envelope biogenesis in *Mycobacterium tuberculosis*. *Future Microbiol* **8**(7):10.2217/fmb.13.52.

Jo EK, Yang CS, Choi CH & Harding CV (2007) Intracellular signalling cascades regulating innate immune responses to mycobacteria: branching out from Toll-like receptors. *Cell Microbiol* **9**(5), 1087–1098.

Kieser KJ & Rubin EJ (2014) How sisters grow apart: mycobacterial growth and division. *Nat Rev Microbiol* **12**, 550–562.

Kim HS, Kim J, Im HN, et al. (2013) Structural basis for the inhibition of *Mycobacterium tuberculosis* l,d-transpeptidase by meropenem, a drug effective against extensively drug-resistant strains. *Acta Crystallogr D* **69**(Pt 3), 420–431.

Kishore U, Greenhough TJ, Waters P, et al. (2006) Surfactant proteins SP-A and SP-D: structure, function and receptors. *Mol Immunol* **43**(9), 1293–315.

Koch R (1932) Die aetiologie der tuberculose, a translation by Berna Pinner and Max Pinner with an introduction by Allen K. Krause. *Am Rev Tuberc* **25**, 285–323.

Kondratieva T, Azhikina T, Nikonenko B, Kaprelyants A & Apt A (2014) Latent tuberculosis infection: What we know about its genetic control? *Tuberculosis* **94**(5), 462–468.

Kouidmi I, Levesque RC & Paradis-Bleau C (2014) The biology of Mur ligases as an antibacterial target. *Mol Microbiol* **94**, 242–253.

Kuk ACY, Mashalidis EH & Lee SY (2017) Crystal structure of the MOP flippase MurJ in an inward-facing conformation. *Nat Struct & Mol Biol* **24**, 171–176.

Kumar P, Arora K, Lloyd JR, et al. (2012) Meropenem inhibits D,D-carboxypeptidase activity in *Mycobacterium tuberculosis*. *Mol Microbiol* **86**, 367–381.

Kumar P, Kaushik A, Lloyd EP, et al. (2017) Non-classical transpeptidases yield insight into new antibacterials. *Nat Chem Biol* **13**, 54–61.

Kurosu M, Mahapatra S, Narayanasamy P & Crick DC (2007) Chemoenzymatic synthesis of Park's nucleotide: toward the development of high-throughput screening for MraY inhibitors. *Tetrahedron Letters* **48**, 799–803.

Lavollay M, Arthur M, Fourgeaud M, et al. (2008) The peptidoglycan of stationary-phase *Mycobacterium tuberculosis* predominantly contains cross-links generated by l,d-transpeptidation. *J Bacteriol* **190**, 4360–4366.

Lechartier B, Hartkoorn RC & Cole ST (2012) *In Vitro* Combination Studies of Benzothiazinone Lead Compound BTZ043 against *Mycobacterium tuberculosis*. *Antimicrob Agents and Chemother* **56**(11), 5790–5793.

Lecoq L, Bougault C, Hugonnet JE, et al. (2012) Dynamics induced by β-lactam antibiotics in the active site of *Bacillus subtilis* L,D-transpeptidase. *Structure* **20**, 850–861.

Lerner TR, Borel S & Gutierrez MG (2015) The innate immune response in human tuberculosis. *Cellular Microbiol* **17**(9), 1277–1285.

Li Y, Wang Y & Liu X (2012) The role of airway epithelial cells in response to mycobacteria infection. *Clin Dev Immunol* 2012:791392.

Li WJ, Li DF, Hu YL, Zhang XE, Bi LJ & Wang DC (2013) Crystal structure of L,D-transpeptidase Ldt_{Mt2} in complex with meropenem reveals the mechanism of carbapenem against *Mycobacterium tuberculosis*. *Cell Res* **23**, 728–731.

Lillebaek T, Dirksen A, Baess I, et al. (2002) Molecular evidence of endogenous reactivation of *Mycobacterium tuberculosis* after 33 years of latent infection. *J Infect Dis* **185**(3), 401–404.

Lugton I (1999) Mucosa-associated lymphoid tissues as sites for uptake, carriage and excretion of tubercle bacilli and other pathogenic mycobacteria. *Immunol Cell Biol* **77**, 364–372.

Loudon RG & Roberts RM (1967) Droplet expulsion from the respiratory tract. *Am Rev Respir Dis* **95**(3), 435–442.

Mahapatra S, Scherman H, Brennan PJ & Crick DC (2005a) N-Glycolylation of the nucleotide precursors of peptidoglycan biosynthesis of *Mycobacterium spp*. is altered by drug treatment. *J Bacteriol* **187**, 2341–2347.

Mainardi JL, Fourgeaud M, Hugonnet JE, et al. (2005) A novel peptidoglycan cross-linking enzyme for a beta-lactam-resistant transpeptidation pathway. *J Biol Chem* **280**, 38146–38152.

Makinoshima H & Glickman MS (2005) Regulation of *Mycobacterium tuberculosis* cell envelope composition and virulence by intramembrane proteolysis. *Nature* **436**, 406–409.

Manjunatha UH, Rao SPS, Kondreddi RR, et al. (2015) Direct inhibitors of InhA active against *Mycobacterium tuberculosis*. *Science Transl Med* **7**(269):269ra3.

Martin CJ, Carey AF & Fortune SM (2016) A bug's life in the granuloma. *Seminars in immunopath* **38**(2), 213–220.

Martinelli DJ & Pavelka MS Jr (2016) The RipA and RipB peptidoglycan endopeptidases are individually nonessential to *Mycobacterium smegmatis*. *J Bacteriol* **198**, 1464–1475.

Mavrici D, Marakalala MJ, Holton JM, et al. (2014) *Mycobacterium tuberculosis* FtsX extracellular domain activates the peptidoglycan hydrolase, RipC. *PNAS* **111**, 8037–8042.

McNeil M, Wallner SJ, Hunter SW & Brennan PJ (1987) Demonstration that the galactosyl and arabinosyl residues in the cell-wall arabinogalactan of *Mycobacterium leprae* and *Mycobacterium tuberculosis* are furanoid. *Carbohydrate Res* **166**, 299–308.

Mellroth P, Daniels R, Eberhardt A, et al. (2012) LytA, Major Autolysin of *Streptococcus pneumoniae*, Requires Access to Nascent Peptidoglycan. *J of Biol Chem* **287**(14), 11018–11029.

Mengin-Lecreulx D, Texier L, Rousseau M & Van Heijenoort J (1991) The murG gene of *Escherichia coli* codes for the UDP-N-acetylglucosamine: N-acetylmuramyl-(pentapeptide) pyrophosphoryl-undecaprenol N-acetylglucosamine transferase involved in the membrane steps of peptidoglycan synthesis. *J Bacteriol* **173**, 4625–4636.

Meroueh SO, Bencze KZ, Hesek D, et al. (2006) Three-dimensional structure of the bacterial cell wall peptidoglycan. *PNAS* **103**(12), 4404–4409.

Middleton AM, Chadwick MV, Nicholson AG, et al. (2002) Interaction of *Mycobacterium tuberculosis* with human respiratory mucosa. *Tuberculosis* **82**, 69–78.

Minnikin DE, Lee OYC, Wu HHT, et al. (2015) Pathophysiological Implications of Cell Envelope Structure in *Mycobacterium tuberculosis* and Related Taxa. *Tuberculosis - Exp Knowledge, InTech*. Chapter **7**. doi: 10.5772/59585.

Miranda MS, Breiman A, Allain S, Deknuydt F & Altare F (2012) The Tuberculous Granuloma: An Unsuccessful Host Defence Mechanism Providing a Safety Shelter for the Bacteria*? Clin and Develop Immunol*, Article ID 139127, 14 pages.

Narasimhan P, Wood J, MacIntyre CR & Mathai D (2013) Risk Factors for Tuberculosis. *Pulm Med*, 2013:828939.

Nesbitt NM, Yang X, Fontan P, et al. (2010) A thiolase of *Mycobacterium tuberculosis* is required for virulence and production of androstenedione and androstadienedione from cholesterol. *Infect Immunol* **78**, 275–282.

Niederweis M, Danilchanka O, Huff J, Hoffmann C & Engelhardt H (2010) Mycobacterial outer membranes: in search of proteins. *Trends in Microbiol* **18**(3), 109–116.

Parthasarathy G, Lun S, Guo H, et al. (2012) Rv2190c, an NlpC/P60 Family Protein, Is Required for Full Virulence of *Mycobacterium tuberculosis*. *PLOS ONE* **7**(8): e43429.

Pavkov T, Egelseer EM, Tesarz M, et al. (2008) The structure and binding behavior of the bacterial cell surface layer protein SbsC. *Structure* **16**, 1226–1237.

Payen MC, De Wit S, Martin C, et al. (2012) Clinical use of the meropenem-clavulanate combination for extensively drug-resistant tuberculosis. *Int J Tuberc Lung Dis* **16**, 558–560.

Pazos M, Peters K & Vollmer W (2017) Robust peptidoglycan growth by dynamic and variable multi-protein complexes. *Curr Opin in Microbiol* **36**(0), 55–61.

Petersen TN, Brunak S, von Heijne G & Nielsen H (2011) SignalP 4.0: discriminating signal peptides from transmembrane regions. *Nat Methods* **8**, 785–786.

Petoukhov MV, Franke D, Shkumatov AV, et al. (2012) New developments in the ATSAS program package for small-angle scattering data analysis. *J Appl Cryst* **45**, 342–350.

Peyron P, Bordier C, N'Diaye EN & Maridonneau-Parini I (2000) Nonopsonic phagocytosis of *Mycobacterium kansasii* by human neutrophils depends on cholesterol and is mediated by CR3 associated with glycosylphosphatidylinositol-anchored proteins. *J Immunol* **165**, 5186–5191.

Pieters J (2008) *Mycobacterium tuberculosis* and the Macrophage: Maintaining a Balance. *Cell Host & Microbe* **3**(6), 399–407.

Pitarque S, Larrouy-Maumus G, Payré B, et al. (2008) The immunomodulatory lipoglycans, lipoarabinomannan and lipomannan, are exposed at the mycobacterial cell surface. *Tuberculosis* **88**(6), 560–565.

Plocinski P, Arora N, Sarva K, et al. (2012) *Mycobacterium tuberculosis* CwsA interacts with CrgA and Wag31, and the CrgA–CwsA complex is involved in peptidoglycan synthesis and cell shape determination. *J Bacteriol* **194**, 6398–6409.

Pope, WH, Ferreira CM, Jacobs-Sera D, et al. (2011) Cluster K mycobacteriophages: insights into the evolutionary origins of mycobacteriophage TM4. *PLOS ONE* **6**:e26750.

Prigozhin DM, Mavrici D, Huizar JP, et al. (2013) Structural and Biochemical Analyses of *Mycobacterium tuberculosis N*-Acetylmuramyl-l-alanine Amidase Rv3717 Point to a Role in Peptidoglycan Fragment Recycling. *J of Biol Chem* **288**(44), 31549–31555.

Priyadarshini R, de Pedro MA & Young KD (2007) Role of Peptidoglycan Amidases in the Development and Morphology of the Division Septum in *Escherichia coli*. *J Bacteriol* **189**(14), 5334–5347.

Prosser GA & de Carvalho LP (2013a) Kinetic mechanism and inhibition of *Mycobacterium tuberculosis* D-alanine:D-alanine ligase by the antibiotic D-cycloserine. *FEBS J* **280**, 1150–1166.

Prosser GA & de Carvalho LP (2013b) Metabolomics reveal d-alanine:d-alanine ligase as the target of d-cycloserine in *Mycobacterium tuberculosis*. *ACS Medic Chem Letters* **4**, 1233–1237.

Prosser GA& de Carvalho LP (2013) Reinterpreting the Mechanism of Inhibition of *Mycobacterium tuberculosis* d-Alanine:d-Alanine Ligase by d-Cycloserine. *Biochemistry* **52** (40), 7145–7149.

Rahman, O, Cummings SP, Harrington DJ & Sutcliffe IC (2008) Methods for the bioinformatic identification of bacterial lipoproteins encoded in the genomes of Gram-positive bacteria. *World J Microbiol Biotechnol* **24**, 2377–2382.

Raymond JB, Mahapatra S, Crick DC & Pavelka MS Jr (2005) Identification of the namH gene, encoding the hydroxylase responsible for the N-glycolylation of the mycobacterial peptidoglycan. *J Biol Chem* **280**, 326–333.

Reddy VM, Einck L, Andries K & Nacy CA (2010) *In vitro* interactions between new antitubercular drug candidates SQ109 and TMC207. *Antimicrob Agents Chemother* **54**, 2840–2846.

Robert X & Gouet P (2014) Deciphering key features in protein structures with the new ENDscript server. *Nucl Acids Res* **42**(W1), W320–W324.

Rojas M, Garcia LF, Nigou J, Puzo G & Olivier M (2000) Mannosylated lipoarabinomannan antagonizes *Mycobacterium tuberculosis*-induced macrophage apoptosis by altering Ca2+-dependent cell signaling. *J Infect Dis* **182**, 240–51.

Roy A, Kucukural A & Zhang Y (2010) I-TASSER: a unified platform for automated protein structure and function prediction. *Nat Protoc* **5**(4), 725–38.

Ruggiero A, Marasco D, Squeglia F, et al. (2010) Structure and Functional Regulation of RipA, a Mycobacterial Enzyme Essential for Daughter Cell Separation. *Structure* **18**(9), 1184–1190.

Ruiz N (2015) Lipid flippases for bacterial peptidoglycan biosynthesis. *Lipid Insights* **8**, 21–31.

Rullas J, Dhar N, McKinney JD, Garcia-Perez A, et al. (2015) Combinations of beta-lactam antibiotics currently in clinical trials are efficacious in a DHP-I-deficient mouse model of tuberculosis infection. *Antimicrob Agents and Chemotherapy* **59**, 4997–4999.

Sakula A (1983) BCG: Who were Calmette and Guérin? *Thorax* **38**, 806–812.

Sambou T, Dinadayala P, Stadthagen G, et al. (2008) Capsular glucan and intracellular glycogen of *Mycobacterium tuberculosis*: Biosynthesis and Impact on the Persistence in mice. *Mol Microbiol* **70**(3), 762–774.

Sanders AN, Wright LF & Pavelka MS Jr (2014) Genetic characterization of mycobacterial l,d-transpeptidases. *Microbiol* **160**(Pt 8), 1795–1806.

Sarathy JP, Dartois V & Lee EJD (2012) The Role of Transport Mechanisms in *Mycobacterium tuberculosis* Drug Resistance and Tolerance. *Pharmaceuticals* **5**(11), 1210–1235.

Saunders BM & Cooper AM (2000) Restraining mycobacteria: role of granulomas in mycobacterial infections. *Immunol Cell Biol* **78**, 334–341.

Sivaramakrishnan S & Ortiz de Montellano PR (2013) The DosS-DosT/DosR Mycobacterial Sensor System. *Biosensors* **3**(3), 259–282.

Sauvage E, Kerff F, Terrak M, Ayala JA & Charlier P (2008) The penicillin-binding proteins: structure and role in peptidoglycan biosynthesis. *FEMS Microbiol Rev* **32**, 234–258.

Schatz A, Bugie E & Waksman SA (1944) Streptomycin, a substance exhibiting antibiotic activity against Gram-positive and Gram-negative bacteria. *Proc Exp Biol Med* **55**, 66–69.

Schnappinger D, Ehrt S, Voskuil MI, et al. (2003) Transcriptional adaptation of *Mycobacterium tuberculosis* within macrophages: insights into the phagosomal environment. *J Exp Med* **198**, 693–704.

Schoonmaker MK, Bishai WR & Lamichhane G (2014) Nonclassical transpeptidases of *Mycobacterium tuberculosis* alter cell size, morphology, the cytosolic matrix, protein localization, virulence, and resistance to β-lactams. *J Bacteriol* **196**, 1394–1402.

Shukla S, Richardson ET, Athman JJ, et al. (2014) *Mycobacterium tuberculosis* Lipoprotein LprG Binds Lipoarabinomannan and Determines Its Cell Envelope Localization to Control Phagolysosomal Fusion. *PLOS Pathog* **10**(10): e1004471.

Sievers F, Wilm A, Dineen D, et al. (2011) Fast, scalable generation of high-quality protein multiple sequence alignments using Clustal Omega. *Mol Systems Biol* **7**, 539.

Siricilla S, Mitachi K, Wan B, Franzblau SG & Kurosu M (2015) Discovery of a capuramycin analog that kills nonreplicating *Mycobacterium tuberculosis* and its synergistic effects with translocase I inhibitors. *J of Antibiotics* **68**, 271–278.

Slayden RA, Lee RE & Barry CE (2000) Isoniazid affects multiple components of the type II fatty acid synthase system of *Mycobacterium tuberculosis*. *Mol Microbiol* **38**, 514–525.

Smith NH, Kremer K, Inwald J, et al. (2006) Ecotypes of the *Mycobacterium tuberculosis* complex. *J Theor Biol* **239**, 220–225.

Steiner EM, Schneider G & Schnell R (2017) Binding and processing of β-lactam antibiotics by the transpeptidase Ldt_{Mt2} from *Mycobacterium tuberculosis*. *FEBS J* **284**, 725–741.

Sturgill-Koszycki S, Schlesinger PH, Chakraborty P, et al. (1994) Lack of acidification in Mycobacterium phagosomes produced by exclusion of the vesicular proton-ATPase. *Science* **263**, 678–681.

Supply P, et al. (2013) Genomic analysis of smooth tubercle bacilli provides insights into ancestry and pathoadaptation of *Mycobacterium tuberculosis*. *Nat Genetics* **45**(2), 172–179.

Szwedziak P & Lowe J (2013) Do the divisome and elongasome share a common evolutionary past? *Curr Opin Microbiol* **16**, 745–751.

Tahlan K, Wilson R, Kastrinsky DB, et al. (2012) SQ109 targets MmpL3, a membrane transporter of trehalose monomycolate involved in mycolic acid donation to the cell wall core of *Mycobacterium tuberculosis*. *Antimicrob Agents Chemother* **56**(4), 1797–1809.

Tan TC, Mijts BN, Swaminathan K, Patel BK & Divne C (2008) Crystal structure of the polyextremophilic alpha-amylase AmyB from *Halothermothrix orenii*: details of a productive enzyme-substrate complex and an N domain with a role in binding raw starch. *J Mol Biol* **378**, 852–870.

Tiberi S, D'Ambrosio L, De Lorenzo S, et al. (2016) Ertapenem in the treatment of multidrug-resistant tuberculosis: first clinical experience. *Eur Respir J* **47**, 333–336.

Toossi Z & Ellner JJ (2001) Pathogenesis of tuberculosis. *Tuberculosis*. Friedman, L.N. (ed.). *New York: CRC Press*, 19–47.

Tran AT, Wen D, West NP, Baker EN, Britton WJ & Payne RJ (2013) Inhibition studies on *Mycobacterium tuberculosis* Nacetylglucosamine-1-phosphate uridyltransferase (GlmU). *Org & Biomol Chem* **11**, 8113–8126.

Trunkfield AE, Gurcha SS, Besra GS & Bugg TDH (2010) Inhibition of *Escherichia coli* glycosyltransferase MurG and *Mycobacterium tuberculosis* Gal transferase by uridine-linked transition state mimics. *Bioorg & Medic Chem* **18**(7), 2651–2663.

Turner RD, Vollmer W & Foster SJ (2014) Different walls for rods and balls: the diversity of peptidoglycan. *Mol Microbiol* **91**(5), 862–874.

Typas A, Banzhaf M, Gross CA & Vollmer W (2012) From the regulation of peptidoglycan synthesis to bacterial growth and morphology. *Nat Rev Microbiol* **10**, 123–136.

Udwadia ZF & Pinto LM (2007) REVIEW SERIES: The Politics of TB: The politics, economics and impact of directly observed treatment (DOT) in India. *Chr Respir Disease* **4**(2), 101–106.

von Pirquet C (1907) Der diagnostische wert der kutanen tuberkulinreaktion bei der tuberkulose des kindesalters auf grund von 100 sektionen. *Wr Klein Wochenschr* **20**, 1123–1128.

von Pirquet C (1907) Die allergieprobe zur diagnose der tuberkulose in kindesalter. *Wr Med Wochenschr* **28**, 1369–1374.

Vergne I, Fratti RA, Hill PJ, Chua J, Belisle J & Deretic V (2004) *Mycobacterium tuberculosis* phagosome maturation arrest: mycobacterial phosphatidylinositol analog phosphatidylinositol mannoside stimulates early endosomal fusion. *Mol Biol Cell* **15**, 751–60.

Vollmer W, Blanot D & de Pedro MA (2008) Peptidoglycan structure and architecture. *FEMS Microbiol Rev* **32**, 149–167.

Voskuil MI, Bartek IL, Visconti K & Schoolnik GK (2011) The Response of *Mycobacterium tuberculosis* to Reactive Oxygen and Nitrogen Species. *Front in Microbiol* **2**:105.

Wehrli W (1983) Rifampin: mechanisms of action and resistance. *Rev Infect Dis* **5**(3), S407–11.

WHO (2008) Guidelines for the programmatic management of drug-resistant tuberculosis: emergency update 2008. Geneva.

WHO (2010) Treatment of Tuberculosis: *Guidelines.* 4th edition. Geneva.

WHO (2014) The End TB Strategy Global strategy and targets for tuberculosis prevention, care and control after 2015. Sixty Seventh World Health Assembly.

WHO (2014) Companion Handbook to the WHO Guidelines for the Programmatic Management of Drug-Resistant Tuberculosis. Geneva.

WHO (2015) Guidelines on the management of latent tuberculosis infection. Geneva.

WHO (2016) Global Tuberculosis Report 2016. World Health Organization, Geneva.

Young DB, Gideon HP & Wilkinson RJ (2009) Eliminating latent tuberculosis. *Trends in Microbiol* **17**(5), 183–188.

Zhang L, Koay M, Maher MJ, Xiao Z & Wedd AG (2006) Intermolecular transfer of copper ions from the CopC protein of *Pseudomonas syringae*. Crystal structures of fully loaded Cu(I)Cu(II) forms. *J Am Chem Soc* **128**, 5834–5850.